Miniaturized combinatorial screening

of small molecules, responsive hydrogels, and biomaterials

Zur Erlangung des akademischen Grades eines

DOKTORS DER NATURWISSENSCHAFTEN

(Dr. rer. nat.)

von der KIT-Fakultät für Chemie und Biowissenschaften

des Karlsruher Instituts für Technologie (KIT)

genehmigte

DISSERTATION

von

M. Sc. Alisa Rosenfeld

aus

Archangelsk, Russland

Referent: Dr. Pavel Levkin

Korreferent: Prof. Dr. Ute Schepers

Tag der mündlichen Prüfung: 21.04.2020

Один матрос реставрировал старинную мебель
И хлебнул с ней горя.
Каждую ночь он спускался в гараж
И рыл подземный ход, чтоб добраться до моря.
Тридцать лет - он закончил рыть
И вышел где-то в пустыне.
Он пал на колени в соленые волны
И приник к ним губами, как будто к святыне.

Аквариум «Трамонтана»

Die vorliegende Arbeit wurde unter der Leitung von Dr. Pavel Levkin von März 2017 bis März 2020 am Institut für Biologische und Chemische Systeme (IBCS-FMS) des Karlsruher Instituts für Technologie (KIT, Campus Nord) angefertigt.

Frau Prof. Dr. Ute Schepers möchte ich für die freundliche Übernahme des Korreferats danken.

Eidesstattliche Erklärung

Hiermit versichere ich, dass ich die vorliegende Arbeit selbständig angefertigt und keine anderen als die angegebenen Quellen und Hilfsmittel benutzt sowie wörtlich und inhaltlich übernommene Stellen als solche kenntlich gemacht habe. Die Satzung des Karlsruher Instituts für Technologie (KIT) zur Sicherung guter wissenschaftlicher Praxis in der gültigen Fassung wurde beachtet.

Abstract

The importance of new drugs and advanced materials for the future of humankind cannot be overestimated. A continuing demand for new drugs persists, since there are still many diseases inefficiently cured by existing remedies. Similarly, many niche applications require more and more sophisticated responsive materials, aggravated by the fact that the underlying structure/function relationships are often not fully understood. Nonetheless, despite significant efforts and financial investments are made, the classical workflows of early drug and material discovery remain slow and inefficient. Typically, a library of new small molecules or materials is synthesized one by one, which is time-, material-, and workforce consuming. The synthesis and screening parts are often separated in time and space. In order to address these challenges, miniaturized platforms that allow performing both synthesis and screening steps in a high-throughput manner are sought to be developed.

A miniaturized Droplet Microarray (DMA) platform, comprising a glass slide patterned with hydrophilic regions surrounded by superhydrophobic borders, offers confined microenvironments to various liquids, including aqueous solvents and cell suspensions.

In this PhD work, DMA substrates were modified to be used as a miniaturized platform for combinatorial solid-phase synthesis of small molecules and subsequent biological screenings, which resulted in chemBIOS workflow (chemical synthesis combined with biological read-out on the same glass slide). Due to the compartmentalization, each droplet served first as a separate reaction compartment and later as a microreservoir for culturing cells. Nanoporous poly(2-hydroxyethyl methacrylate-*co*-ethylene dimethacrylate) layers served as a solid phase for the synthesis and were functionalized with a photo-cleavable 4-[4-(1-Hydroxyethyl)-2-methoxy-5-nitrophenoxy]butanoic acid as a linker. The attachment of the linker onto the solid phase was optimized and used as a model reaction to show three possibilities of reaction monitoring on DMA: ToF-SIMS, XPS and ATR-IR. The use of a photo-cleavable linker for solid-phase synthesis allowed controlling the concentration of the final drug in separated individual droplet compartments by changing the irradiation time. Upon irradiation with UV-light, products of the solid-phase synthesis could be released from the porous polymer and delivered into the separate droplets. Thus, the light-induced release of the products allowed controlling the release spatially, temporally and quantitatively. Confinement of liquids, which is an essential part of the whole workflow, was proved by XPS and ToF SIMS methods and protected from leakage from one spot to another. HEK293T cells were tested in regards of maintaining cell viability upon UV irradiation, which manifested in preserved high viability up to 15 min UV irraditation (6 mW/cm^2, 360 nm). Finally, a peptide synthesis was established as a model reaction, totalling a 16-membered tripeptide library.

In chapter 4 it is shown that DMA platform meets the requirements for a cell-compatible polymer microarray and can be used as a benchtop-ready platform for high-throughput combinatorial hydrogel synthesis and, if desired, subsequent cell encapsulation. Photoresponsive materials were chosen as model materials due to importance of light in biological settings and in order to bridge the gap in the state-of-the-art high-throughput syntheses dominated by thermo- and hydroresponsive materials. Poly(ethylenglycol) methacrylate (PEGMA), poly(ethylenglycol) dimethacrylate (PEGDMA), 2-(dimethylamino)ethyl methacrylate (DMAEMA) and (2-(*N*-3-sulfopropyl-*N*,*N*-dimethyl ammonium)ethyl methacrylate (SAMA) were used to construct libraries of inherently photodegradable hydrogels. A spatial gradient of monomers and crosslinkers was produced by dispensing different volumes of these compounds along the x- and y-axes of an array. A PEGMA/DMAEMA/PEGDMA containing 33-membered combinatorial library á 4 replicates was synthesized on a nanoliter scale and used to optimize the photopolymerization parameters (i.e. oxygen scavenging system and proper mixing within droplets). A PEGMA/SAMA/PEGDMA containing 20-membered combinatorial library á 16 replicates was synthesized, and the photodegradation properties of the underlying materials were examined in a high-throughput manner. The findings were proved correct by upscaling, embracing the spectrum from non-degradable to rapidly degradable hydrogels. In total, more than 450 distinct hydrogel micropads were synthesized in a miniaturized high-throughput manner.

The aforementioned PEGMA-based hydrogels, albeit showing rapid photodegradability, are unsuitable for cell encapsulation. In Chapter 5, the need for an inherently photodegradable material suitable for cell encapsulation was addressed. A combinatorial screening of 32 composite gelatin methacrylate/ poly(ethyleneglycol) methacrylate (GelMA/PEGMA)-based photodegradable hydrogels was performed and hydrogels were tested in regards to their photodegradation properties. Mathematical approximation was performed to reveal structure/function relationships between photodegradability and degree of functionalization of GelMA, its amount as well as amount of PEGMA and PEGDMA. Testing revealed a hydrogel that is suitable for cell photoencapsulation, while still being degraded at a rate of 0.5 mm/min, despite GelMA exerting a manifold negative impact on photodegradation properties. The degradation procedure was optimized, proving the medium exchange prior to degradation essential for fast material erosion and still compliant with cells. As an example, an array of free-standing cell-laden hydrogel micropads was produced, and cell viability was proved to remain high upon UV irradiation.

To conclude, Droplet Microarray was modified and used for miniaturized high-throughput combinatorial small molecule and responsive hydrogel synthesis. Both synthetic parts can be

seamlessly combined with biological experiments on the same chip. Due to the high miniaturization and parallelization, the time and material consumption is reduced approximately 100- to 1000-fold. The findings of Chapter 3, i.e. the ability not only to synthesize libraries of compounds but also release them into individual cell microreservoirs with spatio-temporal control, demonstrate the potential to further advance miniaturized and HT cell-based assays. The workflow presented in Chapter 4 can be utilized to facilitate high-throughput experimentation in the field of responsive hydrogels to generate new and more sophisticated responsive materials with novel properties, which may remain undiscovered using the one-by-one synthesis approach. Also, a novel cell-friendly gelatin-based hydrogel was developed that can be photodegraded on demand under cell-compatible conditions without the installation of photolabile groups prior to degradation.

Zusammenfassung

Die Bedeutung neuer Medikamente und fortgeschrittener Materialien für die Zukunft der Menschheit kann gar nicht hoch genug geschätzt werden. Die anhaltende Nachfrage nach neuen Arzneimitteln besteht immer noch, da es weiterhin viele Krankheiten gibt, die durch die auf dem Markt angebotenen Arzneimittel ineffizient geheilt werden. In ähnlicher Weise erfordern viele Spezialanwendungen immer ausgefeiltere Materialien, deren Entwicklung durch die Tatsache erschwert wird, dass die zugrundeliegenden Struktur-/ Funktionsbeziehungen häufig nicht vollständig geklärt sind. Trotz beträchtlicher Anstrengungen und finanzieller Investitionen bleiben die klassischen Workflows der frühen Wirkstoff- und Materialentwicklung jedoch langsam und ineffizient. Typischerweise wird eine Bibliothek neuartiger kleiner Moleküle oder Materialien einzeln synthetisiert, was zeit-, material- und arbeitsintensiv ist. Die Synthese- und Screening sind oft zeitlich und räumlich voneinander getrennt. Um diesen Herausforderungen zu begegnen, wird die Entwicklung einer miniaturisierten Plattform angestrebt, mit der sowohl Synthese als auch biologische Screenings mit hohem Durchsatz durchgeführt werden können.

Eine miniaturisierte Droplet Microarray (DMA) –Plattform stellt einen Glasträger dar, der mit hydrophilen Bereichen, die von superhydrophoben Rändern umgeben sind, gemustert ist. Dadurch können auf dem DMA verschiedenen Flüssigkeiten, einschließlich wässriger Lösungsmittel und Zellsuspensionen, kompartmentalisiert werden.

In dieser Doktorarbeit wurde DMA so modifiziert, dass es als miniaturisierte Plattform für die kombinatorische Festphasensynthese kleiner Moleküle und anschließende biologische Screenings verwendet werden kann. Dies führte zum chemBIOS-Workflow (chemische Synthese wird mit biologischem Auslesen auf demselben Glasträger kombiniert). Aufgrund der Kompartimentierung diente jedes Tröpfchen zunächst als miniaturisiertes Reaktionsgefäß und später als Mikroreservoir für die Kultivierung von Zellen. Nanoporöse Poly(2-hydroxyethylmethacrylat-coethylendimethacrylat)-Schicht diente als feste Phase für die Synthese und wurde mit einem photospaltbaren Linker funktionalisiert. Die Anbindung des Linkers an die Festphase wurde optimiert und als Modellreaktion verwendet, um drei Möglichkeiten der Reaktionsüberwachung auf DMA aufzuzeigen: ToF SIMS, XPS und ATR-IR. Die Verwendung eines photospaltbaren Linkers für die Festphasensynthese ermöglichte die Steuerung der Konzentration des Endproduktes in einzelnen Tröpfchenkompartimenten durch Änderung der Bestrahlungszeit. Bei Bestrahlung mit UV-Licht konnten Produkte der Festphasensynthese aus dem porösen Polymer freigesetzt und in die separaten Tröpfchen abgegeben werden. Die lichtinduzierte Abspaltung der Produkte ermöglichte es somit, die Freisetzung räumlich, zeitlich und quantitativ zu steuern. Der Einsperrung von Flüssigkeiten

ist hierbei eine wesentliche Voraussetzung des gesamten Workflows und wurde mit XPS- und ToF-SIMS-Methoden nachgewiesen. HEK293T-Zellen wurden hinsichtlich der Zellviabilität bei UV-Bestrahlung getestet, was sich in einer bis zu 15 min dauernden UV-Bestrahlung (6 mW/cm^2, 360 nm) bewahrten hohen Lebensfähigkeit äußerte. Schließlich wurde eine Peptidsynthese als Modellreaktion etabliert, die eine 16-gliedrige Tripeptidbibliothek umfasste.

In Kapitel 4 wird gezeigt, dass die DMA-Plattform die Anforderungen für ein zellkompatibles Polymer-Microarray erfüllt und für die kombinatorische Hydrogelsynthese mit hohem Durchsatz und gegebenenfalls für die anschließende Verkapselung von Zellen verwendet werden kann. Die photoresponsiven Materialien wurde aufgrund der Bedeutung des Lichts für biologische Anwendungen als Modellmaterialien ausgewählt, und um die Lücke in den bis dato veröffentlichten Hochdurchsatzsynthesen zu schließen, die von thermo- und hydroresponsiven Materialien dominiert werden. Poly(ethylenglykol)methacrylat (PEGMA), Poly(ethylenglykol)dimethacrylat (PEGDMA), 2-(dimethylamino)ethylmethacrylat (DMAEMA) und (2-(N-3-sulfopropyl-N,N-dimethylammonium)ethylmethacrylat (SAMA) wurden eingesetzt, um Bibliotheken von inhärent durch UV Licht degradierbaren Hydrogelen zu konstruieren. Ein räumlicher Gradient von Monomeren und Vernetzern wurde erzeugt, indem verschiedene Volumina dieser Verbindungen entlang der x- und y-Achse eines Arrays gedruckt wurden. Eine PEGMA/DMAEMA/PEGDMA enthaltende 33-gliedrige kombinatorische Materialienbibliothek, mit jeweils 4 Replikaten von jeder Zusammensetzung, wurde im Nanolitermaßstab synthetisiert und zur Optimierung der Photopolymerisationsparameter (d.h. des Sauerstoffeinfangsystems und des gründlichen Mischens innerhalb der Tröpfchen) verwendet. Eine PEGMA/SAMA/PEGDMA enthaltende kombinatorische Bibliothek, mit jeweils 16 Replikaten von jeder Zusammensetzung, wurde synthetisiert und der Photodegradation unterzogen. Die Eigenschaften der Materialien wurden im Hochdurchsatz untersucht und die Ergebnisse durch Hochskalierung bestätigt, wobei das Spektrum von nicht abbaubaren bis schnell abbaubaren Hydrogelen abgedeckt wurde. Insgesamt wurden mehr als 450 Hydrogel-Mikropads in einer miniaturisierten Weise mit hohem Durchsatz synthetisiert.

Die obengenannten Hydrogele auf PEGMA-Basis zeigen schnelle Photoabbaubarkeit, sind aber für die Einkapselung von Zellen ungeeignet. In Kapitel 5 wird das Bedürfnis nach einem inhärent lichtabbaubaren Material angesprochen, das für die Einkapselung von Zellen geeignet ist. Eine kombinatorische Synthese von 32 Hydrogelen auf Gelatin methacrylat/Poly(ethylenglycol) methacrylat- (GelMA/ PEGMA)-Basis wurde durchgeführt und die Hydrogele wurden auf ihre Photodegradierbarkeit getestet. Es folgte eine mathematische Näherung, um die Struktur/Funktions-Beziehungen zwischen der Photoabbaubarkeit und dem Funktionalisierungsgrad von GelMA, seiner Menge sowie der

Menge an PEGMA und PEGDMA aufzudecken. Die Tests ergaben ein Hydrogel, das für die Photoeinkapselung von Zellen geeignet ist und mit einer Geschwindigkeit von 0,5 mm/min abgebaut werden kann, obwohl GelMA einen vielfachen negativen Einfluss auf die Photoabbaueigenschaften ausübt. Der Abbauworkflow wurde optimiert, wobei sich der Mediumaustausch vor dem Abbau als nötig erwiesen hat. Es wurde gezeigt, dass der Mediumaustausch für einen schnellen Abbau wesentlich ist und dennoch mit den Zellen kompatibel ist. Als Beispiel wurde ein Array von freistehenden zellbeladenen Hydrogel-Mikropads hergestellt, und es wurde nachgewiesen, dass die Lebensfähigkeit der Zellen bei der Arrayproduktion unverändert hoch bleibt.

Zusammenfassend konnte Droplet Microarray modifiziert und für miniaturisierte kombinatorische Synthese von kleinen Molekülen sowie stimuli-responsiven Hydrogelen im hohen Durchsatz verwendet werden. In beiden Fällen lässt sich Synthese nahtlos mit biologischen Experimenten auf demselben Chip kombiniert werden. Durch die hohe Miniaturisierung und Parallelisierung wird der Zeit- und Materialverbrauch um das 100- bis 1000-fache reduziert. Die Ergebnisse der Kapitel 3, unter anderem die Fähigkeit, Bibliotheken von Verbindungen nicht nur zu synthetisieren, sondern sie auch in einzelne zellenthaltende Mikrokompartments mit räumlich-zeitlicher Kontrolle freizusetzen, zeigen das Potenzial, miniaturisierte Hochdurchsatzscreenings weiter voranzutreiben. Der in Kapitel 4 vorgestellte Workflow kann für Hochdurchsatzsynthese von intelligenten Hydrogelen verwendet werden, um komplexere Materialien mit neuartigen Eigenschaften zu entdecken, die unter Verwendung des one-by-one Syntheseansatzes möglicherweise unentdeckt bleiben. Außerdem wurde ein neues zellfreundliches Hydrogel auf Gelatinebasis entwickelt, das bei Bedarf unter zellverträglichen Bedingungen ohne die Installation photolabiler Gruppen photodegradiert werden kann.

List of abbreviations

4-DMAP	4-dimethylaminophenol
AFM	atomic force microscopy
AM	acetoxymethyl
ATR-IR	attenuated total reflection infrared
BE	binding energy
bs	broad singulett
dH_2O	DI water
DIC	diisopropylcarbodiimid
DMA	Droplet Microarray
DMEM	Dulbecco's Modified Eagle's Medium
DMF	dimethylformamide
DoF	degree of functionalization
DPBS	Dulbecco's Phosphate-Buffered Saline
FCS	fetal calf serum
Fmoc-Ala	N-(9-Fluorenylmethoxycarbonyl)-L-alanine
Fmoc-Glu(OtBu)-OH	N-(9-Fluorenylmethyloxycarbonyl)-L-glutamic-acid-tertbutyl ester
Fmoc-Gly	N-(9-Fluorenylmethoxycarbonyl)-L-glycine
Fmoc-Leu	N-(9-Fluorenylmethoxycarbonyl)-L-leucine
Fmoc-Val	N-(9-Fluorenylmethoxycarbonyl)-L-valine
FTIR	Fourier-transform infrared spectroscopy
GelMA	gelatin methacrylate
HEMA-*co*-EDMA	2-hydroxyethyl methacrylate-*co*-ethylene dimethacrylate
HL	hydrophilic
HEK	human embryonic kidney cells
HeLa	cervical cancer cells
HTS	high-throughput screening
kDa	kilodalton
LAP	lithium phenyl-2,4,6-trimethylbenzoylphosphinate
LCST	low critical solution temperature
MTT	3-(4,5-dimethylthiazol-2-yl)-2,5-diphenyltetrazolium bromide
MWCO	molecular-weight cut-offs
NHDF	normal human dermal fibroblasts
NMR	nuclear magnetic resonance
PEG	poly(ethylenelgycol)
PEGDMA	poly(ethylenelgycol)-dimethacrylate

PEGMA	poly(ethylenelgycol) methacrylate
s	singlet
SAP	sodium phenyl-2,4,6-trimethylbenzoylphosphinate
SH	superhydrophobic
TLC	thin layer chromatography
TMS	tetramethylsilane
TNBSA	2,4,6-trinitrobenzene sulfonic acid
ToF-SIMS	Time of Flight - Secondary Ion Mass Spectrometry
UHV	ultra high vacuum
UV	ultraviolet
WCA	water contact angle
XPS	X-ray photoelectron spectroscopy

1. Introduction[1]

1.1 Combinatorial high-throughput synthesis of small molecules

1.1.1 State-of-the-art early drug discovery pipelines

Drugs play a pivotal role in the history of the humankind. The demand for new drugs is high, not only because of drug resistant pathogens, and the need for better, less toxic drugs, but also because there are just on average only 8 novel first-in-class drugs per year, approved by the FDA.[1-2] The world is undersupplied with drugs, mainly because of the inefficiency and the high costs of the whole drug discovery pipeline, which is reflected in averaged 15-25 years and US$800 million- US$2 billion required for a single drug to enter the market,[3-5] despite enormously high investment in this field and more than 10.000 biotechnology and pharmaceutical companies worldwide.

There are about 18 million purchasable drug-like compounds available in various commercial chemical libraries,[6] such as ChemBridge or ChemDiv. These libraries have been accumulated over the last 20-30 years from different sources but usually from individual syntheses performed by different researchers worldwide. Notably, a one-by-one synthesis of compounds that will be included in a chemical library, performed according to standard wet chemistry approaches, requires large amounts of reagents and solvents. Taken with the need of consequent characterization and isolation of new compounds it makes the efficiency of synthesis of drug-like molecules extremely low and not compatible with the demand for high-throughput screenings (HTS). To solve this problem, pharmaceutical companies use combinatorial chemistry and high-throughput screening methods to synthesize and test large chemical libraries. Cell screenings are usually performed in 96- or 384-well plates, so in order to achieve a high throughput, thousands of microtiter plates have to be used. This approach suffers from several drawbacks, such as consumption of relatively large amounts of cells and high-cost reagents and the need to use robotics in order to screen thousands of chemicals per day, as well as difficulty to remove chemicals from cell monolayer once the screening has to be stopped, which influences the accuracy of experiments.[7-8] The general methodological drawback is separation of chemical synthesis from the biological screenings in time and space. So, the library of compounds can be synthesized in one laboratory at one point of a time and has to be bought and transported to another laboratory at some other time point to be subjected

[1] This chapter is adapted from following publications:
Alisa Rosenfeld; Pavel A. Levkin. High-Throughput Combinatorial Synthesis of Stimuli-Responsive Materials. *Advanced Biosystems*, **2019**, 1800293; **Alisa Rosenfeld**; Marius Brehm; Alexander Welle; Vanessa Trouillet; Stefan Heissler; Maximilian Benz; Pavel A. Levkin. Solid-phase combinatorial synthesis using microarrays of microcompartments with light-induced on-chip cell screening. *Materials Today Bio*. **2019**, 3, 100022.

to cell screenings. In the light of increasingly competitive industrial environment, it becomes difficult to ignore the cost-related issues of such screenings and syntheses and makes both synthesis and biological experiments not compatible with ultra high-throughput screenings.

1.1.2 Miniaturized high-throughput synthesis approaches

Miniaturization and array formats, accompanied by parallelisation, can solve some of these problems. The microarray technology enables rapid synthesis of various compounds, including DNA,[9-11] peptides,[12-13] proteins,[14] small molecules,[12, 15-16] oligosaccharides,[17-18] synthetic polymers.[19] DNA microarray technology, given a momentum in early 1990´s,[20] was the first successful example of miniaturized highly parallel high-throughput synthesis, based on immobilized single-strand probe nucleic acid.[10-11, 21] Small molecule and peptide microarrays were pioneered by Lam et al.[12] and Schreiber et al.[15], followed by protein microarray developed by MacBeat and Schreiber[14], with a standard (2.5 cm by 7.5 cm) slide comprising 10,800 spots. Light directed spatially addressable parallel synthesis of peptides, reported by Fodor et al., in which a photolithographic mask is used to reach a high level of spatial control, resulted synthesis of 1,054 peptides on the area as small as 2.56 mm^2.[22] Breitling et al. proposed a synthesis of 40,000 peptide spots per cm^2 by using electrical fields generated by individual pixel electrodes of a microchip.[23] The feature density could be further increased to 62,500 spots per cm^2 using scanning-probe-lithography based approach.[24] SPOT synthesis, taking advantage of cheap cellulose, has emerged as a rapid and simple method to generate peptides[13] and was extended to small molecules.[16] Other examples of synthetic microarrays include formation of oligosaccharides[25-26] and synthetic polymers.[19] Extensive research is done on biological display methods, such as phage, yeast, bacterial, CIS, mRNA and ribosome display.[27] They are based on close association between peptide and nucleic acid from which it was expressed, e.g. peptide is displayed on the surface of phage or yeast. Lithography techniques enable confining liquids and performing reactions in volumes on a femto- to atooliter scale.[28]

While these methods have provided significant development in the field of miniaturized high-throughput synthesis in the past years, they still face numerous challenges. Most of the techniques are restricted to peptide and nucleic acid chemistries, lacking thereby synthetic diversity. Final biological assays are usually performed in the bulk solution. Several types of cell screenings can be performed in bulk without compartmentalization, e.g. high-throughput screening of cell-surface interactions with biomaterial arrays or gradients,[29-31] to find biomaterials supporting growth, expansion or differentiation of cells. In these cases, cell responses are initiated by contact with a material, which is attached to the planar surface. Peptides obtained via SPOT can be used in biological assays, where they either stay attached to the cellulose in studying of bacteria-surface interactions[32] as well as protein, antibody and

metal binding assays.[33-34] However, since confinement of liquids on the cellulose surface is challenging, solution based cell screenings can be only achieved by tedious procedures. Ultra high throughput DNA sequencing allows simultaneous miniaturized screening in bulk solution of large DNA-encoded libraries containing up to 10^{15} compounds. Yet, it requires decoding strategies and is dependent on nucleic acid-friendly reactions.[35] Still, a considerable amount of cell experiments (e.g. investigation of cell-cell interactions and cell interaction with soluble cues) need to be done in confined volumes. Also, issues of cross-contamination caused by lateral diffusion of compounds and low spatial and temporal control can be solved by introducing compartmentalized microreservoirs. Additionally confinement in small volumes enables or significantly facilitates the detection of low-abundance molecules and analytes that cannot be amplified, as well as sensitivity of (single)-cell screening by minimalizing of diffusion losses and dilution.[36]

The ultimate goal to advance drug discovery would therefore be a miniaturized platform that 1) facilitates high throughput synthesis, 2) employs diverse chemistry, thus covering larger chemical space, 3) utilizes combinatorial approach and 4) after completing synthesis can be directly used in cell screening with high spatial and temporal control.

1.2 Combinatorial high-throughput synthesis of smart materials

1.2.1 Smart materials – definition

Stimuli-responsive materials, also called smart or adaptive materials, are attracting growing attention in different fields, including biotechnology and medicine, as these materials are able to respond to minute changes in their surrounding environment by changes in their chemical, physical or biological properties. By applying a specific stimulus, stimuli-responsive materials can be altered at molecular scale in different ways (e.g. conformational transition, hydrophilicity, charge, solubility, chemical bond cleavage, etc.), resulting in changes in the materials' macroscopic features such as changes in volume, shape, performance, wettability, color, mechanical motion, release/capture of molecules, degradation, aggregation, precipitation, etc. A plethora of stimuli can be used to trigger a specific material response, and corresponding materials are comprehensively reviewed in the literature. These stimuli include temperature,[37-38] light,[39-41] mechanical forces,[42] electric and magnetic field,[40] ultrasound,[40, 42] pH,[43-44] ionic strength,[45] humidity,[46] various small molecules (e.g. glucose,[47-48] CO_2,[49-50] redox agents[51-52]), enzymes,[53] and some more complex combinations of stimuli.[54-56]

Sophisticated diverse examples of stimuli responsiveness and adaptivity are often found in natural biological systems. In the course of evolution and in order to interact with their dynamic environments, biological systems have acquired various complex responsive, adaptive and

dynamic properties. On every level of life, from dynamic ecosystems down to tissues, cells and biopolymers, responsiveness plays a crucial role and is a remarkable and ubiquitous biological property (sperm chemotaxis toward the egg, gravitropism of plant roots, and coral reef response to sea temperature as an illustration). A bioinspired design of responsive synthetic materials can benefit from millions of years of evolution and is an important means of accelerating the development of functional materials, improving their performance, and for fundamental research. For example, self-healing is an omnipresent feature of living organisms that has inspired the development of self-healing smart materials.[57] Bioinspired routes for preparing stimuli-responsive materials can, for example, use enzyme-cleavable linkers to achieve degradation of a polymer network in the presence of a corresponding enzyme.[58] Self-oscillating materials based on the Belousov-Zhabotinsky reaction[59] carry an analogy to autonomous oscillation in living systems like heart contractions and pulsatile secretion of hormones. However, they stand apart from other responsive materials, as they oscillate in a self-governed manner and need no oscillating external stimuli.[60]

1.2.2 Benefits of a combinatorial approach

Many high-end technologies, such as tissue engineering,[61] soft robotics,[62] sensors,[63] etc., require responsive materials perfectly adapted for each application. Usually, such multifunctional materials are rationally constructed by incorporating building blocks with known responsive behavior (e.g. pH-responsive and temperature-responsive functional groups). They reveal predictable, combined characteristics (e.g. pH- and temperature-responsiveness) that are independently traceable to installed building blocks.[54] Nonetheless, the functionality and tempo of development of new responsive materials remain far behind the broad-ranging demands of the aforementioned fields. To fulfil the miscellaneous needs and realize novel applications, we need to overcome the undersupply of responsive materials by covering larger chemical space and creating new materials faster. Combinatorial methodology is a powerful approach to quickly generate a vast number of structurally and functionally diverse materials using just a few functional building blocks **(Figure 1)**.

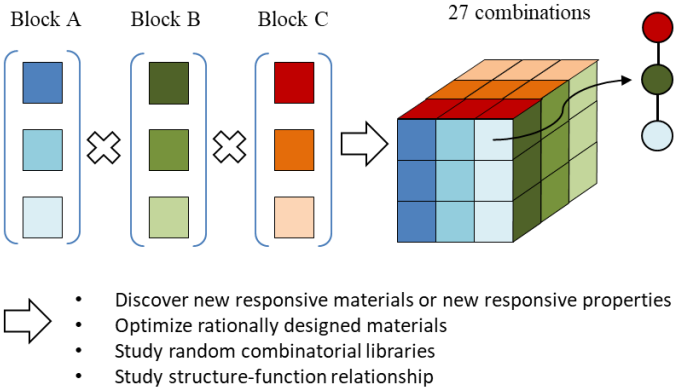

Figure 1. Operating principle and benefits of combinatorial library. Combinatorial approach allows quick generation of chemically diverse responsive materials and their investigation. Alisa Rosenfeld; Pavel A. Levkin. High-Throughput Combinatorial Synthesis of Stimuli-Responsive Materials. Advanced Biosystems, 2019, 1800293, Copyright Wiley-VCH GmbH. Reproduced with permission.

A multitude of design parameters and an even larger number of their combinations can essentially contribute to the precise fine-tuning of a responsive material for a specific application. However, stimuli-responsive materials are usually synthesized and evaluated iteratively one-by-one. The drawback of this approach is the paucity of possible combinations that can be practically tested for the purpose of saving time, consumables and manpower. This forces researchers to follow the beaten track - to investigate only some of the commonest and most obvious combinations of triggers and responses, and to change only one parameter at a time, despite the large variety of possibilities. Therefore, although a considerable amount of research is being devoted to the field of responsive materials, the actual development of such materials remains slow and inefficient and the design principles, including structure-function relationships, are often not fully understood.

1.2.3 The benefits of a high-throughput approach

To overcome slow and inefficient, one-by-one synthesis and screening, miniaturization, parallelization and high-throughput (HT) methodologies must be employed (**Figure 2**).

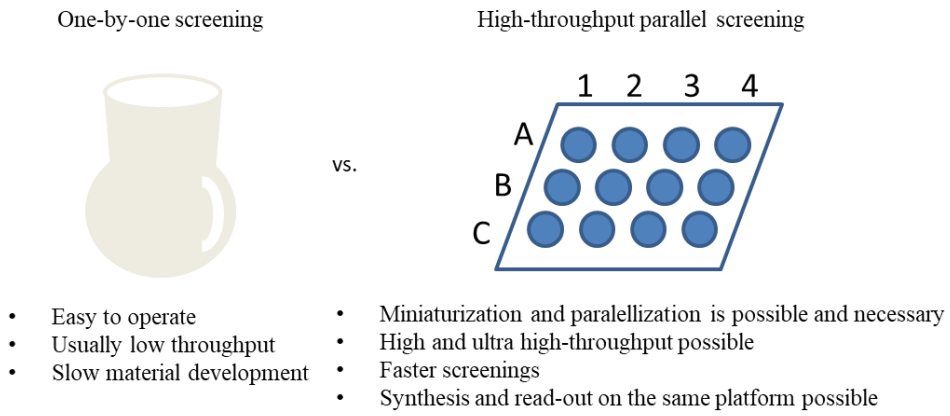

Figure 2. Comparison of classical one-by-one screening with high-throughput screening. Stimuli-responsive materials are usually synthesized sequentially one after another; therefore, the number of testable combinations is

limited. High-throughput techniques combined with the combinatorial approach enable us to cover otherwise inaccessible chemical space, and make possible material optimization for fundamental research and the discovery of novel properties.

HT synthesis and screening proved themselves initially as a powerful strategy in the pharmaceutical industry; HT syntheses and screenings have recently been applied in material discovery.[19] Besides saving time, consumables and work force, there are several other considerable benefits of employing combinatorial HT synthesis and screening in responsive material development. For rationally constructed materials possessing predictable characteristics, the combinatorial HT approach can enhance their focused screening and optimization. By varying known design parameters, rapid material fine-tuning for a particular application is achievable, and varied parameters can be mapped, providing insights into structure-function relationships. Yet, with the growing number of components being introduced, it becomes difficult to predict or rationally design the interplay between them. Combinatorial screening over a multitude of building blocks can reveal inhibitive (retarding) or cumulative (synergetic) effects that are otherwise unpredictable. This is particularly useful for deepening our understanding of synergetic and antagonistic interactions between different building blocks. Combinatorial HT screening of random libraries is therefore particularly useful if the ability to rationally design a responsive material is limited by theoretical knowledge that does not happen to be available. For example, the sheer complexity of the extracellular matrix and rather seldom predictability of mutual cell-material interactions make combinatorial methods and HT strategies powerful tools in stimuli-responsive material synthesis for tissue engineering applications. An intrinsically HT method also encourages the employment of counterintuitive, creative combinations of starting materials to discover materials with novel properties, functions, and responses. In light of the unpredictability of mutual component interactions and large, random (diversity-based) sets of combinations, combinatorial HT synthesis and screening offer a convenient opportunity to explore a variety of properties and functions that are accessible only with great effort in one-by-one synthesis or that cannot be rationally designed. In doing so we can transform a vast quantity of combinations and components into novel quality. Screening random libraries can therefore be performed to pursue novel discoveries, to acquire a key competitive advantage in what has become an aggressive environment of patenting policies.

1.2.4 Combinatorial high-throughput synthesis of stimuli-responsive materials – state-of-the-art

In the following paragraphs selected state-of-the-art examples of applying combinatorial HT synthesis and screening to accelerate the development of responsive and adaptive materials

are reviewed. Big libraries (>60 members) made in combinatorial but low-throughput one-by-one manners are also included.

1.2.4.1 Thermoresponsive materials

Thermoresponsive materials are one of the most well-studied and understood stimuli-responsive materials, including the most thoroughly investigated poly(*N*-isopropylacrylamide) (pNIPAAm). Its responsive properties have been extensively exploited in various biological applications, e.g. for controlled, temperature-triggered cell binding and release.[64] There are several examples of combinatorial HT synthesis of thermoresponsive materials. Combinatorial HT synthesis of thermoresponsive materials for mild cell release was established by Bradley group in 2009.[65] Water soluble *N*-isopropylacrylamide (NIPAAm) and *N*,*N*-diethylacrylamide (DEAA), that are known to confer thermoresponsive properties to final hydrogels, as well as other monomers were used to produce a 2280-membered library on a single glass slide via inkjet printing **(Figure 3**):

Figure 3. Fluorescence image of a 2280-membered library with captured fluorescent HeLa cells. Cell numbers calculated at different temperatures correlate with polymer composition and temperature. Reproduced from [65]

In the initial screen, the hydrogels were quantified in terms of their cell-binding and cell releasing properties upon cooling from 37°C to 20°C and 10°C **(Figure 4):**

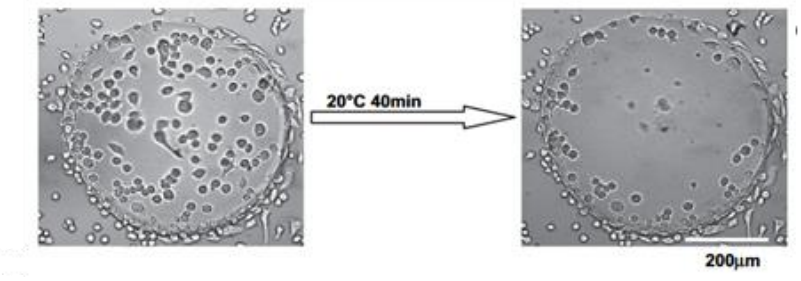

Figure 4. Bright-field image showing cell detachment from a polymer spot upon cooling. Reproduced from [65]

Following the initial screen, 23 “hit”-hydrogels were reprinted in “hit”-microarray in multiple copies, and their cell-binding and cell-releasing properties were assessed regarding the average area of a hydrogel spot. Finally, three best hydrogels were scaled up and scrutinized one-by-one. Their study revealed that these hydrogels offered strong cell-detachment

efficiency: up to 91% of cells could be released upon a thermal switch with the high viability of released cells (>85%). Being shrunk and dehydrated at 37°C, the hydrogels swell at lower temperatures, resulting in cellular detachment. A subsequent screen of “hit”-microarray on five cell lines (HeLa, L929, HEK-293T, mouse embryonic stem cells E14tg2a and B16F10) enabled the discovery of an optimal cell binding/releasing material for each cell type. The ability of NIPAAm-based thermoresponsive materials to release cells in response to temperature changes was exploited by Bradley group to identify a long-lasting cell-adhesive material that permitted the much-in-demand, gentle, reagent-free harvesting of human embryonic stem cells (hESCs). After their initial discoveries,[65] Bradley group synthesized an arrayed library of 609 hydrogels from 18 monomers.[66] In their initial screens, hESC attachment, viability, and the marker expression of cells attached to hydrogels were studied in a HT manner, then the best 25 polymers were scaled up and tested to see how efficient the thermally-triggered cell release was. Their study ultimately resulted in a chemically well-defined hydrogel that supported the long-term growth of hESCs while preserving their pluripotency and enabling non-destructive serial passaging and dissociation via thermal modulation and excellent (>90%) releasing capacity. These discoveries reveal the hidden potential of the combinatorial HT synthesis of responsive biomaterials and HT assessment of their biological properties. The design of the libraries was based on incorporating NIPAAm to confer thermoresponsive properties. However, with the number of monomers they used, it was difficult to rationally predict, but easy to test the properties of each unique polymer. The resulting diverse, large libraries made it possible to rapidly identify and optimize biocompatible materials with specific responsive properties. Without miniaturization and parallelization, the screening of hundreds of materials would require not only large quantities of chemical precursors but also an enormous amount of expensive stem cells and is thus quite unrealistic.

So far, thermo-responsiveness has been measured by the number of cells released from the material after the temperature modulation. An essentially different cell-free approach to define thermally responsive materials was also established based on temperature-correlated changes in wettability **(Figure 5**)[67]:

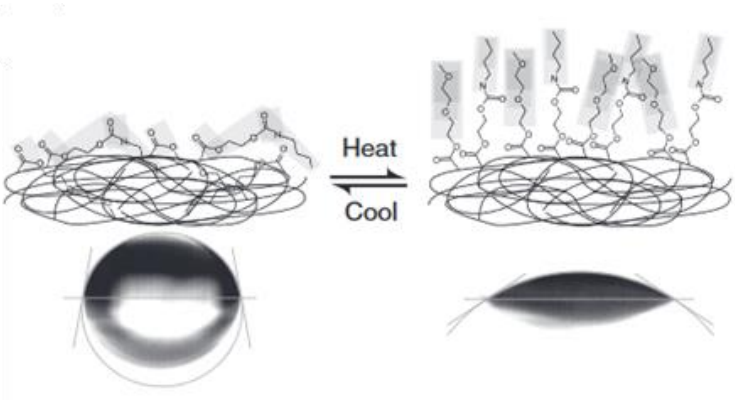

Figure 5. Schematic depiction of conformational changes in an exemplary copolymer upon temperature changes, which causes changes in water contact angle. These changes are compatible with high-throughput combinatorial screenings and can be utilized as a readouts for measuring thermoresponsiveness of materials.

HT measurements of the water contact angle (WCA) were taken to identify materials with thermoresponsive properties among 279 unique materials arranged in array format **(Figure 6):**

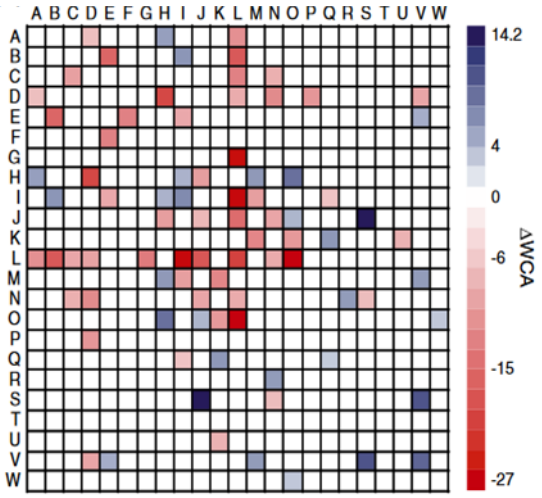

Figure 6. Intensity map of WCA changes upon heating of a polymer library. Letters indicate the monomers mixed at 50/50% ratio.[67]

Subsequently, time-of-flight secondary ion mass spectrometry (ToF-SIMS) enabled the detection of temperature-dependent molecular conformational changes in “hit” materials. The two polymers identified in this study later proved themselves as competent materials for thermally triggered *E.coli release* revealing noteworthy (up to 96%) efficiency, with possible application in self-cleaning bacterial filtration systems.[68]

Polymer microarray technology was recently employed to discover a responsive material able to alter an incorporated dye’s fluorescence upon a shift in temperature.[69] An array of 275 polymer features in quadruplicates was produced by ink-jet printing and differentiated in terms

of their fluorescence enhancement or quenching of entrapped fluorescent dye. Five representative combinations were up-scaled to produce polymer beads to further investigate optothermoresponsive properties at temperatures ranging from 25°C to 55°C.

Another cell-free approach, turbidimetry, was used to scrutinize thermoresponsive behaviour of polymers. Beger et al. synthesized a library of 60 oligo(ethyleneglycol)methacrylate-based polymers (partially in automated parallel and partially in individual one-by-one manner); 32 polymers were subjected to turbidimetry to investigate the responsive properties by measuring the cloudy point at different pH values, the pH-responsiveness being attributed to the incorporation of acidic monomer units.[70] Interestingly, several copolymers exhibited both thermo- and pH-responsiveness, although their homopolymers revealed no LCST behavior. This effect was only detectable by systematic random library screening of counterintuitive monomer combinations, thus showing the importance of such screenings to find unexpected, novel effects.

1.2.4.2 Hydroresponsive materials

Water is a ubiquitous solvent and is conveniently applicable as a trigger of various responses. An atomic force microscopy (AFM) surface high-throughput characterization study of a 576-membered acrylate library revealed four different topographies (flat surfaces and surfaces containing pits or nodules or particles). Pits were only observed in copolymers of 4-tert-butylcyclohexyl-acrylate with either (oligo)ethylene glycol acrylate or 3-(dimethylamino)propyl acrylate. The difference in hydrophilicity of these monomers leads to a phase-separation and therefore to pits, composed of hydrophilic monomer, dispersed in bulk hydrophobic monomer. Almost all of pit-polymers exhibited a rapid pit-to-bumpy transition upon exposure to water **(Figure 7)**.[71]

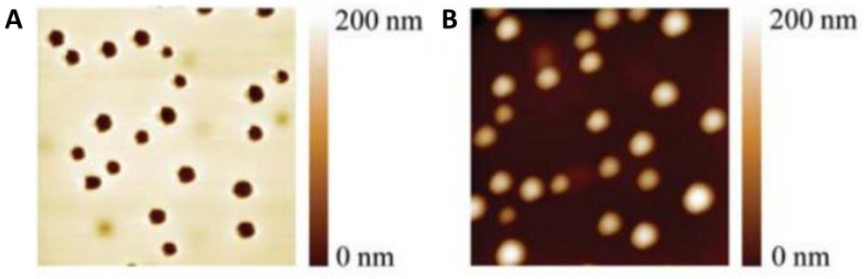

Figure 7. A 576-membered acrylate library, constructed from chemically very diverse monomers with different hydrophilicity, was characterized by HT-AFM. The screening revealed four different topographies, including a nano-structured pit-topography (A). Such polymers were discovered to be hydroresponsive and deliver a bumpy-topography (B) upon immersion in water, based on swelling of phase-separated hydrophilic pits.[71]

These transitions, based on swelling of hydrophilic pits, were almost all reversible for at least one wet-dry-wet cycle. Remarkably, this interesting response was only detectable via HT analysis methodologies, emphasizing their importance in high-throughput smart material development. The materials could probably not have been discovered if smaller sample sets had been used. This example accentuates the compatibility of combinatorial HT synthesis and screening methods to discover novel responsiveness and stresses the importance of random (diversity-based) combinatorial HT screening for discovering novel materials.

Hydrolytic degradation is an important parameter in various biological settings. Typically, ester linkages are installed to induce hydroresponsiveness under biological conditions. The Langer group investigated hydrolytically labile poly(β-aminoesters) as promising synthetic transfection vectors by first synthesizing a 140-membered-library in vials,[72] followed by half-automated 2350-membered library synthesis in 96-well plates.[73] From the first screening two polymers (~1% from the library) and from the second screening 46 polymers (~2% from the library) exceeded the performance of conventionally employed synthetic transfection agent poly(ethylene imine). The significantly larger second library, enabled by automatization strategies, delivered more “hits”, having almost the same success rate as the first library, emphasizing the importance of the throughput. Bradley group investigated another class of hydrolytically labile materials and synthesized a 61-member library of poly(ε-caprolactone)-based polyurethanes in bulk, and then in form of polymer microarray to identify 57 copolymers that facilitate cellular attachment and growth.[74] Hydrolysis experiments were performed in bulk on a larger scale on certain representative materials and demonstrated fasted degradation of more amorphous structures than semi-cristalline copolymers. Notably, the hits from both studies were selected and optimized in terms of their water solubility and gene delivery ability or cell responses, respectively, and not in terms of their hydroresponsiveness or degradation properties. Combinatorial HT (random) screening can be particular useful for investigating these features, as the mechanism of the degradation and its determining parameters (e.g. polymer hydrophobicity, pH and temperature of aqueous solution) are not always known, and the kinetics of degradation/rate of hydrolysis can be adapted and optimized for specific clinical applications (e.g. drug delivery or tissue engineering) by manipulating the material composition.[75] This issue was addressed by Burdick group.[76] A 120-member library of photocrosslinked, hydrolytically labile poly-(β-aminoesters) was synthesized and characterized in terms of degradation properties, albeit in a one-by-one manner **(Figure 8):**

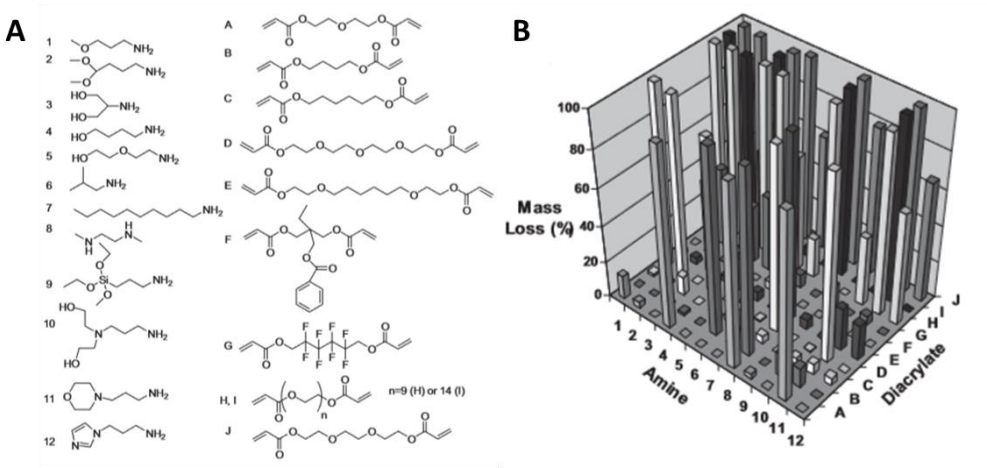

Figure 8. A) Acrylates and amines used to synthesize a library of polymerizable molecules, which then were used to form a library of hydrolytically labile polymers. B) Degradation behavior of the polymers based on the presence of ester linkages was detected by mass loss after 1 day of incubation in PBS at 37°C; faster degradation was attributed to hydrophilic diacrylates, whereas slower degradation was attributed to hydrophobic amines.[76]

The library was later screened against bulk properties, cell toxicity and attachment to identify an osteoconductive material.[77] The screening over a multitude of starting material combinations has proved the importance of the combinatorial approach, as a hydrolytical degradation trend cannot easily be derived from the chemical structure of educts. Combinatorial HT synthesis and screening has great potential and should be used to investigate other structure-function relationships and triggers. A 80-membered 2-oxazoline-based library including 40 potentially degradable poly(2-oxazoline)-co-polyesters was synthesized in bulk. To lay a foundation for future experiments on correlation of hydrophobic character of the gels with the degradation rate, as a proof of concept authors have tested one exemplary polymer to prove the pH-dependency of degradability and the degradability by esterases.[78] The degradation rate was evaluated by quantification of released Eosin B, which was incorporated prior to polymerization, and was found to be the highest at pH 8 and in the presence of porcine liver esterase.

Interestingly, some efforts were made to combine hydrolytical lability with UV-triggered degradation, albeit in a one-by-one manner resulting in small libraries.[79] Combinations of triggers demand more intense investigation. Such research can be accelerated by combinatorial HT synthesis.

1.3 Photoresponsive hydrogels

Light as a stimulus is of utter importance in various biological settings due to the unique combination of its intrinsic properties: 1) remote; 2) non-contaminant, thus no by-products are formed; 3) highly adjustable irradiation parameters, such as wavelength (allowing for orthogonal photoreactions), light intensity and irradiation time (allowing for control over the

degree of photoreactions); 4) spatial control both in 2D (single-photon induced photoreaction, by using corresponding photomasks) and 3D (two-photon induced photoreaction, overcoming light absorption issues); 5) temporal control by turning the light source on or off; 6) cheap.[41] Various hydrogel responses upon exposure to light can be observed. A hydrogel can be formed or degraded by light (partially or completely). Further, a hydrogel can endure volume changes (swelling/shrinking due to changes in crosslinking degree and/or hydrophilicity) or a photothermal excitation (i.e., a local increase in temperature that affects an adjacent thermoresponsive material). Gel-to-sol transition upon hydrogel degradation, hydrogel swelling as well as near infrared light induced photothermal excitation are promising approaches in targeted drug delivery.[80-81] Light-mediated manipulation of hydrogel-based cell microenvironments is readily used to mimic the native dynamic extracellular matrix, making a plethora of different applications possible. These include remote uncaging of reactive sites, such as RGD,[82] tethering of biomolecules via consequent light-induced polymerization,[83-84] release of biomolecules and cells,[85] changing the hydrogel stiffness to control stem cell differentiation[86-87] and cell morphology[88]. Moreover, photoresponsive hydrogels can be utilized to construct dynamic surfaces capable of light-induced changes in surface roughness (e.g. swelling based, subsequently exposing and hiding different regions),[89] or surface wettability (e.g. spiropyrane-based systems, zwitterionic antiadhesive state being used to release cells).[90]

Despite the variety of applications and significant efforts made to develop and improve photoresponsive hydrogels, conventional “one at a time” synthesis failed to extent most of the reviewed hydrogels beyond the proof-of-concept stage. These materials often compromise more biologically damaging high energy light, low quantum yield and slow kinetics. In addition, in order to systematically study structure/function relationships and hydrogel design parameters, larger combinatorial libraries should be synthesized and evaluated. Cell experiments, i.e. proving the biocompatibility of material itself, intermediates and products of photoreaction, can and should be studied in high throughput and preferably in a miniaturized format to reduce the amount of cells and consumables. Development of high-throughput methodologies for fast synthesis and screening of photoresponsive materials is therefore of vital importance.

1.4 Droplet microarray (DMA) platform

Droplet microarray (DMA) comprises a standard microscopic glass slide with a 6-12 µm thin layer of nanoporous poly(2-hydroxyethyl methacrylate-*co*-ethylene dimethacrylate) (HEMA-*co*-EDMA) chemically immobilized to the glass surface (**Figure 9).** The HEMA-*co*-EDMA polymer surface is functionalized via esterification with 4-pentynoic acid, followed by patterning via the UV-induced thiol-yne click reaction[91] with either cysteamine hydrochloride or 1*H*,1*H*,2*H*,2*H*-perfluorodecanethiol to form hydrophilic spots with various shape and size (HL, static water

contact angle (WCA), θ_{st} = 4.4°)[91] surrounded by superhydrophobic (SH, θ_{adv} = 173°, $\theta_{st.}$ = 170° and θ_{rec} = 164°)[91] borders (**Figure 9**):

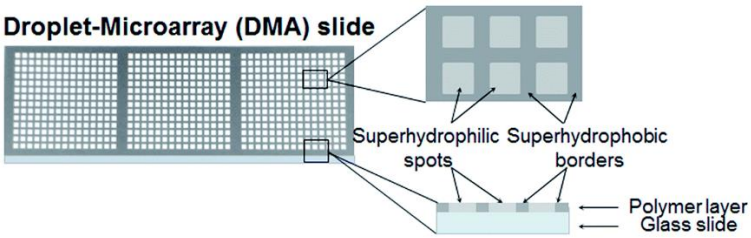

Figure 9. Graphical schematic of superhydrophobic-hydrophilic microarray (Droplet Microarray), adapted from [92]

Due to the extreme difference in wettability between SH and HL areas, aqueous solutions, such as cell suspension, applied onto such surface spontaneously form an array of separated microdroplets via discontinuous dewetting.[93] Some organic solvents, such as DMF and DMSO can also be confined into hydrophilic spots, despite their low surface tensions (37.10 and 43.54 mN/m, respectively). Various non-contact liquid dispensing techniques can be used to deposit liquids directly into the hydrophilic spots, without the need for manual handling.

DMA has proved itself to serve as a convenient and versatile platform for HT screening of single cells,[94] suspension and adherent cells,[92, 95] cell spheroids,[96] bacteria,[97] and even single fish-embryos.[98] DMA was also used to perform HT screening on stem cells,[99-100] embryoid bodies,[101] and are optimized for reversed cell transfection[91].

Previously two general workflows for screening of compound libraries were established. The first method involves a library transfer using the "sandwiching approach" **(Figure 10)**[102]:

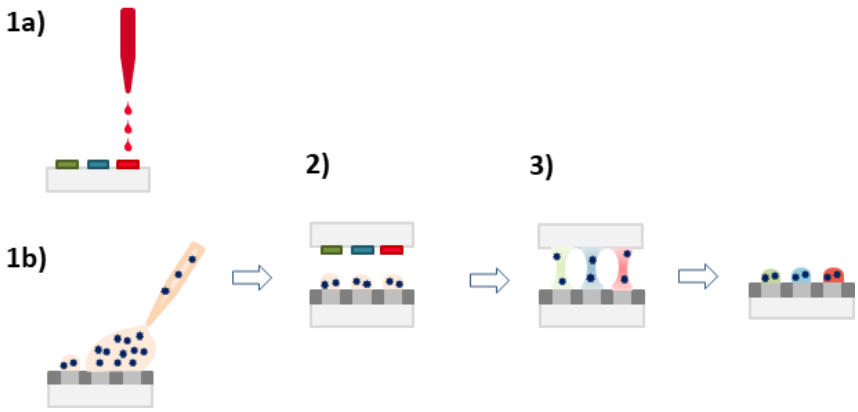

Figure 10. A workflow for compound library screening, sandwiching approach: 1a) drug library is printed on glass slide; 1b) cells are seeded on DMA 2) DMA and drug library slide are aligned parallel to each other; 3) cells get in contact with drugs upon sandwiching, which starts the compound screening.[102]

In the "reversed drug treatment approach", the library of compounds is printed directly onto the spots of a DMA slide (**Figure 11**)[92]:

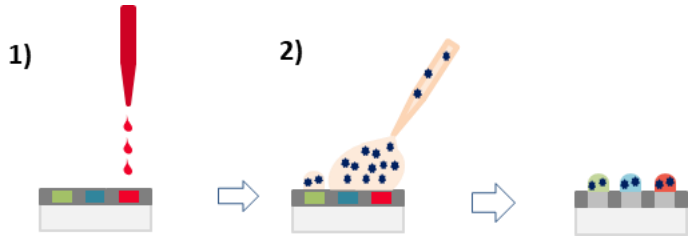

Figure 11. A workflow for compound library screening, reversed drug treatment approach 1) drug library is printed into hydrophilic spots of DMA; 2) cells are seeded onto the DMA with preprinted drugs, which starts the compound screening.[92]

In these approaches, the transfer of purchased drug libraries onto DMA slide requires solution handling and therefore presents some logistical challenges. To avoid the transfer step, chemical libraries can be synthesized directly in the hydrophilic spots of the DMA and subsequently subjected to biological screenings. ChemBIOS workflow combines both chemical synthesis and biological screening on the same platform.[103-105] It was previously validated for liquid-based synthesis of lipidoids, and later cell-screening to identify transfection reagents.[104] DMA was also proved itself as a convenient platform to produce an array of identical alginate hydrogels for miniaturized 3D cell culture.[106]

1.5 Objectives

The process of drug discovery includes individual synthesis and characterisation of drug candidates, followed by a biological screening. Both processes are separated from each other in space and time. This approach suffers from low throughput and associated high costs, which in turn lead to inefficiency in the field of drug discovery. Droplet Microarray comprises a polymer-coated glass slide patterned with hydrophilic spots and superhydrophobic borders, which due to compartmentalization of liquids can serve as a convenient platform for miniaturized high-throughput cell experiments. In course of these experiments, drug libraries are printed on DMA, and the screening is started in all spots simultaneously. However, this workflow is limited to the purchasable compounds. Liquid-phase organic synthesis on DMA expands the number of accessible compounds and benefits from combinatorial approach by systematically covering the chemical space. Cell screening can be conducted on the same slide where the synthesis was performed, forming a chemBIOS workflow. The synthesized compound starts to interact with cells as soon as they get in contact with each other and in only one concentration, which is determined by the yield of corresponding reaction and the solubility of the reaction product in cell medium. Liquid-based organic synthesis also requires consequent purification steps. Therefore, despite numerous advantages of this workflow, the temporal and quantitative control over the screening is missing. The first aim of this PhD work was to develop chemBIOS workflow for solid-phase synthesis, therefore eliminating the

purification step. The product is bound to the solid phase, and cells can be seeded and allowed to accommodate prior to the start of the screening, ensuring temporal control. The installation of a photolabile solid-phase linker and therefore light-induced release variable in time and light intensity also allow controlling the product release quantitatively.

Similar to drug discovery, the traditional pipeline of material, i.e. hydrogel development includes individual one-by-one synthesis and characterization. The drawback of this approach is the scarceness of possible combinations that can be practically tested for the purpose of saving time, consumables and manpower. However, covering larger chemical space is particularly useful in the field of stimuli-responsive materials, since it allows rapid identification and refinement of “hit” structures, studying structure-function relationships, and mimicking biological systems irrespective of the eventual lack of theoretical knowledge, while seeking novel responsive functions. High-throughput methods are therefore important to accelerate discovery of stimuli-responsive materials and to screen for biological interactions of interest in parallel. Still, as an alternative approach to classical one-by-one synthesis, high-throughput development of stimuli-responsive hydrogels is still tremendously under-represented, despite the urgent requirement for such techniques. This can be seen by the fact that during the last decades less than 20 studies on high-throughput combinatorial synthesis of stimuli-responsive materials were published, focusing mostly on thermo- and hydroresponsive materials. Hence, the second objective of this PhD work was to use DMA for high-throughput combinatorial stimuli-responsive hydrogel synthesis and screening, focusing on photoresponsive materials, which are both polymerized and degraded by UV light. Here, hydrophilic regions of hydrophilic/superhydrophobic pattern are used for deposition of various precursor solutions. In contrast to established high-throughput methodologies, which limit biological screening to interactions with material surface, DMA provides the confinement of liquids, thus allowing encapsulation of cells within the hydrogel, and enables variation in hydrogel height and width. An arrayed format makes decoding of the “hit” composition simple and is particularly suitable for high-throughput synthesis, subsequent screening for particular responses or biological screening, and surface-sensitive analytical methods.

Light-triggered material polymerization and degradation is especially important in biological settings, benefiting from non-contact spatially and temporarily controlled manipulation of soft matter. However, the photoresponsiveness of hydrogels is generally not intrinsic and requires complex synthetic procedures wherein photoresponsive crosslinking groups are incorporated into the hydrogel. As mentioned before, PEG-based methacrylates are intrinsically photodegradable, but lack cell adhesion sites and therefore are not suitable for cell encapsulation. The third aim of this PhD work was to develop an intrinsically photodegradable material that can be used to culture cells in 3D for at least 14 days. Combinatorial approach

was employed to find the optimal balance between cell adhesion and photodegradation properties and systematically screen for structure/function relationships. The “hit” composition should be then used to produce an array of free-standing cell-containing hydrogel micropads, as an example of on-demand light-triggered material manipulation.

2. Materials and methods

2.1 Experimental details for Chapter 3

2.1.1 Materials

The glass slides were purchased from Schott Nexterion (Jena, Germany). Ninhydrine, piperidine were purchased from Alfa Aesar (Ward Hill, Massachusetts, USA). 4-Pentynoic acid was purchased from Apollo Scientific (Bredbury, UK). Fmoc-Glu(OtBu)-OH and Fmoc-Gly-OH was purchased from Bachem (Bubendorf, Switzerland). Fmoc-Val-OH, Fmoc-Ala-OH and Fmoc-Leu-OH were purchased from Iris Biotech (Marktredwitz, Germany) and kindly provided by Dr. Parvesh Wadhwani, Institute of Biological Interfaces, KIT**.** Hydrochloric acid (37 %), ethanol, ethanol absolute, acetone, 4-(dimethylamino)pyridine, 4-[4-(1-Hydroxyethyl)-2-methoxy-5-nitrophenoxy]butanoic acid (hydroxyethyl photolinker), pyridine, methanol, *N*,*N*-dimethylformamide, acetic acid anhydride, phenol were purchased from Merck (Darmstadt, Germany). 1-Hydroxybenzotriazole was purchased from Molekula (Newcastle upon Tyne, UK). Sodium hydroxide, 3-(trimethoxysilyl)propyl methacrylate, 2-hydroxyethyl methacrylate, ethylene dimethacrylate, 1-decanol, cyclohexanol, 2,2-dimethoxy-2-phenylacetophenone, 1*H*,1*H*,2*H*,2*H*-perfluorodecanethiole, cysteaminium chloride, potassium cyanide were purchased from Sigma-Aldrich (St. Louis, Missouri, USA). Calcein AM was purchased from Life Technologies GmbH (Darmstadt, Germany), Propidium iodide from Invitrogen (Merelbeke, Belgium).

If not stated differently, all chemicals have been used without further purification.

2.1.2 Functionalization of DMA slide with the linker

The DMA slides were prepared according to the previously published procedure.[94, 102] Briefly, microscope glass slide was coated with a layer of nanoporous poly(2-hydroxyethyl methacrylate-*co*-ethylene dimethacrylate) (HEMA-*co*-EDMA) (using fluorinated glass slide during photopolymerization), taped with sticky film to increase roughness of the surface and subsequently esterified using 4-pentynoic acid. The pattern of repeating superhydrophobic and hydrophilic properties was created by utilizing the corresponding photomask via thiol-yne photoclick reaction using 1*H*,1*H*,2*H*,2*H*-perfluorodecanethiole and cysteaminium chloride or β-mercaptoethanol, respectively. To functionalize the hydrophilic spots with the linker, (4-[4-(1-hydroxyethyl)-2-methoxy-5-nitrophenoxy]butanoic acid), diisopropyl carbodiimide (DIC), 1-hydroxybenzotriazol were mixed in DMF to a final concentration of 0.03 M, 0.3 M and 0.3 M, respectively. In each 2.83 mm spot of the DMA slide functionalized with cysteaminium chloride 10 µL of solution was pipetted and incubated in the dark at room temperature for 18 h (overnight). The DMA slide was then washed with acetone and dried in nitrogen flow. The unreacted amino groups of cysteamine were then capped using a 10%-solution of pyridine in

acetic acid anhydride. In each spot, 10 µL of capping solution was pipetted. After 5 minutes, the DMA slide was washed with acetone and dried in nitrogen flow.

2.1.3 Analytics and reaction monitoring

The static contact angle was measured using Drop Shape Analyzer DSA25 (Krüss, Hamburg, Germany) by applying 50 µL deionized water on a non-functionalized hydrophilic surface and on a hydrophilic surface, functionalized with linker and capped with acetic anhydride.

For reaction monitoring experiments (ATR-IR, ToF-SIMS), several spots of a DMA slide were functionalized with the linker as described above, with different exposure time of the hydrophilic spots to the linker solution (e.g. in the range of 1 h to 18 h). After functionalization with the linker, capping of the unreacted amino groups and thorough washing in acetone and drying in nitrogen flow, the DMA slide was subjected to the respective analytical method. For ToF-SIMS depth profiling, different polymer thicknesses were adjusted during the polymerization process by using Teflon film spacers of 6 and 25 µm thickness. The exact final thickness of the polymer layer was determined by profilometry (Dektak XT Stylus Profiler, Bruker Nano, Karlsruhe, Germany).

XPS measurements were performed on the DMA slide, which was exposed to the linker solution for 18 h.

2.1.3.1 XPS measurements (Vanessa Trouillet, IAM, KIT)

XPS measurements were performed using a K-Alpha+ XPS spectrometer (ThermoFisher Scientific, East Grinstead, UK). Data acquisition and processing using the Thermo Avantage software is described elsewhere.[34] All samples were analyzed using a microfocused, monochromated Al Kα X-ray source (400 µm spot size). The K-Alpha+ charge compensation system was employed during analysis, using electrons of 8 eV energy, and low-energy argon ions to prevent any localized charge build-up. The spectra were fitted with one or more Voigt profiles (BE uncertainty: ± 0.2 eV) and a Shirley background. Scofield sensitivity factors were applied for quantification.[107] All spectra were referenced to the C 1s peak (C-C, C-H) at 285.0 eV binding energy controlled by means of the well-known photoelectron peaks of metallic Cu, Ag, and Au, respectively. The K-alpha+ snapmap option was used to image an area of 3 × 3 mm with an X-ray spot of 200 µm (5 iterations were run to reach a better statistic).

2.1.3.2 ToF-SIMS measurements (Dr. Alexander Welle, IFG, KIT)

ToF-SIMS (Time-of-Flight Secondary Ion Mass Spectrometry) was performed on a TOF.SIMS5 instrument (ION-TOF GmbH, Münster, Germany) equipped with a Bi cluster primary ion source, and argon cluster source for depth profiling, and a reflectron type time-of-

flight analyzer. UHV base pressure was < 10^{-8} mbar. For high mass resolution the Bi source was operated in “high current bunched” mode providing short Bi_3^+ primary ion pulses at 25 keV energy, a lateral resolution of approx. 4 µm, and a target current of 1 pA at 20 kHz repetition rate. The short pulse length of 1.1 ns allowed for high mass resolution. The primary ion beam was rastered across a 500×500 µm² field of view on the sample, and 128×128 data points were recorded. Larger fields of view were recorded by scanning the primary beam and moving the sample stage. Primary ion doses were kept below 10^{11} ions/cm² (static SIMS limit). For charge compensation an electron flood gun providing electrons of 21 eV was applied and the secondary ion reflectron tuned accordingly. Spectra were calibrated on the omnipresent C^-, C_2^-, C_3^-, or on the C^+, CH^+, CH_2^+, and CH_3^+ peaks. Based on these datasets the chemical assignments for characteristic fragments were determined.

For depth profiling a dual beam analysis was performed in non-interlaced mode: The primary ion source was again operated in “high current bunched” mode with a scanned area of 100 × 100 µm² (3 frames with 64×64 data points) and a sputter gun (operated with Ar_{1500}^+ ions, 20 keV, scanned over a concentric field of 300×300 µm, target current 9 nA) was applied to erode the sample followed by a 1.5 s pause for charge compensation. Thereby, the sputter ion dose density was >1000 times higher than the Bi ion dose density. This approach allows the recording of larger molecular fragments, like $C_4H_5O_2^-$ from the base polymer backbone throughout the eroded polymer layer of several µm thickness.

2.1.3.3 FTIR spectroscopy (Stefan Heissler, IFG, KIT)

A Bruker Tensor 27 Fourier transform IR spectrometer (Bruker Optik GmbH, Ettlingen, Germany), was employed to obtain the IR-spectra of the samples.

All samples were measured in attenuated total reflection (ATR) geometry without additional preparation on a Bruker Platinum ATR accessory equipped with a diamond crystal, 45° angle of incidence, one reflection. 4000-370 cm^{-1} spectral range was recorded with a scanner velocity of 10 kHz and a spectral resolution of 4 cm^{-1} (32 scans). The reference spectra were taken from air. All spectra were evaluated using the Bruker OPUS software.

2.1.3.4 Linker loading determination and photorelease kinetic measurements

Two stock solutions have been prepared and stored at 8 °C:

- Solution 1: 40 g phenol (425 mmol) were dissolved in a mixture of 49 mL pyridine and 10 mL ethanol abs. and 1 mL of a 10 mM of aqueous KCN solution was added. Final concentrations were 7.1 M phenol and 0.17 mM KCN.

- Solution 2: 2.5 g ninhydrin (14 mmol) were dissolved in 50 mL ethanol abs. to yield a 281 µM solution

To perform the Kaiser test, the solution 1 was mixed with solution 2 in a 4:1 ratio immediately before the experiment. 10 µL of the mixture were pipetted manually in each spot. As a negative sample, a DMA slide with the same pattern size but with hydrophilic spots functionalized with β-mercaptoethanol instead of cysteamine was treated in the same way. Both samples were heated on a heating plate at 50°C for 5 minutes, the liquid of 2 spots was pipetted off, diluted to 1 mL with a methanol/H_2O (1:1) solution and the absorbance at 570 nm was measured.

To study the photorelease properties of the linker, glycine was attached to the linker, as described below, and then the kinetics of its phototriggered detachment was studied. After UV irradiation (0.5 – 15 min, 9 datapoints), the liquid from two spots was pipetted off and added to a mixture of 100 µL solution 1 and 25 µL solution 2 in a vial. For the negative control, deionized water was used instead of the droplet volume. Both were then heated in a waterbath at 50°C for 5 minutes, diluted to 1 mL with methanol/H_2O (1:1) and measured using LAMBDA™ 35 UV-spectrometer (PerkinEmler, Waltham, Massachusetts, USA). ε = 15700 $L \cdot mol^{-1} \cdot cm^{-1}$ has been used as molar extinction coefficient to calculate the concentration by the Beer-Lamberts law.

2.1.3.5 Fmoc-based peptide synthesis

DMA slide was functionalized with linker as described before. For attaching the first amino acid onto the linker 24 µL of a 0.1 M solution of the corresponding Fmoc protected amino acid in DMF, 8 µL of a 0.1 M solution of 4-DMAP in DMF and 8 µL DIC were premixed in a vial and applied along one row of the DMA slide (4 spots). This was repeated for glycine, valine, alanine and leucine according to the scheme. During the reaction time of 18 hours, the DMA slide was stored in the dark at room temperature. Subsequently, the slide was extensively washed with acetone and immersed in DCM for 1 h. For coupling the following amino acids 24 µL of a 0.1 M solution of the corresponding Fmoc protected amino acid in DMF, 8 µL of 0.3 M solution of 1-HOBt in DMF, 8 µL DIC were premixed in a vial, applied in the same manner according to a scheme along one row of the DMA slide (4 spots) and incubated at room temperature in the dark for 4 hours. Next, the slide was extensively washed with acetone and immersed in DCM for 1 h. The coupling step was repeated two times to obtain a library of 16 tripeptides.

Before each coupling step, the amino acids have to be deprotected. The deprotection of amino group was carried out by immersing the whole slide into a solution of 20% piperidine in DMF for 1 h.

2.1.3.6 Cell viability assays

Four DMA slides were functionalized with linker and capped with acetic anhydride as described above, followed by sterilization by immersing in 70 % ethanol in water for 1 h in dark. Slides were then air-dried for at least 15 minutes. While drying, a 2.2 % (w/v) gelatine solution was prepared by adding 3 mL of sterile cell medium to 66 mg gelatin from bovine skin. To increase the solubility of gelatin, the solution was gently warmed in a waterbath at 37 °C. Once gelatin was completely dissolved, the solution was sterilized by filtering through sterile 0.22 µm filter. The gelatin solution was then applied onto all DMA spots via rolling droplet to produce evenly distributed droplets. The DMA slide was then incubated for 1 h at 37 °C, followed by air drying of gelatin for 1 h. In each spot 8 µL of HEK293T cell suspension ($4.23 \cdot 10^5$ cells/ml) were pipetted, followed by incubation for 3 h at 37 °C. Three slides were illuminated with UV light (364 nm) for 5, 10 and 15 minutes respectively, one slide served as a control. Four slides were incubated overnight at 37°C and stained, using live/dead staining with PI and calcein AM.

2.2 Experimental details for Chapter 4

2.2.1 Materials and reagents

Poly(ethylene glycol)methyl ether methacrylate (*M*n approximately 500 g/mol), poly(ethylene glycol) dimethacrylate (*M*n approximately 750 g/mol), 2-(*N*-3-sulfopropyl-*N*,*N*-dimethyl ammonium)ethyl methacrylate, 2-(dimethylamino)ethyl methacrylate, 2-butanone and D-(+)-glucose were purchased from Sigma–Aldrich (St. Louis, MI, USA). Ethyl (2,4,6-trimethylbenzoyl)phenylphosphinate was purchased from FluoroChem (Hadfield, Derbyshire, UK). Glucose oxidase (from *Aspergillus niger*) was purchased from VWR (Darmstadt, Germany). Sodium iodide was purchased from Fluka (Munich, Germany). DMA glass slides were purchased from Aquarray GmbH (Eggenstein-Leopoldshafen, Germany) and used without further changes.

2.2.2 Synthesis of photo initiator sodium phenyl-2,4,6-trimethylbenzoylphosphinate (SAP)

Ethyl (2,4,6-trimethylbenzoyl)phenylphosphinate (1 g, 0.003 mol) was dissolved in 10 mL 2-butanone. After the addition of sodium iodide (0.6 g, 0.004 mol), the reaction mixture was stirred overnight at 60°C. The precipitate was collected by filtration, washed with 2-butanone and dried. Sodium phenyl-2,4,6-trimethylbenzoylphosphinate (yield: 0.7 g, 79%) was yielded as a white solid. The identity of the product was confirmed by NMR:

*^{1}H-NMR (400 MHz, D_2O): δ/ppm = 7.78-7.48 ($H_{aromatic}$, phenyl), 6.92 (s, $H_{aromatic,}$ benzoyl), 2.27 (s, para-CH_3), 2.06 (s, ortho-CH_3): (***Figure 12***):*

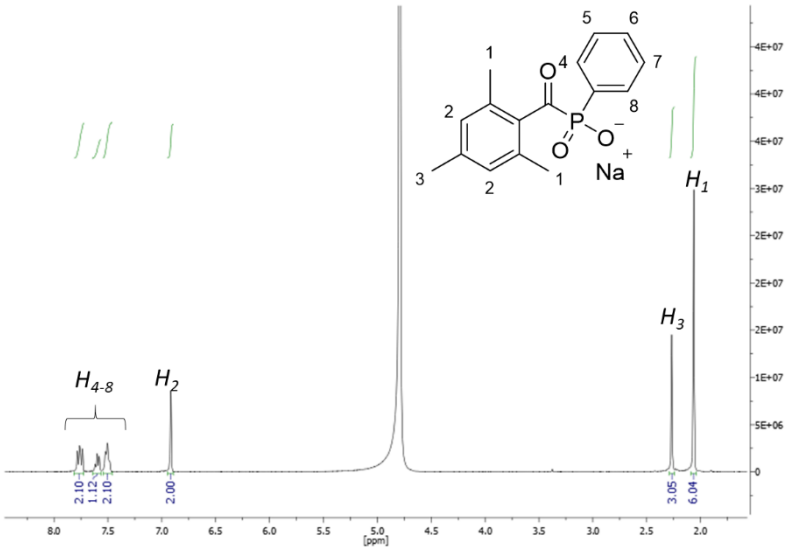

Figure 12. ^{1}H NMR (400 MHz, D_2O) spectrum of sodium phenyl(2,4,6-trimethylbenzoyl)phosphinate

2.2.3 Printing procedures

Monomers were de-inhibited prior to use by passing over a short column of basic aluminum oxide (Alfa Aesar, Ward Hill, MA, USA). All printing experiments were performed using non-contact liquid dispensing technology (Immediate Drop On-Demand technology (I-DOT) liquid dispenser; Dispendix GmbH, Stuttgart, Germany). The viscosity of aqueous monomer stock solutions was adjusted for reproducible printing by non-contact liquid dispensing technology. Printing of solutions was calibrated, allowing precise dosage of solutions in the nanoliter range. The humidity was maintained at 70% during printing.

2.2.4 Confirmation of adequate mixing of components in droplets

Even distribution of two monomers within droplet after printing was confirmed by fluorescence, Raman spectroscopy measurements and multiple particle tracking.

2.2.4.1 Fluorescence measurements

PEGMA solution was supplemented with rhodamine B and the solution of 2-(dimethylamino)ethyl methacrylate (DMAEMA) as an example monomer and the second monomer was supplemented with fluorescein. The solutions of PEGMA, DMAEMA, sodium phenyl-2,4,6-trimethylbenzoylphosphinate (SAP) and PEGDMA (5 mol%) were then printed sequentially in quadruplicate. PEGMA was printed in descending volumes (60 to 10 nL; 12 dilutions), and DMAEMA was printed in ascending volumes (10 to 60 nL; 12 dilutions), and SAP and PEGDMA were printed in constant volumes (30 nL). The homogeneity of fluorescein and rhodamine distribution was assessed qualitatively by fluorescence microscopy (Keyence) and the mean intensity was determined via ImageJ (100 × 100-pixel square sections in the middle of each droplet).

2.2.4.2 Raman spectroscopy measurements (Stefan Heissler, IFG, KIT)

Raman spectroscopy measurements were obtained from a composition comprising 30 nL SAP, 60 nL PEGMA, 10 nL DMAEMA and 30 nLl PEGDMA (5 mol%) with a Bruker Senterra spectrometer (Bruker Optics, Germany). For focusing of the excitation laser and collimation of backscattered light an Olympus MPLAN 20× objective (NA 0.4) was used, resulting in a spot diameter of 5 micron on the sample surface. The excitation laser (λ = 532 nm) was operated at 10 mW output power. Each spectrum was integrated over 60 s with three coadditions (3×20 s). The total number of measurement spots per hydrogel micropad was 144, arranged in a 12×12 matrix. Dr. Richard Thelen (IMT, KIT) performed white light scattering experiments to confirm the 3D form of the hydrogel.

2.2.4.3 Multiple particle tracking (Dr. Claude Oelschlaeger, AME, KIT)

To determine the microrheological properties of the hydrogel, an exemplary composition comprising 30 nL SAP, 60 nL PEGMA, 10 nL DMAEMA and 30 nL PEGDMA (5 mol%) was polymerized. SAP solution contained glucose oxidase and glucose and was further supplemented with green fluorescent polystyrene microspheres of diameter 0.5 µm (Bangs Laboratories, USA) as tracers, from which the Brownian motion was tracked. Then the resulting particle trajectories were transformed into mean square displacement (MSD) traces and quantitative information about the rheological properties were obtained based on a relation between the MSD $\langle \Delta r^2(\tau) \rangle$ as a function of lag time τ and the macroscopic complex shear modulus G*(ω) as a function of the frequency ω.[28] The Laplace transform of the particle MSD $\langle \Delta \tilde{r}^2(\mathrm{i}\omega) \rangle$ is related to the complex modulus G* of the sample via a generalized Stokes–Einstein equation (GSE)[29]

$$G^*(\omega) = \frac{k_B T}{\pi a i\omega \langle \Delta \tilde{r}^2(\mathrm{i}\omega) \rangle} = G'(\omega) + iG''(\omega) ,$$

where a is the radius of the embedded beads, k_B is the Boltzmann constant and T is the temperature. Additionally, to perform the statistical analysis and characterize the microstructure heterogeneity, we examined the distribution of displacements (Van Hove correlation function) and calculated[26] the non-Gaussian parameter α:

$$\alpha = \frac{\langle x^4(\tau)\rangle}{3\langle x^2(\tau)\rangle^2} - 1$$

This parameter is zero for a Gaussian distribution, expected for a homogeneous, uniform sample, while deviations from this distribution result in large α values, reflecting the presence of heterogeneities.

The experimental setup was based on an inverted fluorescence microscope (Axio Observer D1, Carl Zeiss, Germany) equipped with a Fluar 100× objective (numerical aperture 1.3, 100× magnification, oil immersion lens). Two-dimensional (2D) images (field of view 127 × 127 µm, frame rate 50 f/s) of these fluorescent beads were recorded using a sCMOS camera Zyla X (Andor Technology). The videos of the fluctuating microspheres were analyzed using the software Image Processing System (iPS, Visiometrics, Germany) and a self-written Matlab code,[30] based on the widely used Crocker and Grier tracking algorithm.[31]

2.2.5 Confinement studies

Due to compartmentalization, different volumes of precursors can be deposited onto hydrophilic pattern of the DMA. To highlight this fact, 240 resp. 120 nl of prepolymerization mixture were printed onto the 1 x 1 mm patterned DMA, subsequently polymerized and incubatied in rhodamine B solution for better visualization. In addition, 40 nL of prepolymerization mixture was deposited onto the 500 x 500 µm patterned DMA, subsequently polymerized and incubatied in rhodamine B solution for better visualization.

To show the possibility of cell encapsulation within the hydrogels, a suspension of HeLa cells (10 nL, $5{\cdot}10^6$ cells/ml) was printed directly after the hydrogel precursors. After the polymerization (360 nm, 6 mW/cm^2, 10 min) cells were stained with 1 µg ml^{-1} *Hoechst* 33342 by immersing the DMA slide in the *Hoechst* stain solution for 20 min.

2.2.6 Construction of libraries

For optimization of the degassing procedure, a 36-member DMAEMA/PEGMA library (ratios varying from 6:1 to 1:6) with 2.5, 5.0 and 10.0 mol% PEGDMA was synthesized in quadruplicates. We varied the GOx concentration from 1 µM to 40 µM. After the polymerization and incubation in rhodamine B solution, the hydrogel widths were measured manually. After optimization, a typical printing procedure was performed using SAP solutions supplemented with glucose oxidase (40 µM) and glucose (0.1 M) and glucose oxidase solution being freshly

prepared for every experiment, SAP/glucose oxidase/glucose solution being freshly prepared immediately before printing. All solutions were prepared with PBS and reactions were typically performed at room temperature.

In a typical printing procedure, hydrogel libraries were printed as follows: printing of 30 nL SAP (2.6 mg/ml in PBS) supplemented with glucose oxidase and glucose; overprinting with PEGMA (40 wt% in PBS) with the volume descending from 60 to 10 nL per spot; overprinting with 30 nL PEGDMA (e.g. 77,3 mg/ml in PBS for 5 mol% w.r.t. monomers), overprinting with SAMA (230 mg/ml in PBS) with the volume ascending from 10 to 60 nL per spot. To prevent evaporation, humidifying rows consisting of only 130 nL PBS per spot were printed so that each spot containing prepolymerization mixture was surrounded either by another prepolymerization mixture spot or by PBS spot. The DMA produced in this way was irradiated for 10 minutes at 6 mW/cm^2 in a closed petri-dish containing cellulose pads soaked in water to provide a humid environment and washed with PBS. Some starting material combinations could not be polymerized due to both low crosslinker and PEGMA concentration and were not considered further. All degradation studies were carried out using 270 nm UV light source (UVACUBE 2000, Dr. Hönle AG, Gräfelfing, Germany) with irradiance of 22 mW/cm^2.

2.3 Experimental details for Chapter 5

2.3.1 Materials

Lithium phenyl(2,4,6-trimethylbenzoyl)phosphinate (LAP) was purchased from TCI Chemicals Deutschland (Eschborn, Germany). Dulbecco's phosphate buffered saline (DPBS), Dulbecco's modified Eagle medium (DMEM), fetal calf serum (FCS), penicillin-streptomycin, and calcein-AM were purchased from Gibco® life technologies (Carlsbad, USA). The CellTiter 96® non-radioactive cell proliferation assay (MTT) was purchased from Promega GmbH (Mannheim, Germany). Dialysis tubes (MWCO *12-14* kDa) were obtained from VWR International GmbH (Darmstadt, Germany). All other chemicals were purchased from Sigma-Aldrich Chemie (Steinheim, Deutschland). Normal human dermal fibroblasts (NHDF) and HeLa cells were purchased from PromoCell GmbH (Heidelberg, Germany).

2.3.2 Nuclear magnetic resonance (NMR) spectroscopy (Tobias Göckler, IFG, KIT)

Nuclear magnetic resonance (NMR) measurements were performed using a 400 MHz NMR spectrometer (AVANCE 400; Bruker, Rheinstetten, Germany). Chemical shifts are given in parts per million (δ/ppm) downfield from tetramethylsilane (TMS) and referenced to D_2O (4.80 ppm) as internal standard. In the description of signals, s = singlet and bs = broad singlet. ^{1}H NMR spectra of gelatin and GelMA were recorded at a temperature of 315 K to avoid gelation of the sample during the measurement.

2.3.3 Synthesis of water-soluble photoinitiator (please refer to Chapter 2.2.2)

2.3.4 Synthesis of gelatin methacrylate (GelMA) (Tobias Göckler, IFG, KIT)

The synthesis and purification of gelatin methacrylate (GelMA) was performed as previously described in literature.[108-109] In brief, 1 g gelatin (type A, gel strength ~300 g bloom, 0.266 mmol NH_2 groups, 1 eq) was dissolved in 10 mL DPBS, and the solution was heated to 50 °C. After complete dissolution of gelatin, 39.6 µL methacrylic anhydride (0.266 mmol, 1 eq) was added dropwise and the reaction mixture was stirred at 50 °C for 2 h. Next, the solution was diluted with 10 mL dH_2O, transferred into dialysis tubes (MWCO: 14 kDa), and dialyzed against dH_2O at 40 °C for 7 days. The purified solution was frozen at −80 °C and lyophilized (Lyophilisator Christ Aplha 1-4, Christ Gefriertrocknungsanlagen GmbH (Osterode am Harz, Germany). The product was obtained as a white solid and stored at −20°C. GelMA with various degrees of modification (low, medium, or high) was obtained by varying the amount of methacrylic anhydride (1 eq, 8 eq, 30 eq referred to NH_2 groups in gelatin).
^{1}H-NMR (400 MHz, D_2O): δ/ppm = 7.46-7.22 ($H_{aromtic}$, gelatin), 5.73 ($H_{vinyl,a}$), 5.48 ($H_{vinyl,b}$), 5.08-0.83 (gelatin), 3.04 (bs, NH_2), 1.95 (s, CH_3) **(Figure 13 A,C).**

2.3.5 2,4,6-trinitrobenzene sulfonic acid (TNBSA) assay (Tobias Göckler, IFG, KIT)

The percentage of modified free amino groups in GelMA was determined colorimetrically via TNBSA assay. The TNBSA assay was performed according to an established protocol using protein solutions of 500 µg mL^{-1} gelatin and GelMA (low, medium, or high), respectively.[109] For each blank, the protein solutions were first mixed with HCl before adding the TNBSA reagent. The absorption of each sample was measured at 335 nm (SmartSpec 3000; Bio-Rad Laboratories GmbH (Munich, Germany); all measurements were performed in triplicate. The degree of functionalization (DoF) was derived from the ratio of the absorption values of functionalized and non-functionalized gelatin (**Figure 13 B**)

$$\text{DoF}\ [\%] = \left(1 - \frac{\text{A (GelMA)}}{\text{A (gelatin)}}\right) \times 100\%$$

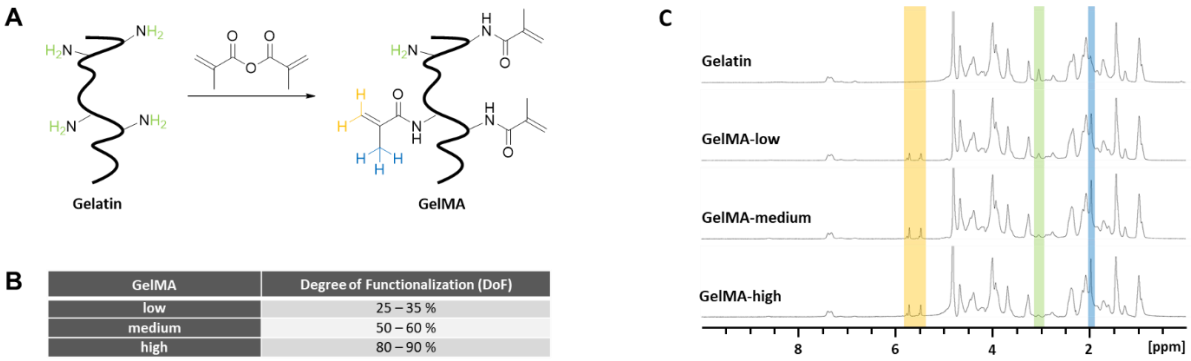

GelMA	Degree of Functionalization (DoF)
low	25 – 35 %
medium	50 – 60 %
high	80 – 90 %

Figure 13. (A) Chemical modification of gelatin to GelMA. (B) Degree of Functionalization (DoF) determined by TNBSA Assay. (C) ^{1}H NMR (400 MHz, D_2O, 315 K) spectra of unmodified gelatin and GelMA of different DoF (Low, Medium, High).

2.3.6 Combinatorial library synthesis

Monomers were de-inhibited prior to use by passing over a short column of basic aluminum oxide from Alfa Aesar (Ward Hill, Massachusetts, USA). Each prepolymerization mixture according to the scheme (240 µL) was deposited into a silicone mold (14 x 5 x 3 mm) and subsequently photopolymerized with UV light (360 nm, 6 mW/cm^2) for 2 min. The photodegradation of each hydrogel was assessed by weighting the hydrogel before and after irradiation under UV light (270 nm, 22 mW/cm^2); excess released liquid was removed prior to weighting.

2.3.7 Cell encapsulation and long-term cultivation

NHDF (used between passage 6 and 8) and HeLa cells were suspended in either PEG or corresponding gelatin containing precursor solutions with 0.3% (w/v) LAP. To reduce harmful exposure of uncrosslinked PEGDMA and PEGMA monomers, cells were added last with a final cell density of 2.5 × 10^6 cells mL^{-1} followed by immediate photocuring. Hydrogel formation and cell encapsulation were induced by exposure to long-wave UV light (360 nm, 6 mW/cm^2, 2 min) and performed in a µ-slide 8 well (ibidi, Martinsried, Germany). Hydrogels had a volume of 200 µL and were covered with 200 µL DMEM after photopolymerization. Entrapped cells were cultured in DMEM with 10% FCSand 1% penicillin-streptomycin for 14 days (37 °C, 5% CO_2). The cell culture medium was refreshed every 2-3 days.

2.3.8 UV photodegradation

Cell-laden gelatin-PEG hydrogel solutions were prepared as described previously in this section. Hydrogels were produced by casting 1 mL of the precursor solution against a Teflon mold (37.6 x 13.8 x 3 mm), followed by immediate photocuring. The hydrogel films were subsequently released from the Teflon mold, transferred into a Petri dish, and swollen overnight in DMEM. To ensure rapid UV photodegradation, FCS had to be removed using one of the following methods: (a) exchanging DMEM against DPBS for 3 h; (b) exchanging DMEM against FCS-free DMEM for 3 h; or (c) swelling the hydrogels overnight in FCS-free DMEM. The photodegradation process was induced by irradiation at 270 nm for 10 min at 22 mW/cm^2. Patterning of the hydrogels was performed using a quartz-chromium photomask. After UV degradation, the hydrogels were transferred back into Petri dishes and cultured overnight in DMEM supplemented with FCS (37 °C, 5% CO_2).

2.3.9 Live/dead staining (Tobias Göckler, IFG, KIT)

Cell viability of encapsulated NHDF and HeLa cells within the hydrogel was monitored using live/dead staining with calcein-AM and propidium iodide. Staining was performed after 1 day, 7 days, and 14 days of cultivation for NHDF and on day 1 post-photodegradation for HeLa cells. The supernatant cell culture medium was removed before hydrogels were stained with calcein-AM (4 ng mL^{-1}) and propidium iodide (20 ng mL^{-1}). The staining solution was removed after 20 min incubation. The hydrogels were then washed several times with DPBS and covered with DMEM. A confocal microscope (Leica TCS SPE) was used to visualize z-stacks of approximately 300 µm thickness (step size: 5 µm) per sample, which were converted into 3D images using Leica LAS X software.

3. High-Throughput Combinatorial Synthesis of Small molecules[2]

3.1 Introduction

The process of drug discovery classically includes individual synthesis and characterisation of drug candidates, followed by a biological screening, which is separated from synthesis in space and time. This approach suffers from low throughput and associated high costs, which in turn lead to inefficiency in the field of drug discovery. Droplet microarray (DMA) platform aims to solve these problems. It comprises a pattern of hydrophilic compartments, surrounded by superhydrophobic borders. Due to extreme differences in wettability, these hydrophilic spots provide confined microenvironment and can accommodate both solutions of drug candidates and cell suspensions. Two drug library-screening approaches were previously validated.[92, 102] In order to harness the power of combinatorial chemistry and eliminate the necessity of purchasing compounds, chemBIOS workflow for liquid-phase synthesis was established.[104] However, in all three approaches, the screening is started as soon as cells get in contact with printed compounds and in all droplets simultaneously for sandwiching approaches, thus the spatiotemporal control is limited. In addition, liquid-phase synthesis often requires tedious purification steps, impairing the simplicity of the synthetic procedure. Therefore, in order to give more control over time and position where the screening is performed, as well as to eliminate the purification steps, a miniaturized platform combining combinatorial solid-phase synthesis with high-throughput cell screenings is highly anticipated.

In this chapter, the chemBIOS method combining both chemical solid-phase synthesis and biological screening on the same chip has been demonstrated. The nanoporous poly(2-hydroxyethyl methacrylate-*co*-ethylene dimethacrylate) inside the hydrophilic spots was used as a support to conduct solid-phase synthesis. The hydrophilic spots were filled with droplets containing either reagents for synthesis or live cells. Due to compartmentalization, each droplet served both as a separate reaction compartment and as a microreservoir for culturing cells, rendering library transfer step redundant and enabling high spatial control. The light-induced release of the products, based on installation of photocleavable solid-phase bound linker, allowed controlling the release also temporally and quantitatively. Upon irradiation with UV-light, products of solid-phase synthesis were released from the porous polymer and diffuse into separate droplets. The quantitative control over the concentration of the final drug in separated individual droplet compartments by changing the irradiation time was demonstrated. Since standard methods to control the course of liquid-phase chemistry reactions such as thin

[2]This chapter is adapted from the following publication: **Alisa Rosenfeld**; Marius Brehm; Alexander Welle; Vanessa Trouillet; Stefan Heissler; Maximilian Benz; Pavel A. Levkin. Solid-phase combinatorial synthesis using microarrays of microcompartments with light-induced on-chip cell screening. *Materials Today Bio*. **2019**, 3, 100022. Marius Brehm performed the kinetic measurement of linker cleavage as well as compound library synthesis.

layer chromatography (TLC) and nuclear magnetic resonance (NMR) spectroscopy cannot be trivially transferred to a miniaturized solid-phase synthesis, attenuated total reflection infrared spectroscopy (ATR-IR), Time-of-flight Secondary-Ion Mass Spectrometry (ToF-SIMS), and X-ray photoelectron spectroscopy (XPS) were used to monitor the reaction on DMA. These methods were used to follow the course of linker attachment onto the solid phase. In order to demonstrate the usability of the platform for chemical synthesis, the confinement within single hydrophilic spots and their sealing with superhydrophobic borders were demonstrated. Also, a peptide synthesis was implemented as a model reaction to create an exemplary chemical library. Finally, high cell viability after UV-triggered small molecule release was proved and highlighted the convenience and future potential of the chemBIOS method.

3.2 Results and discussion

3.2.1 Linker choice and its installation onto the DMA

In order to integrate solid-phase synthesis into the chemBIOS workflow, both suitable anchoring strategy to the solid phase and cleavage strategy from the solid-state were identified, resulting in installation of an *o*-nitrobenzene-based [4-(1-hydroxyethyl)-2-methoxy-5-nitrophenoxy]-butanoic acid as the photocleavable linker[110]:

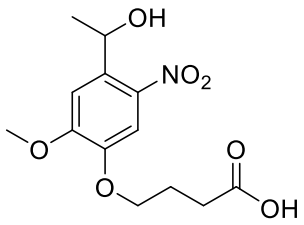

Figure 14. The chemical structure of the nitrobenzene-based photocleavable linker

Photolytic cleavage of small molecules from the solid phase offers several crucial advantages over the chemical one.[111] Photolabile linkers can only be cleaved upon exposure to the light, which broadens the scope of reactions that can be employed in small molecule synthesis in comparison to chemically cleavable linkers, which can be cleaved e.g. under acidic conditions. Another important factor is the non-contaminant and noncontact nature of light. It is critical if small molecules released from the solid phase are directly used in biological assays.[93] The cleavage upon light irradiation also has higher spatial and temporal resolution than chemical one, which is essential for screening applications. Furthermore, the intensity and wavelength of light as well as duration of illumination can be adjusted and controlled, which enables facile fine-tuning of releasing properties. This linker releases acids by UV-irradiation at 364 nm, which has been proven not to affect cell viability.[112-113] The side product of cleavage remains bound to the solid phase. The mechanism of the cleavage is depicted in **Figure 15.**

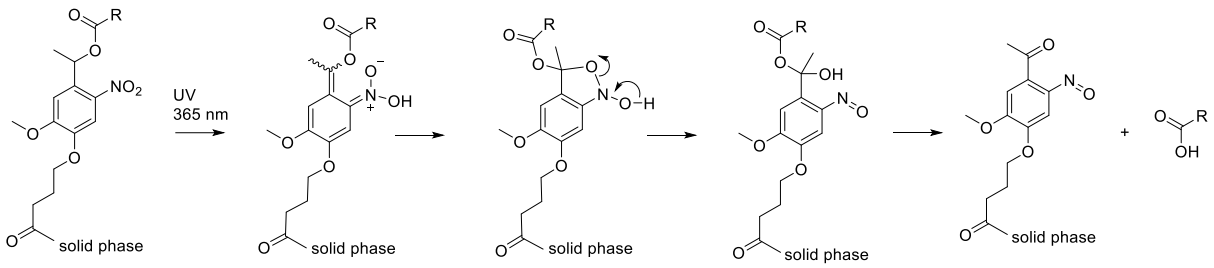

Figure 15. The mechanism of photolytical cleavage of the linker.[111]

This linker also met the selection criteria for the linker attachment onto the solid phase. These included a facile one-step reaction with amino groups of the hydrophilic spots and formation of a less reactive bond between the solid phase and the linker. This was important in order to prevent linker leakage into the droplets during further reactions. Therefore, in order to render the hydrophilic spots of DMA suitable for solid-phase synthesis, linker carrying carboxylic group was anchored to the polymer layer of DMA slide as an amide in a simple one-step reaction **(Figure 16).** Each pentynoic acid tethered to the HEMA-*co*-EDMA polymer layer acts as a branching point, bears two linker molecules, and thus doubles the overall number of reaction sites**:**

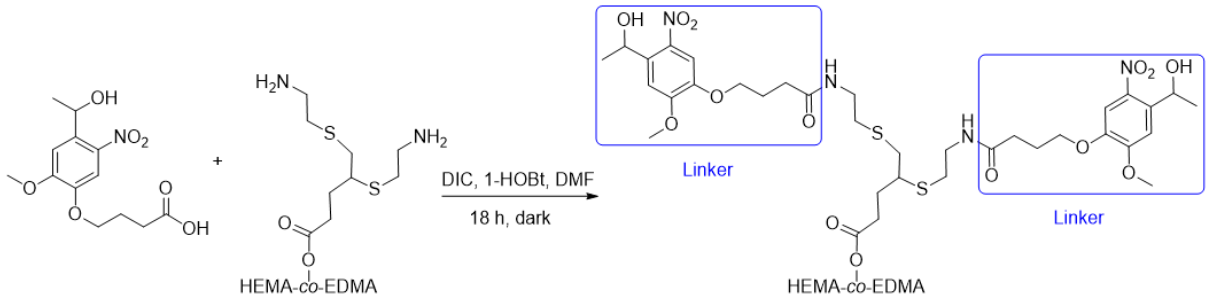

Figure 16. Reaction scheme for attachment of the linker onto the solid phase.

Due to compartmentalization of DMF of DMA, this reaction was in droplets, by pipetting 10 µL of linker-containing solution into each hydrophilic spot. In the next step, the unreacted amino groups were inactivated by formation of an amide with acetic acid anhydride and pyridine as an acid scavenger:

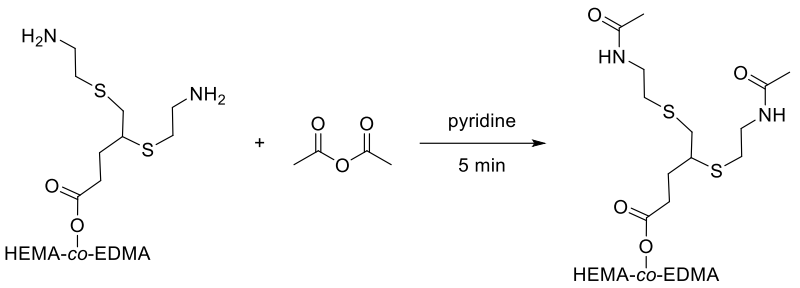

Figure 17. Reaction scheme for capping of unreacted amino groups with acetic acid anhydride.

This reaction was performed by immersing the whole DMA slide into the acetic acid/pyridine solution for 5 minutes. Spots functionalized with the linker and capped with acetic acid anhydride stay hydrophilic, with predictably elevated static WCA of 29±1° in comparison to the non-functionalized spot (static WCA = 4.4°). After capping, the linker content on the surface was determined spectrophotometrically by the Kaiser test[114] to be 1.63 nmol/mm².

3.2.2 Kinetics of linker cleavage

In order to demonstrate the quantitative control over the concentration of the final drug in separated individual droplet compartments, the concentration of a photoreleased compound in the droplet was measured upon exposure to the UV light after distinct time periods. Glycine was used as a model compound and was attached, deprotected and photoreleased as following:

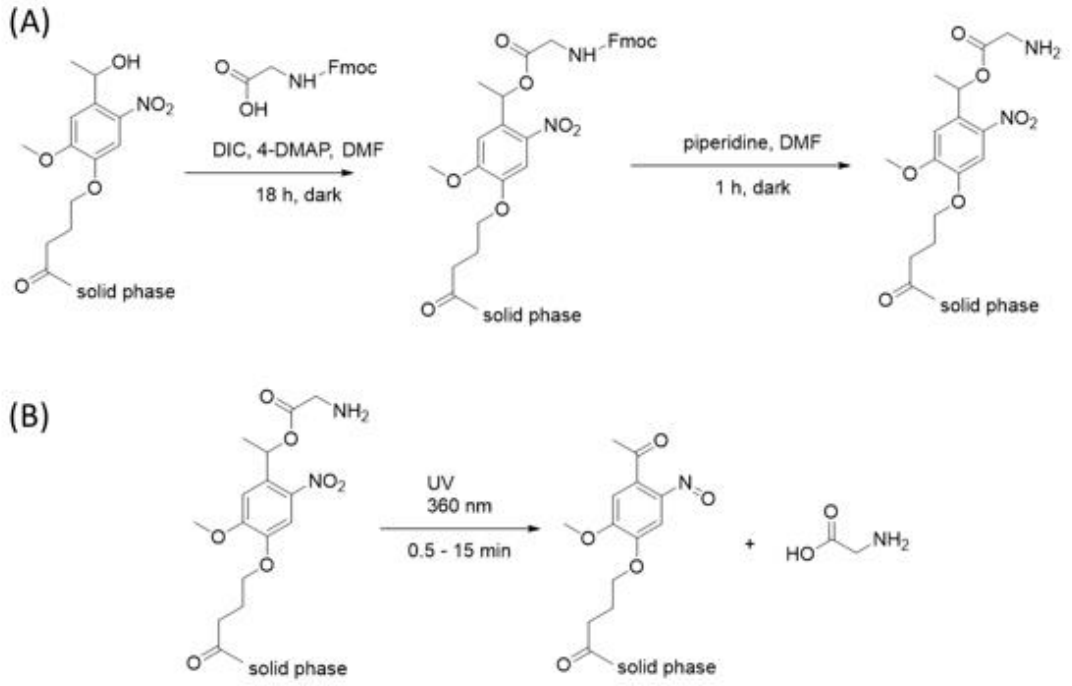

Figure 18. Reaction scheme of (A) attachment of Fmoc-protected glycine to the solid-phase bound linker and subsequent deprotection; (B) photoinduced glycine release from the solid phase.

The concentration of glycine photoreleased after UV irradiation was determined spectrophotometrically via Kaiser test for all irradiation times. The concentration of glycine in the droplet was calculated and plotted against the irradiation time, yielding the release curve:

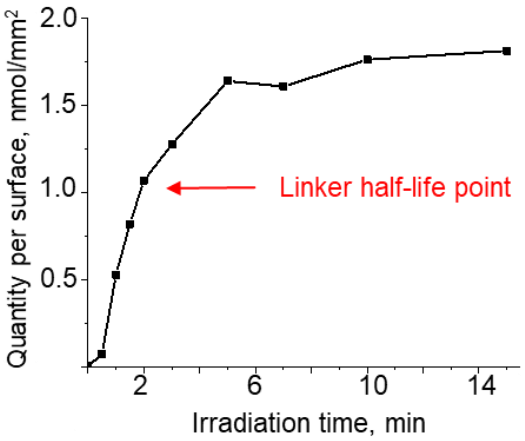

Figure 19. The release curve, depicting phototriggered release of glycine from the surface after different irradiation times, expressed in nmol of glycin per mm^2 of linker-functionalized surface. The amount of released glycine was measured by the Kaiser test.

Therefore, it was proved, that the amount of released glycine can be controlled by varying the exposure time, thus emphasizing not only the temporal control (flexibly selectable starting time)

of the release, but also quantitatively controlling the released amount. The linker half-life (time, at which half of the molecules attached to the linker are cleaved) under UV exposure was measured to be around 2 minutes. The rapid photolytic cleavage of the linker in aqueous environment is important for the application of UV-induced drug release process under biologically relevant conditions. The half-life value is comparable with literature known values for photolysis in liquid phase.[110] The DMA slide, therefore, does not suffer from typical obstacles of resin-bound photolabile linkers, like swelling of resin or light scattering, shadowing and shielding effects, which would increase the half-life of the linker.[110] Complete cleavage was achieved after 15 minutes of UV irradiation (**Figure 19**), which is six times faster than in a comparable SPOT-system, requiring dry cleavage.[115]

3.2.3 Reaction monitoring on DMA

For reaction monitoring experiments (ATR-IR, ToF-SIMS), several spots of a DMA slide were functionalized with the linker as described above, with different exposure time of the hydrophilic spots to the linker solution (e.g. in the range of 1 h to 18 h). After functionalization with the linker, capping of the unreacted amino groups and thorough washing in acetone and drying in nitrogen flow, the DMA slide was subjected to the respective analytical method. Surface sensitive analytical techniques attenuated total reflection infrared spectroscopy (ATR-IR), Time-of-flight Secondary-Ion Mass Spectrometry (ToF-SIMS), and X-ray photoelectron spectroscopy (XPS) were used to monitor the reaction on DMA.

3.2.3.1 ATR-IR measurements for reaction monitoring

ATR-IR spectral data were collected for hydrophilic spots before incubation with linker and after incubation with linker for 1h and overnight. Incubation of a hydrophilic spot with a 0.03 M linker solution, supplemented with 0.3 M diisopropyl carbodiimide and 0.3 M 1-hydroxybenzotriazol, for 1 h led to the emergence of two new signals in IR spectra that could be assigned to the introduced nitro group (1518 cm^{-1} for N-O asymmetric vibration and 1336 cm^{-1} for N-O symmetric stretch).[116] The intensity of these characteristic signals increased as the reaction proceeds overnight (**Figure 20**):

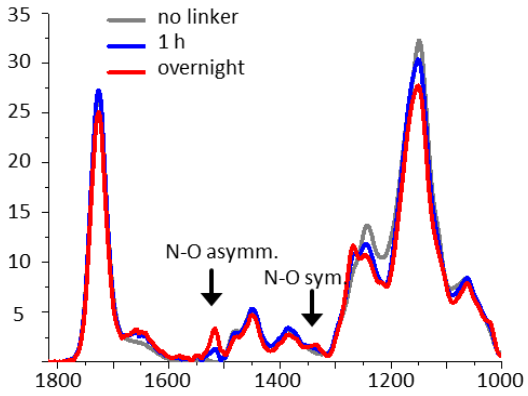

Figure 20. ATR-IR measurements of hydrophilic spots incubated with the linker solution for different periods of time.

3.2.3.2 XPS measurements for reaction monitoring

XPS measurements were performed on the spot before and after incubation with 0.03 M linker solution, supplemented with 0.3 M diisopropyl carbodiimide and 0.3 M 1-hydroxybenzotriazol for 18 h (**Figure 21**). Before incubation, the N 1s XP spectrum indicated the presence of cysteamine with a component at 399.2 eV and a protonated form with a peak at 401.4 eV. After incubation with linker solution (**Figure 21, line 2**), the signal at 399.2 eV is shifted to 399.8 eV, proving the emergence of amide groups. An additional signal at 406.0 eV indicates the presence of the linker nitro group, thus revealing the successful attachment of the linker to the solid phase.

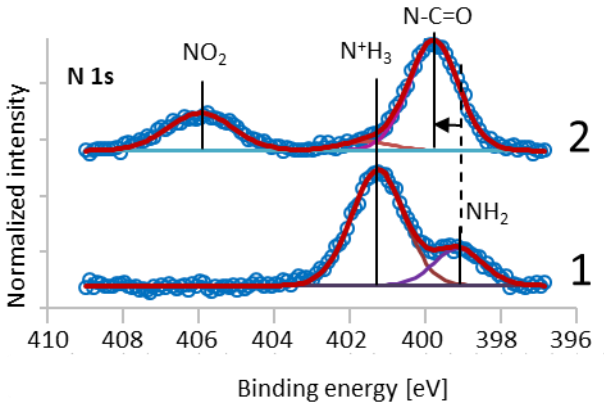

Figure 21. N 1s XP spectra before (1) and after (2) functionalization with the linker.

3.2.3.3 ToF-SIMS measurements for reaction monitoring

In order to investigate the kinetics of linker immobilization as well as the loading of the linker as a function of polymer thickness, ToF-SIMS measurements of polymer substrates with different polymer thicknesses and different linker incubation time were conducted. Despite the semi-quantitative nature of ToF-SIMS, the relative intensity change of respective ions provides useful information about the kinetics of the reaction. A clear trend of NO_2^- intensity changing can be observed for different linker incubation times (**Figure 22**):

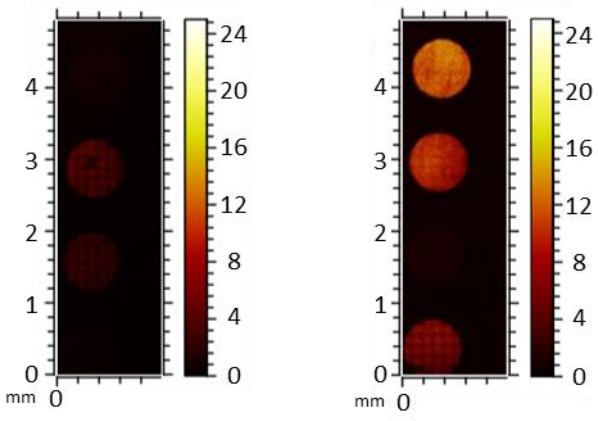

Figure 22. ToF-SIMS stage scans for NO_2^- signals of hydrophilic spots reacted with the linker solution for different periods of time (from top to bottom, left: no linker, 2h, 1h, no linker; right: 18h, 6h, no linker, 3h).

Therefore, to achieve complete loading, it is important to incubate DMA slide with linker solution overnight. Another important finding was that no NO_2^- signal was detected on spots without linker. This means that compartmentalization of liquids within DMA works well and each spot serves as a confined microreactor with no evidence of cross contamination.

The big surface area of the porous polymer layer (9 m^2/g) provides numerous accessible reaction sites, while the permeability enables diffusion of chemicals, so the linker can react throughout the polymer layer and not only on the topmost surface. Therefore, it is important to prove, whether the distribution of the linker is even throughout the whole polymer layer, to take advantage of its whole volume. In addition, the incubation time with the linker solution has to be adjusted to ensure maximal loading. The distribution of the linker (loading of the linker as a function of polymer thickness and incubation time) was determined via depth profiling via dynamic SIMS under argon cluster erosion after incubation of hydrophilic spots of different thicknesses (6 and 26 µm) for different times (1-18 h). Typically, DMA comprises a glass slide with a polymer layer of 6 µm. If linker solution is incubated on hydrophilic spots overnight, the distribution of the linker in 6 µm thick polymer is uniform (**Figure 23**):

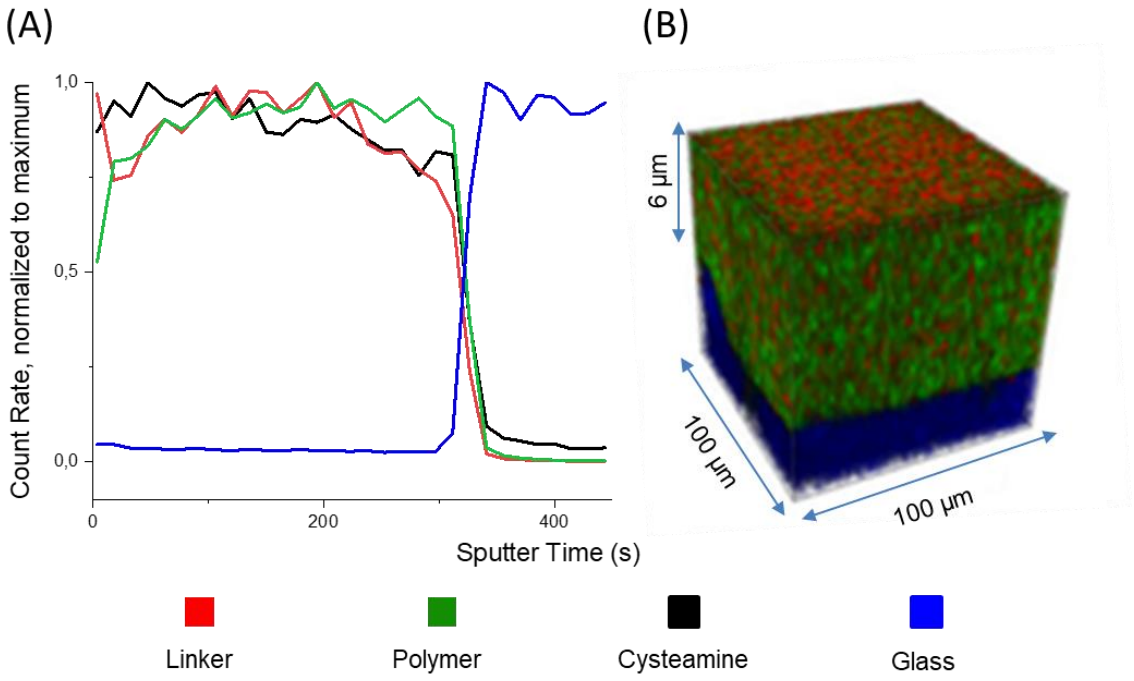

Figure 23. ToF-SIMS characterization of 6 µm polymer layer loaded with linker. A) ToF-SIMS depth profile for 6 µm thick polymer layer incubated with linker solution overnight. Signals for cysteamine (characterized by CN^-, black) and linker (characterized by NO_2^-, red) have the same intensity throughout the polymer layer (characterized by $C_4H_5O_2^-$, green). The linker is uniformly distributed. Glass substrate signals are characterized by SiO_2^-, SiO_3^-, and SiO_3H^-, blue; B) 3D rendering of ToF-SIMS depth profile for 6 µm thick polymer film; X-Y-Dimensions are 100x100 µm, Z-Dimension is 6 µm.

However, hydrophilic spots patterned on thicker polymer layers (26 µm), incubated with linker solution overnight, show a gradient of uniformly decreasing amount of linker towards the surface opposite of irradiation according to the NO_2^- -signal in ToF-SIMS **(Figure 24 A**). This finding can be attributed to the decreasing amount of the cysteamine (CN^--signal in ToF-SIMS), onto which the linker is covalently attached.

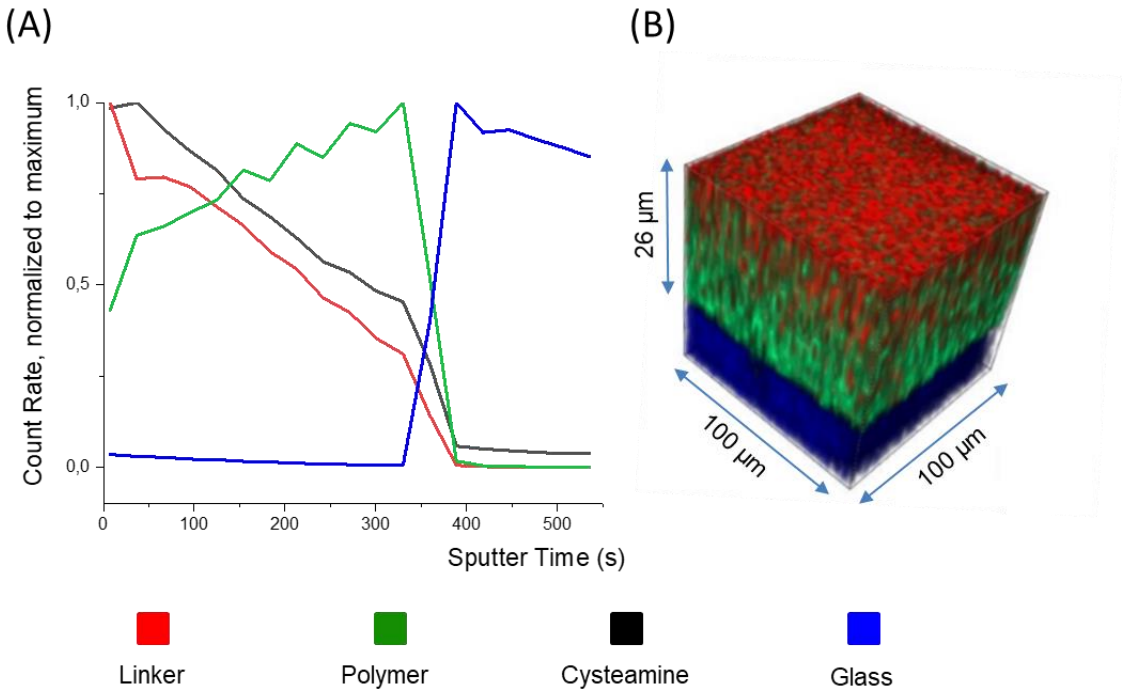

Figure 24. ToF-SIMS characterization of 26 µm polymer layer loaded with linker. A) ToF-SIMS depth profile for 26 µm thick polymer layer incubated with linker solution overnight. Signals for cysteamine (characterized by CN^-, black) and linker (characterized by NO_2^-, red) decrease throughout the polymer layer (characterized by $C_4H_5O_2^-$, green) towards glass substrate. The linker is not distributed uniformly. Glass substrate signals are characterized by SiO_2^-, SiO_3^-, and SiO_3H^-, blue; B) 3D rendering of ToF-SIMS depth profile for 26 µm thick polymer film; X-Y-Dimensions are 100x100 µm, Z-Dimension is 26 µm.

The signal of the linker decreased even faster for shorter incubation times (**Figure 25)**. Despite uneven distribution of the linker in the 26 µm thick polymer, the depth integrated signals of linker are the highest for the sample, which was produced by incubating the hydrophilic spots with linker solution overnight. The signals decrease simultaneously with the incubation time, which again stressed the importance of incubation of hydrophilic spots with linker solution overnight (**Figure 25**).

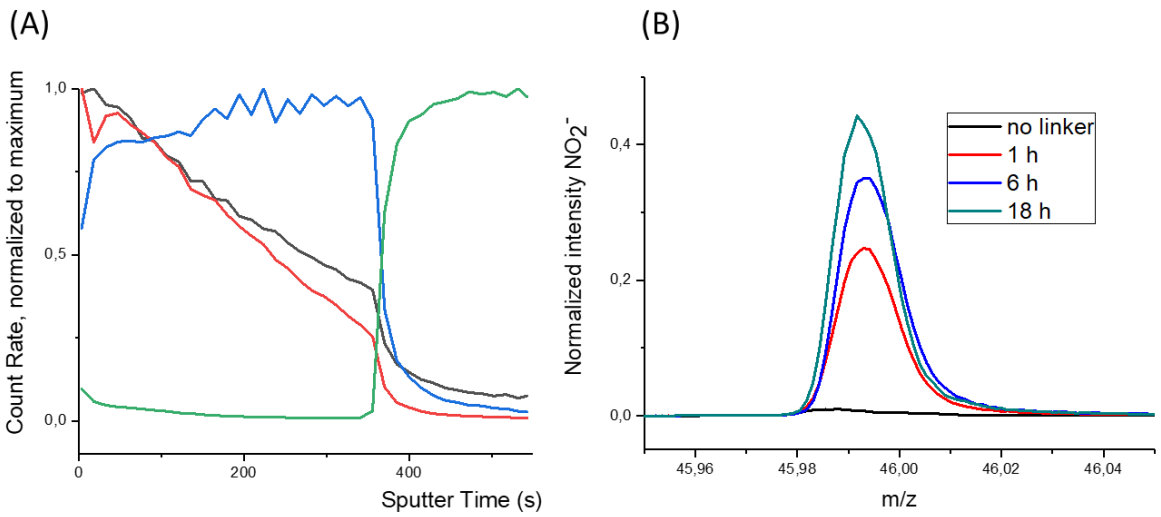

Figure 25. A) ToF-SIMS depth profile for 26 µm thick polymer layer incubated with linker solution for 6 h. Signals for cysteamine and linker decrease nonuniformly towards glass slide. B) Depth integrated NO_2^- signals for different incubation times with linker solution, obtained by dynamic SIMS under argon cluster erosion, normalized versus polymer signal $C_4H_5O_2^-$ to compensate for thickness differences.

Later, the slides with 6 µm thick polymer layer were used, and overnight incubation with linker solution was utilized to ensure maximal loading.

3.2.3 Confinement on DMA

The confinement of solution is an essential prerequisite for using hydrophilic spots as distinct microreservoirs without cross contamination between the individual spots. I have proved the confinement of solutions in the bulk of polymer as well as on top of the slide by XPS (**Figure 26** representing area between the spots) and depth profiling via ToF-SIMS (**Figure 27**, cut-out of the spot incl. surrounding). The linker-containing liquid could wet only hydrophilic spots, so the linker was attached only to the cysteamine of the hydrophilic spots, as seen from the intensity of combined N 1s signals of amide and nitro groups (referred to the presence of linker inside the hydrophilic spots; **Figure 26 A**).

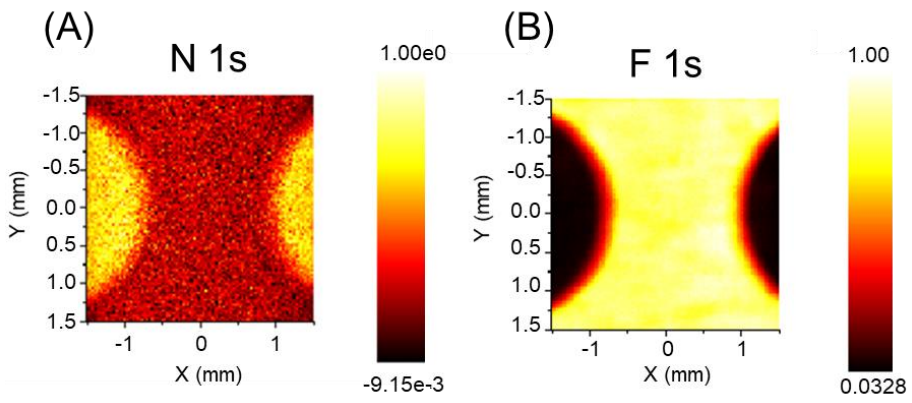

Figure 26. XPS image of the area between spots depicting (A) the abundance of nitrogen inside the spots (assigned to the amide and nitro group, N 1s, 400.2 and 406.0 eV respectively); (B) the abundance of fluorine outside the spots (assigned to the fluorine, F 1s, 689.0 eV).

XPS image of the area between spots, on the other hand, depicts the high abundance of fluorine (right image, assigned to the fluorine, F 1s, 689.0 eV). The ToF-SIMS assisted depth profiling of the interface area of the spot and the surrounding has shown NO_2^- signal only inside the spots, and F^- signal outside the spots. No NO_2^- signal was found within fluorinated borders, implying that linker-containing solution could not penetrate the fluorinated boarders, confirming the fluorinated borders seal the spot securely from the surrounding in the bulk of polymer (**Figure 27**):

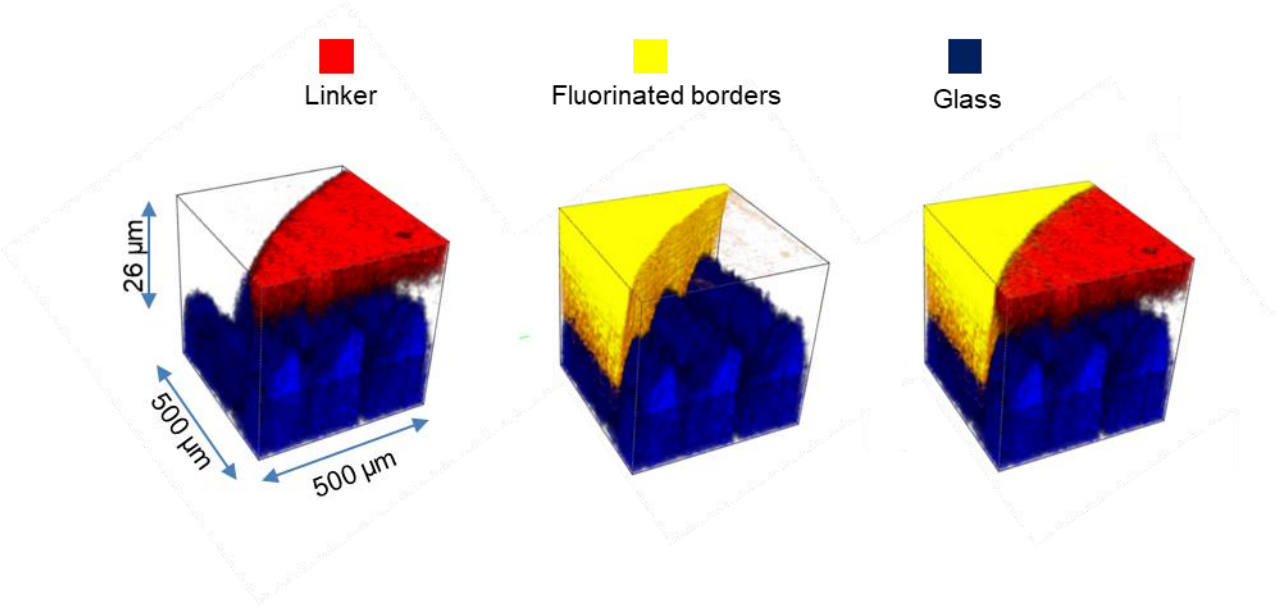

Figure 27. 3D rendering of ToF-SIMS depth profiles; linker, characterized by NO_2^- (red), fluorinated borders, characterized by F- (yellow) and glass substrate (SiO_2^-, SiO_3^-, and SiO_3H^-) (blue). X-Y-Dimensions are 500x500 µm, Z-Dimension is 26 µm.

Both XPS and ToF-SIMS measurements show the absence of the linker (and with it lack of active sites for solid-phase synthesis) within the fluorinated boarders, thus rendering them inert

and unqualified to act as a solid-phase. These results clearly indicate that compartmentalization of liquids within the DMA works well and each spot serves as a confined microreactor with no evidence of cross contamination.

3.2.4 Combinatorial chemistry on DMA

To show the general possibility of combinatorial solid phase synthesis on DMA, standard Fmoc-chemistry (**Figure 28**) for an exemplary 16-membered library of tripeptides was performed.

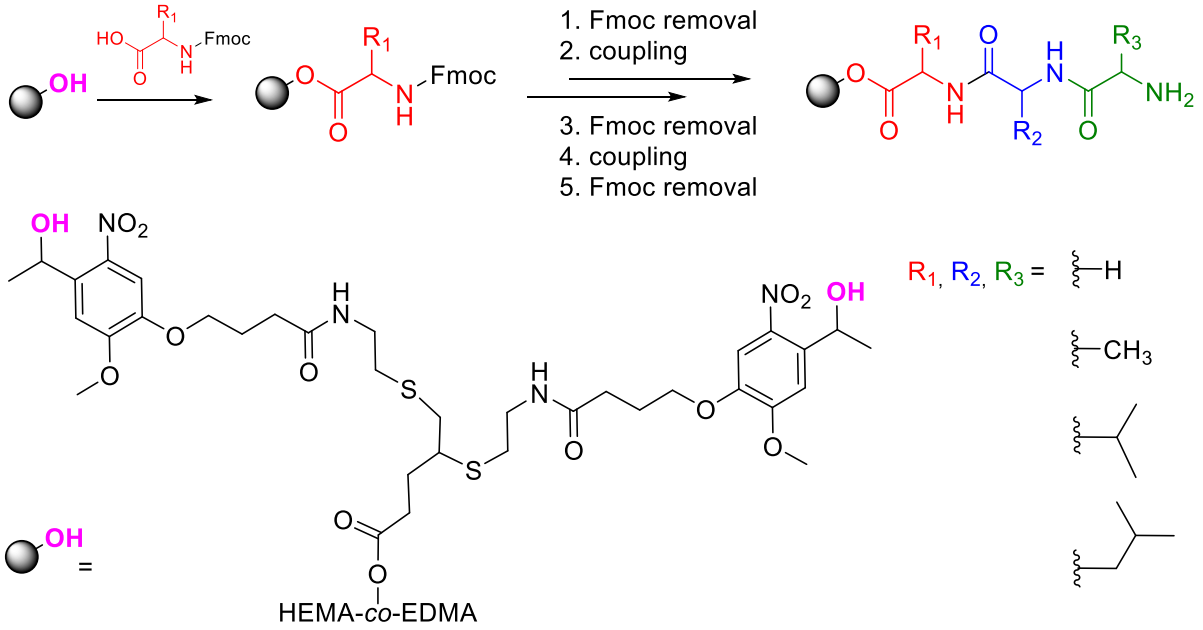

Figure 28. Reaction scheme utilizing Fmoc chemistry (corresponding combinatorial scheme of tripeptide synthesis s. Figure 29).

For this, the hydrophilic spots were functionalized with the linker, as described above and distinct tripeptides were synthesized according to the scheme (**Figure 29**).

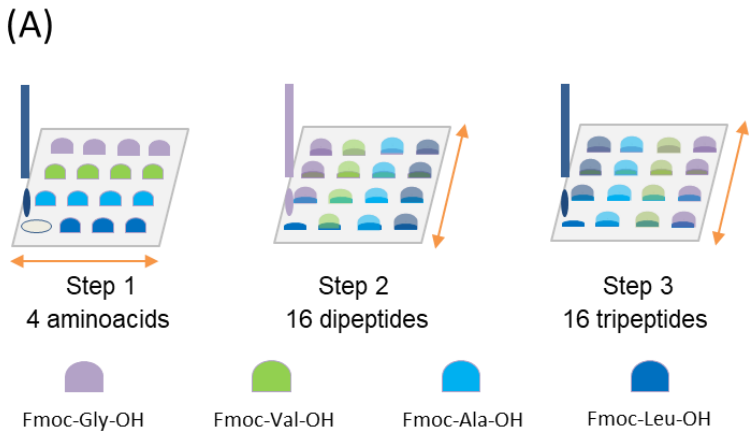

(B)

GGL	GVA	GAV	GLG
VGL	VVA	VAV	VLG
AGL	AVA	AAV	ALG
LGL	LVA	LAV	LLG

Figure 29. A) A schematic representation of the construction of 16-membered combinatorial library on 16 hydrophilic spots of DMA, using 4 different amino acids, arrows indicating the direction of distribution relative to each other. First, aminoacids are applied in rows and immobilized on the solid phase. In the second and third steps, amino acids are applied in columns; B) Overall combinatorial library scheme for synthesis of tripeptides on the array. Array format allows for simple decoding. G – glycine, V – valine, A – alanine, L – leucine.

The combinatorial approach was realized by applying the *N*-protected Fmoc amino acids glycine (Fmoc-Gly-OH), valine (Fmoc-Val-OH), alanine (Fmoc-Ala-OH) and leucine (Fmoc-Leu-OH) row- and columnwise (**Figure 29 A**). Amino acids were applied along the rows of the DMA slide, starting with Fmoc-Gly-OH in row 1 and continuing with Fmoc-Val-OH in row 2, Fmoc-Ala-OH in row 3 and Fmoc-Leu-OH in row 4. All amino acids could be deprotected simultaneously by immersing DMA slide in 20 vol% solution of piperidine in DMF. To conduct the second coupling step, amino acids were applied along the columns, starting with Fmoc-Gly-OH in column 1, continuing with Fmoc-Val-OH in column 2, Fmoc-Ala-OH in column 3 and Fmoc-Leu-OH in column 4. After repeating the deprotection step, amino acids were applied for the third coupling step in the following pattern: Fmoc-Leu-OH in column 1, Fmoc-Ala-OH in column 2, Fmoc-Val-OH in column 3, Fmoc-Gly-OH in column 4. After the final Fmoc deprotection step, the tripeptides were cleaved from the surface upon UV irradiation for 15 minutes (**Figure 30**).

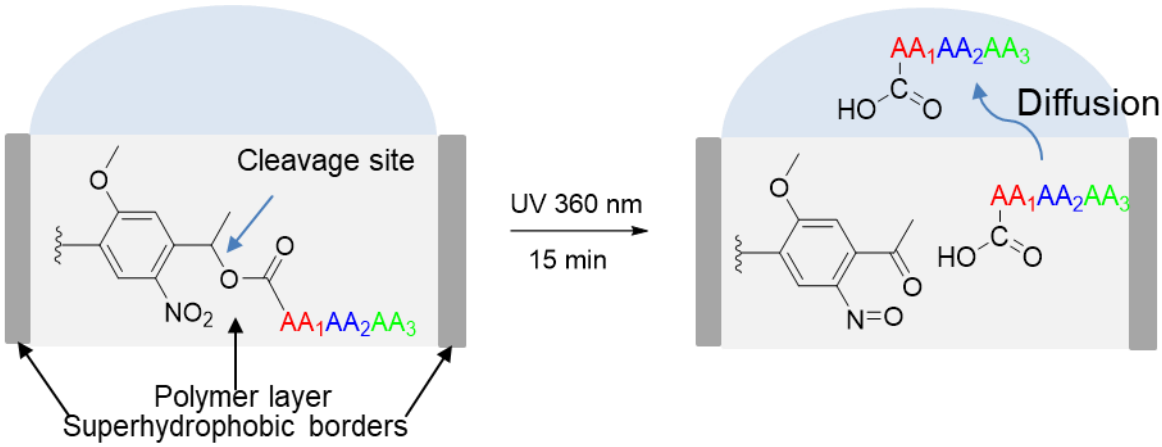

Figure 30. General reaction scheme of tripeptides´ ($AA_1AA_2AA_3$) cleavage from the solid phase; tripeptides bear a free carboxy group at the C-terminus. The photolinker stays attached to the solid phase. After the cleavage, tripeptides diffuse into separate water droplets, and can be subjected to ESI-MS analysis or to interaction with cells, cells being seeded prior to cleavage.

The tripeptides then diffuse into the droplets, where they either can be collected for further analysis or can directly interact with cells, if cells seeded before cleavage. The presence of tripeptides in the droplets was confirmed via ESI-MS by the corresponding [M+H$^+$] signals (**Figure 31**).

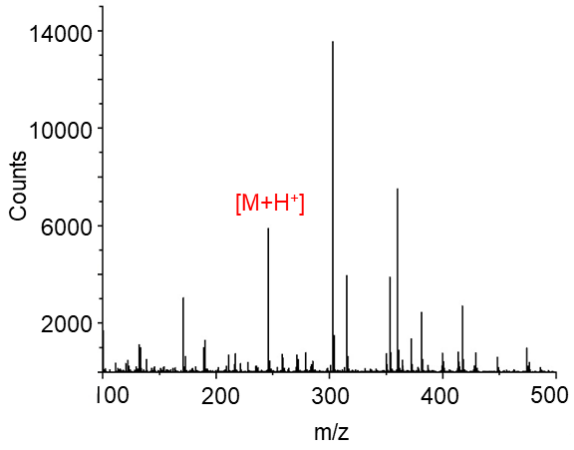

Figure 31. Exemplary positive mode ESI-MS spectra of the tripeptide GGL (244.1 m/z).

Only one tripeptide per spot could be detected, which confirms that solid-phase synthesis of peptides in confined 10 µL volumes and their release into the corresponding droplets via photo-triggered cleavage can be performed without detectable cross-contamination. The fact, that the hydrophobic tripeptides could be released from the solid-phase in the aqueous solution, proves the suitability of the DMA for synthesis and release of drug-like molecules, which are mostly hydrophobic. The 16-membered exemplary library could be constructed within 3 days, requiring <1 hour of active participation. Each 2.83 mm in diameter spot can accommodate up to 10 µL liquid, so liquid handling was conveniently done by manual pipetting.

3.2.5 Cell compatibility of the photo triggered release

One of the key features of the combinatorial solid-phase synthesis using the chemBIOS workflow is the possibility to perform cell-based screenings directly on the same DMA slide after the synthesis part is accomplished, and without the need to transfer the compounds onto another DMA slide or into the wells of microtiter plates. The 4-[4-(1-hydroxyethyl)-2-methoxy-5-nitrophenoxy]butanoic acid as UV-triggered linker, used for the solid-phase synthesis, can be cleaved using 360 nm UV light. In order to prove the harmlessness of the 360 nm UV light for cells cultured on DMA slide, a series of experiments on adherent HEK293T cells was constructed. Cells were seeded onto 4 separate DMA slides functionalized with the linker as described above. Three slides were illuminated with 364 nm UV light for 5, 10 or 15 minutes. After incubation for 18 hours the cell viability was assessed by live/dead staining. These experiments demonstrate that the UV light (360 nm, 6 mW/cm^2, up to 15 minutes) used for triggering the compound release from the solid phase as well as surface bound product of linker cleavage do not affect viability of HEK293T cells, as seen from life/dead staining on **Figure 32 and 33:**

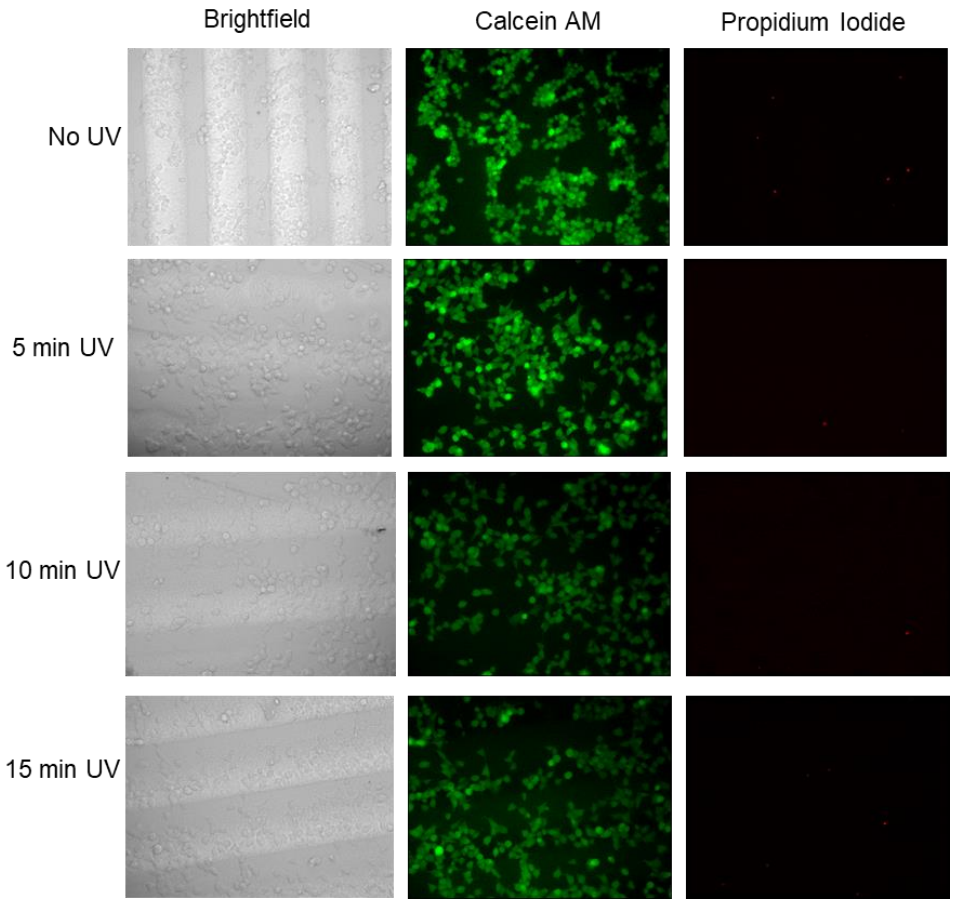

Figure 32. Live/dead staining of HEK293T cells with calcein-AM (green, live cells) and propidium iodide (red, dead) upon 18 h incubation after UV irradiation (360 nm, 6 mW/cm^2, 0-15 minutes).

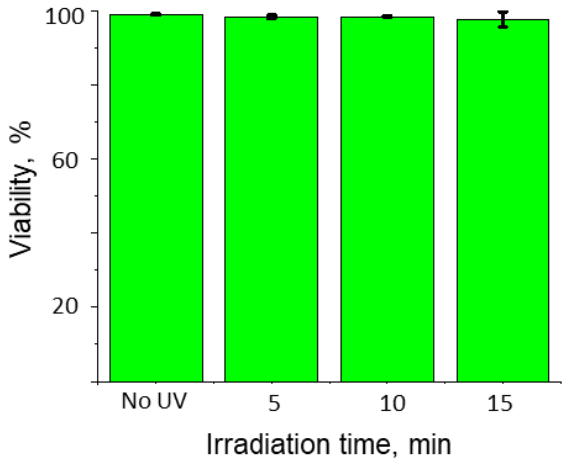

Figure 33. Graph representing cell viability changes upon irradiation with the UV light (360 nm, 6 mW/cm^2, irradiation time 0-15 minutes, followed by incubation for 18 h).

4 Miniaturized high-throughput synthesis and screening of responsive hydrogels using nanoliter compartments[3]

4.1 Introduction

Hydrogels are widely applied in different biological and medical settings, including their use as matrices for three-dimensional (3D) cell culture, as drug delivery systems, and in regenerative medicine. Therefore, discovery of new hydrogel materials, as well as optimization of known materials to meet particular requirements, is of outstanding importance. Typically, hydrogels are synthesized and evaluated iteratively in a one-by-one manner. The drawback of this approach is the paucity of possible combinations that can be practically tested as well as the high cost in terms of time, consumables and labor. Therefore, the process of discovery of novel hydrogels remains slow and the design principles, including structure-function relationships, are often not fully understood. Miniaturized high-throughput technologies, enabled by technologies such as droplet microfluidics[117] and polymer microarrays, are therefore important in facilitating and accelerating the discovery of novel hydrogels and screening of biological interactions of interest in parallel. Pioneered by Anderson et.al.[19] and Tourniaire et.al.[118] in the mid-2000s, polymer microarray technologies for biomaterial discovery have the advantage of an arrayed format. These techniques have been used successfully for the discovery of biomaterials for broad-ranging applications, ranging from materials for bone repair[119] and heart valve engineering,[120] to materials for parasite removal[121] and bacteria-repellent medical devices.[122] High-throughput techniques have been widely used to study the effects of biomaterials on stem cells.[66, 123-124] Biomaterial microarrays have been extensively reviewed.[125] Interestingly, reports of high-throughput synthesis of responsive materials are rare.[105] Responsive hydrogels have particular advantage of being synthesized in a high-throughput manner. Structure-function relationships between multiple responses cannot be easily forecast and thus, require experimental investigation in a process that does not lend itself to the classical iterative synthesis. The discovery of novel properties is facilitated by screening of a much larger range of chemical structures than can easily be achieved in conventional one-by-one synthesis. Therefore, high-throughput synthesis of responsive materials offers the potential to narrow the gap between the demand and supply of responsive materials.

Millions of cells are usually necessary to screen for cell-material interactions.[19] In the case of stem and primary cells, this can soon become expensive and therefore, restricts the number of possible combinations that can be tested. Solutions often have to be premixed before

[3] This chapter is adapted from the following publication: **Alisa Rosenfeld**; Claude Oelschlaeger; Richard Thelen; Stefan Heissler; Pavel A. Levkin. Miniaturized high-throughput synthesis and screening of responsive hydrogels using nanoliter compartments, submitted.

printing.[19, 65, 126] Furthermore, cell-material assays are usually performed without compartmentalization of the individual materials. This can lead to cross-contamination issues in the case of cell-cell signaling studies, and is particularly important for the microenvironment of stem cells, thus demanding independent control of contact-mediated signalling. Introducing soluble factors after seeding cells can be conveniently achieved by compartmentalization. Compartmentalization also renders microarray add-ons[127] obsolete.

A platform utilizing compartmentalized hydrophobic/hydrophilic patterns was developed by Le et.al., in which a pattern of varying wettability on gold-coated glass slides was utilized to study processes such as hMSC encapsulation.[127] However, the manual handling involved in this technique considerably limits the throughput. Therefore, a platform that allows simple high-throughput fabrication of arrayed combinatorial library of responsive hydrogels in separated nanoliter compartments has not yet been developed.

The DMA, being a platform that comprises a glass slide photopatterned with hydrophilic regions/spots separated by superhydrophobic liquid-impermeable barriers, has been used for alginate-based hydrogel microarray production.[106] These hydrogel microarrays comprised only one hydrogel composition. Following deposition of a unique prepolymerization mixture in each spot, the superhydrophobic barriers prevent cross-contamination, providing compartmentalization and opening the possibility to test different compositions in a combinatorial manner. Moreover, such assay miniaturization provides the ability to test a greater number of combinations of starting compounds, ensuring, if required, an almost spatially continuous gradient that can be used to study structure/function relationships. Specialized printing technique also allow precise deposition of compounds at the nanoliter level. DMA platform can be also used to perform multiple microbeads or cell encapsulation experiments in a parallel.

In this chapter, high-throughput combinatorial synthesis of hydrogels using DMA was demonstrated. Polymerization on nanoliter scale was optimized with regards to oxygen scavenging, which was proved by synthesis of 33-membered combinatorial hydrogel library in quadruplicates. The proper mixing behavior was confirmed by fluorescence measurements, Raman mapping and multiple particle tracking experiments. Synthesis in confined environment was shown to be beneficial for cell encapsulation and to study polymer´ buckling properties. Two combinatorial libraries of UV-responsive hydrogels (totaling 20 unique members á 16 replicates), all of which manifested a well-defined spatial gradient of components, were synthesized to highlight the convenience and future potential of DMA as a platform for responsive material synthesis.

4.2 Results and discussion

4.2.1 General array production

In this study, a platform in which hundreds of highly adjustable combinations of polymerization starting materials and additives can be simultaneously synthesized and assayed was developed. To implement the combinatorial approach and support a high-throughput aspect, a liquid dispensing device based on non-contact liquid dispensing technology was used to dispense droplets containing components of a hydrogel library.[128] The I-DOT printer is a noncontact printer that utilizes compressed air pulses to dispense precise dosage of solutions in the nanoliter range. The non-contact liquid dispensing technology printer was equipped with a humidifier, thus allowing printing of aqueous solutions without adding humectants or oil films. Droplets can be dispensed directly onto the hydrophilic spots of the DMA without cross-contamination, since superhydrophobic borders provide confined surroundings to hydrophilic regions. These wall-less microreactors allow synthesis of a unique material in each spot. The non-contact liquid dispensing technology printer facilitates the creation of a typical library of 144 unique pre-polymerization mixtures within several minutes. This process requires less than 20 µL of reagent solution in total and is executed in more than 800 pipetting steps. To construct a similar library in a conventional one-by-one manner on 1 ml scale would be much more time-consuming and require approximately 7,000 times more solution (144 mL) (**Figure 34**):

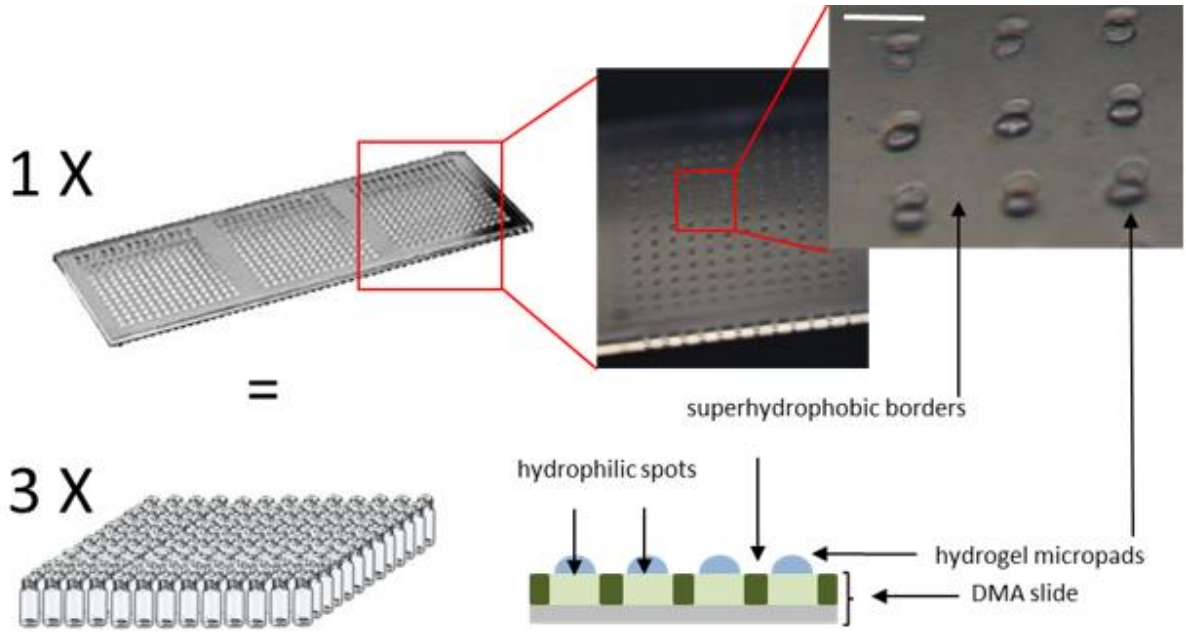

Figure 34. Schematic comparison of high-throughput screening of 588 hydrogels in vials and on DMA. Confined hydrophilic regions on a DMA slide act as wall-less reaction microvessels, enabling the single DMA slide to substitute 588 vials. Scale bar 1 mm.

Recently, Li and Scheiger et al. has shown that commonly used methacrylate-based hydrogels are inherently degradable by 270 nm UV light.[129-130] Most of the high-throughput smart material libraries reported to date are based on temperature and water responses;[105] therefore, it was aimed to complement these studies with a study of methacrylate-based photoresponsive hydrogels (**Figure 35**):

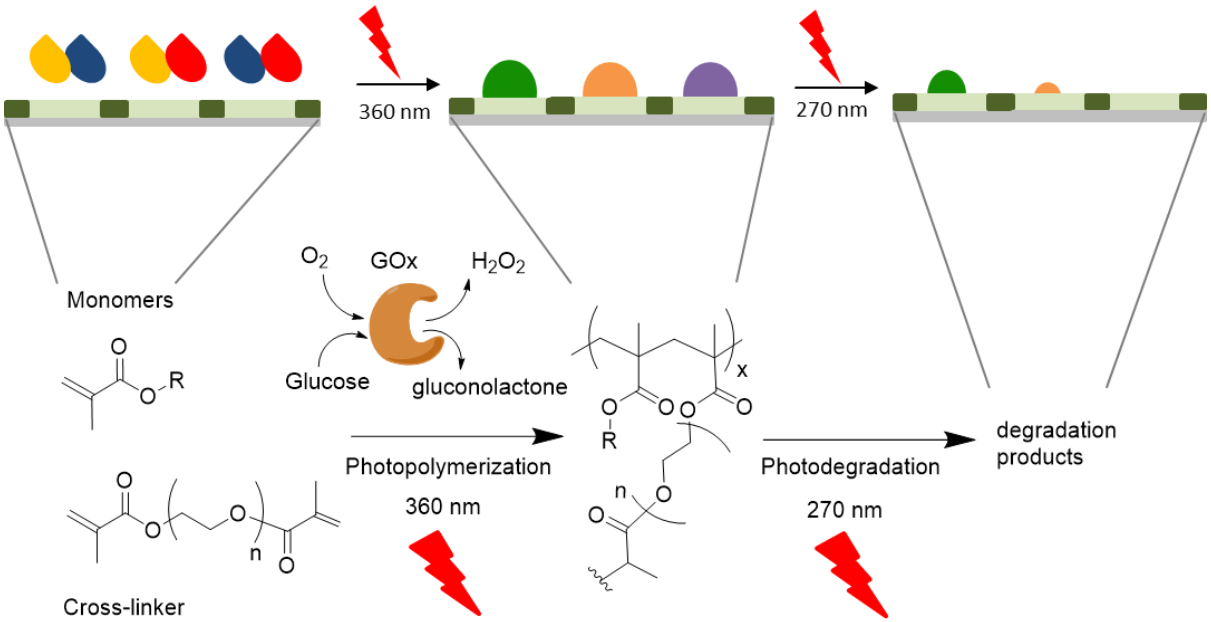

Figure 35. Schematic description and reaction scheme of high-throughput on-chip photoinduced synthesis of combinatorial library of photodegradable hydrogels and assessment of degradation properties. Based on this reaction, three libraries have been synthesized: 3-membered PEGMA/PEGDMA library, 33-membered PEGMA/DMAEMA/PEGDMA library and 17-membered PEGMA/SAMA/PEGDMA library; PEGMA/DMAEMA/PEGDMA library was used to optimize the photopolymerization protocol; PEGMA/PEGDMA and PEGMA/SAMA/PEGDMA libraries were assessed with regard to their photodegradation properties.

Photopolymerization was selected because it is a fast, non-contact, controllable (in terms of wavelength, exposure time and intensity), proceeds under physiological conditions and under high spatiotemporal control.[131] SAP was used as a photoinitiator; therefore, photopolymerization occurred at 360 nm and photodegradation occurred at 270 nm.

4.2.2 Polymerization on a nanoliter scale

Despite many benefits, the open infrastructure of DMA involves the contact of droplets containing prepolymerization mixture with oxygen, which can dramatically decrease the efficiency of radical polymerization. Conventional methods of oxygen removal, such as degassing via nitrogen purging, working under an inert atmosphere or freeze-pump-thaw cycles, require additional infrastructure or are not readily applicable to reactions carried out in submicroliter volumes.[132] Therefore, to perform miniaturized HT radical polymerization under

ambient conditions and overcome its inherent intolerance to oxygen, the initiator solution was supplemented with glucose oxidase (GOx) and glucose (Glu), which function in combination as an oxygen scavenger system.[132-134] A 33-membered PEGMA/DMAEMA library was used as a sample library for optimization of the degassing procedure. Without the GOx/Glu degassing system, the average hydrogel micropad size decreased as the concentration of DMAEMA increases. For these compositions, the conversion was low due to presence of oxygen, resulting in partial crosslinking of polymers, which were consequently unable to adhere to the underlying substrate and were removed during washing step. For the GOx/Glu degassed polymerization, 40 µM GOx was sufficient to reproducibly synthesize hydrogel microarrays in all prepolymerization mixtures tested. Changes in pH of the precursor solutions did not result in better polymerization (**Figure 36**):

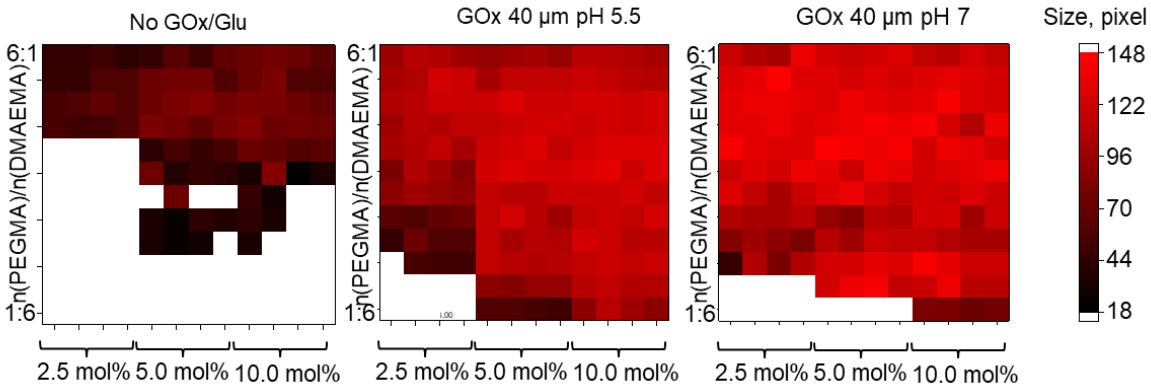

Figure 36. Size distribution derived from the brightfield microscopy of a hydrogel library polymerized with/without GOx/Glucose oxygen scavenger system. White spots indicate compositions, which could not be polymerized.

The high surface-to-volume ratio of submicroliter droplets combined with the shorter pathways for oxygen diffusion, as well as the suboptimal reaction temperature for GOx justifies the increased (200×) GOx concentration required for complete conversion of monomers within the hundred nanoliter-sized droplets compared to reactions conducted in the submilliliter range.[135]

4.2.3 Confinement

For inkjet printing on flat surfaces with homogeneous wettability, the size of hydrogels is controlled by changing the number of droplets printed per spot. In contrast, the size and shape of the hydrogel features printed on DMA can be controlled by changing the freely selectable pattern of the photomask used for production of slides (**Figure 37**). Prepolymerization mixtures deposited onto different patterns of choice can be therefore polymerized into arbitrary shapes and with freely selectable density of the hydrogel micropad due to precise setting of the pitch between spots. Superhydrophobic borders prevent liquid-spreading and therefore, allow deposition of volumes up to 1,000 nL in a 1×1 mm spot. Deposition of different volumes

provides control over the hydrogel height and width, which would not be possible on a nonpatterned surface.

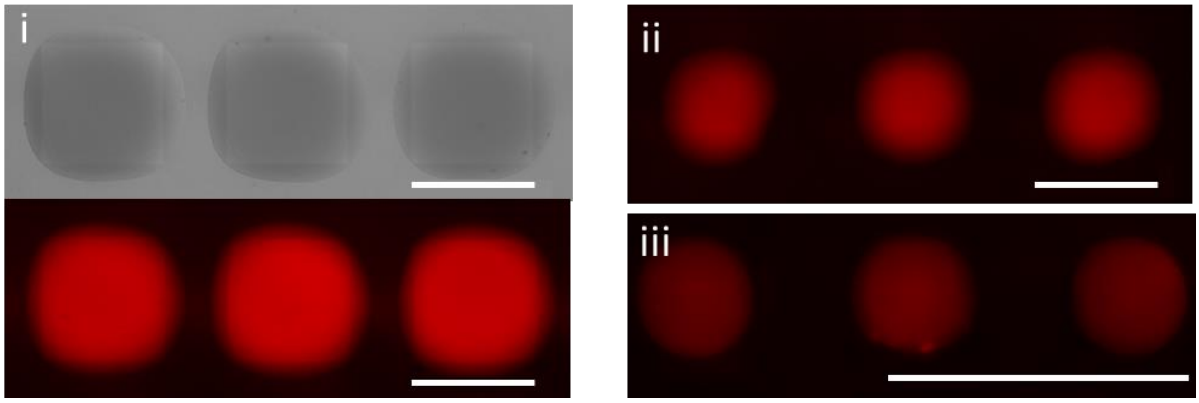

Figure 37. Brightfield and fluorescent images of hydrogels, which were polymerized in nanoliter-sized compartments using (i) and (ii) 1000 µm squared pattern, 240 nL resp. 120 nL prepolymerization mixture (iii) 500 µm squared pattern, 40 nl prepolymerization mixture. Fluorescence was achieved by immersing the hydrogel array into the 0.01 M Rhodamine B solution. Scale bars are 1 mm.

Furthermore, in the absence of an oxygen scavenger system during the polymerization, we observed surface instabilities because of the oxygen gradient and hence, different degrees of crosslinking from the surface of the hydrogel to its core. Since the hydrogel micropads are laterally confined on rigid hydrophilic spots, initially smooth hydrogels may become unstable upon swelling in water and develop various surface patterns (**Figure 38 A**):

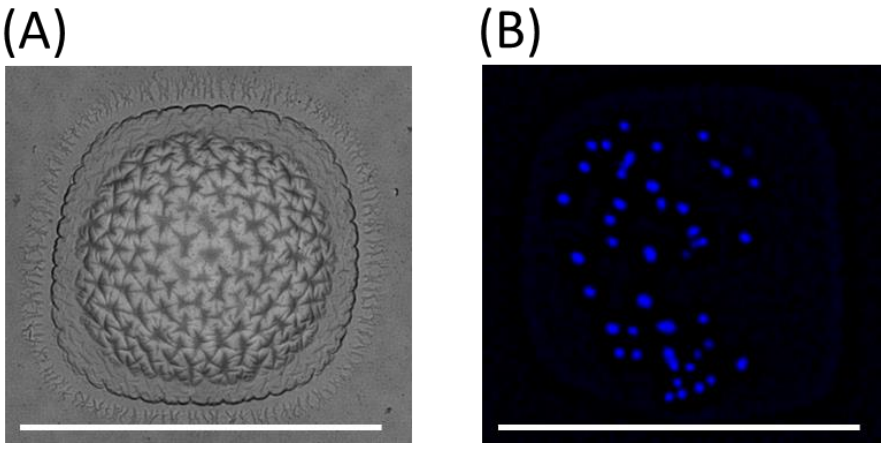

Figure 38. Examples of utilizing confined microenvironment. A) A brightfield image of an exemplary hydrogel showing surface instabilities upon extensive swelling. B) HeLa-cells encapsulated within the hydrogel pad and stained with Höchst. Scale bars are 1 mm.

Therefore, combinatorial synthesis of hydrogels using DMA can be utilized for high-throughput assessment of thin film buckling properties depending on the starting composition.

The possibility of encapsulation of cells within hydrogels was demonstrated (**Figure 38 B**) by overprinting the prepolymerization solution with a cell-suspension. Confinement shows the possibility to study cell encapsulation parameters (rapid optimization of hydrogel composition to promote a certain biological outcome), to develop 3D cell culture matrices as well as to study cell-material interactions without crosstalk between cells encapsulated in neighbouring hydrogels prevented by superhydrophobic borders.

4.2.4 Mixing within droplets

During the printing process, the droplet of one solution impacts on the droplet of another solution to induce a vortex, which enables fluid mixing. To ensure the reaction occurs throughout the whole reaction volume, the mixing behavior of the reagents in consecutively printed droplets was evaluated. The printed solutions were colored one-by-one with fluorescein/rhodamine B and printed on top of each other in different proportions, one colored solution at a time, as described in the literature.[136] The overprinting of colorless droplet with a colored one (and vice versa) induced significant turbulence in the spots, resulting in even distribution of the fluorescent dye (**Figure 39**) in the typical range of droplet volumes (60 nL to 10 nL). The mixing time was estimated to be several seconds.

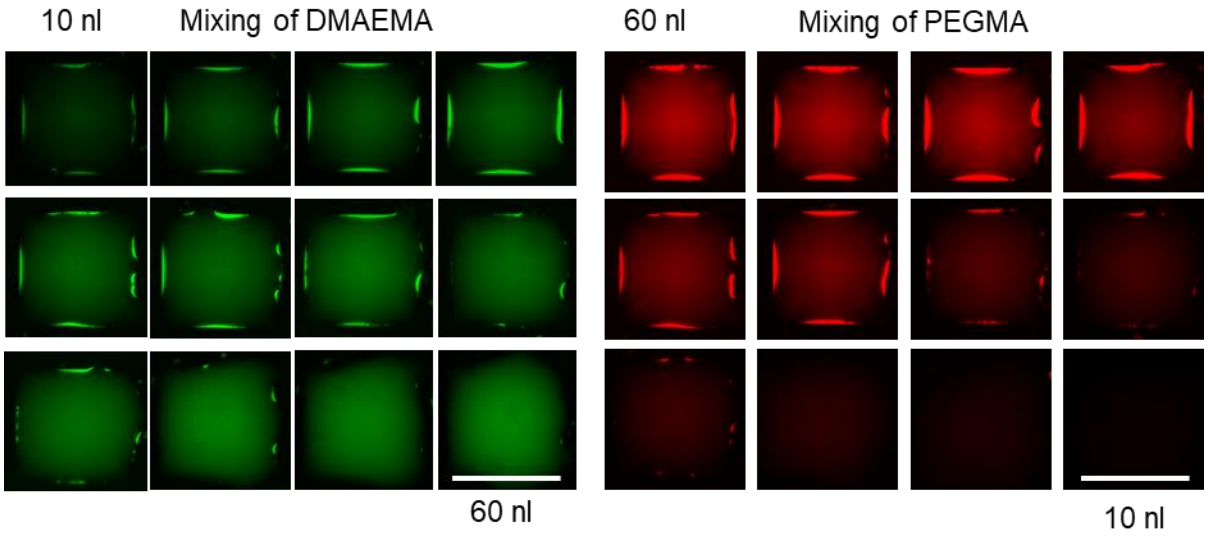

Figure 39. Mixing within droplets after drop-on-drop printing of components of prepolymerization solutions, examples for DMAEMA and PEGMA. Scale bars are 1 mm.

Next, Raman spectroscopy measurements on one selected hydrogel composition were performed to confirm the homogeneous distribution of chemicals within droplets. The total

number of measurement spots per hydrogel micropad was 144, arranged in a 12×12 matrix (**Figure 40**).

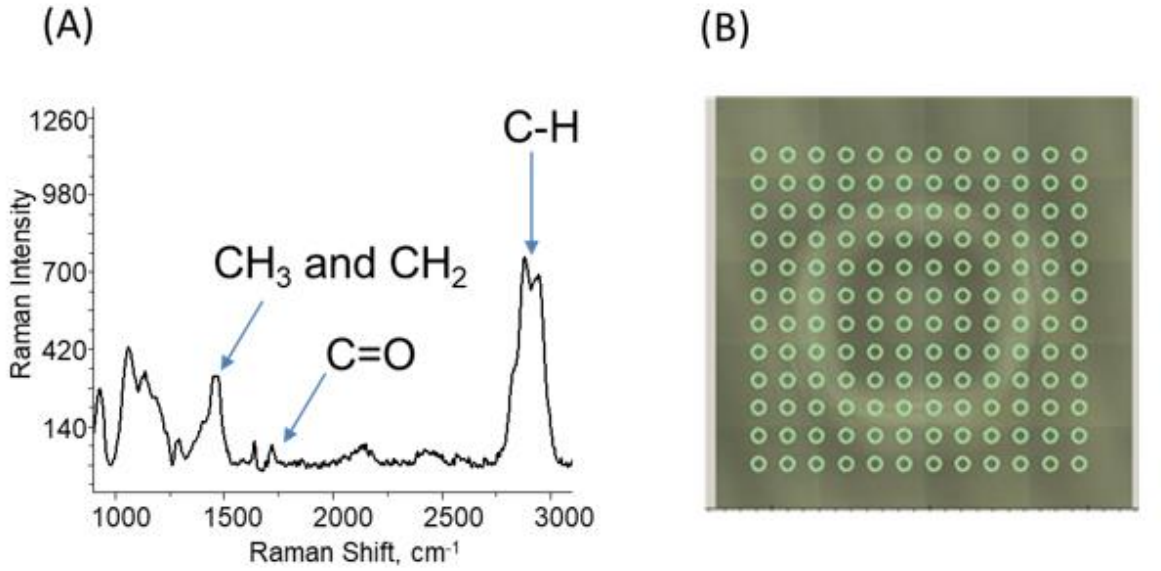

Figure 40. A) Raman spectrum of one point of the hydrogel reveals the carbonyl, CH_3 and CH_2 as well as C-H vibrations. B) Arrangement of 144 Raman measurements as a 12×12 matrix (1x1 mm spot).

As shown in **Figure 41** the distribution of C-H (3015 to 2790 cm^{-1}), CH_3 and CH_2 (1500 to 1400 cm^{-1}) as well as carbonyl vibrations (1730 to 1700 cm^{-1}) was radially even.

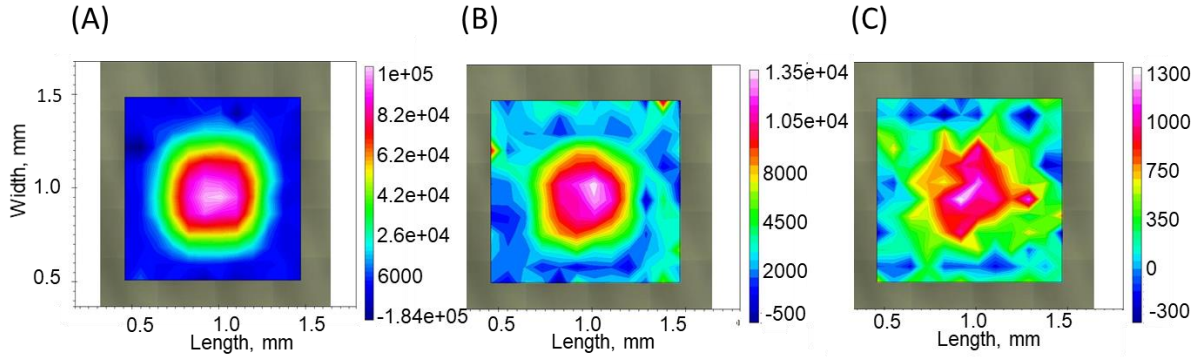

Figure 41. **Raman mapping on a representative hydrogel** (A) integrated over 3015-2790 cm^{-1}, corresponds to C-H (B) integrated over 1500-1400 cm^{-1}, corresponds to CH_3 and CH_2; (C) integrated over 1730-1700 cm^{-1}, corresponds to carbonyl group.

The higher intensity of vibrations toward the top of the hydrogel micropad correlated with its height and the overall bulged form, and thus with the abundance of corresponding functional groups. The consistency of bulge formation was confirmed by white light scattering measurements (**Figure 42**):

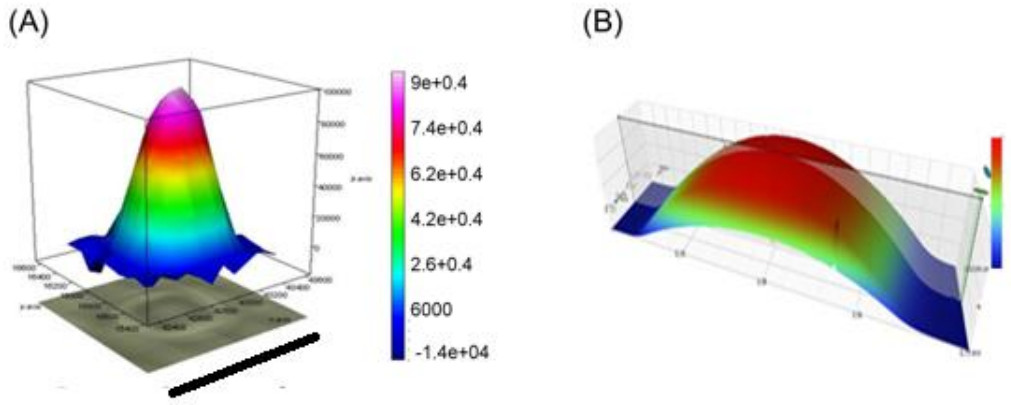

Figure 42. A) 3D depiction of the C-H signals, showing higher intensity of vibrations toward the top of the hydrogel micropad, which correlates with its height and the overall bulge formed; B) White light scattering experiment, proving the bulged form of the hydrogel. Scale bar is 1 mm.

Finally, rheological and heterogeneity properties of the hydrogel micropad were assessed by performing multiple particle tracking (MPT) microrheology (results are summarized in the **Figure 43**).

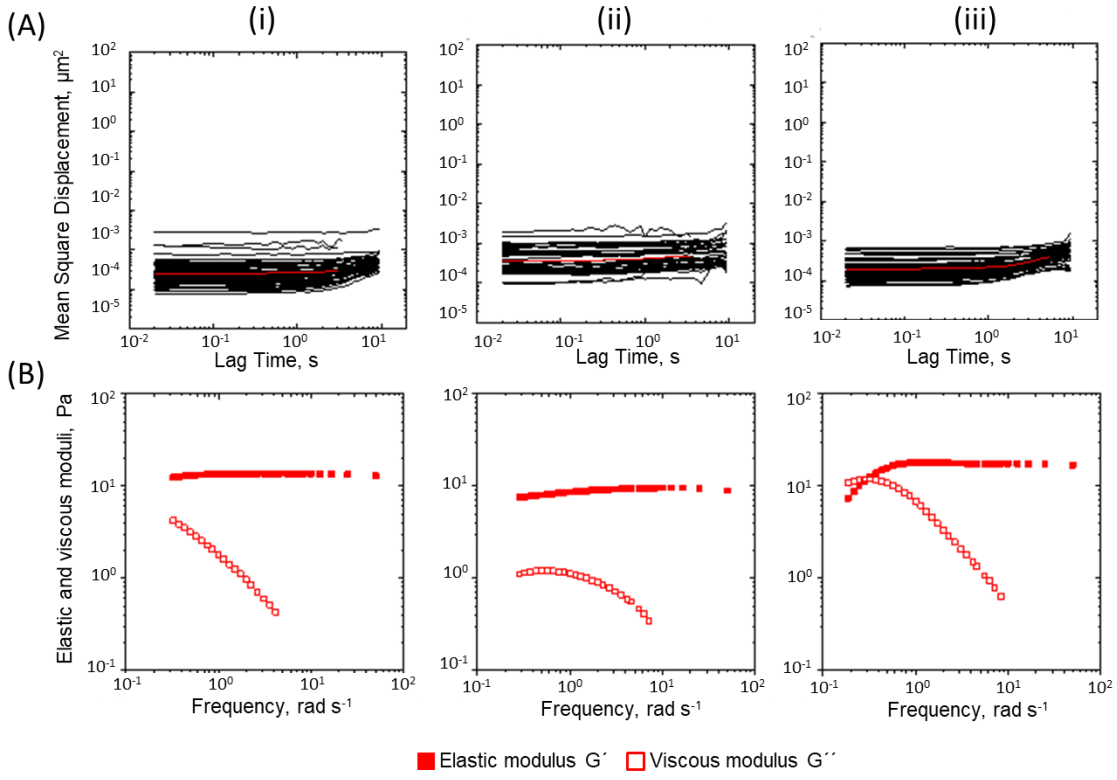

Figure 43. A) Mean square displacement values of tracer particles for three regions of the hydrogel (i) central region, 55 tracer particles; (ii) left region, 43 tracer particles, and (iii) bottom region, 62 tracer particles; B) Elastic and viscous moduli behaviour as function of applied frequency, revealing a significant degree of elasticity.

In order to incorporate polystyrene tracer particles into the hydrogel prior to polymerization, SAP/glucose oxidase/glucose solution containing particles was printed instead of SAP solution. After polymerization, the mean square displacement (MSD) of the tracer was measured. **Figure 43 A** shows the variation of MSDs as a function of lag time (τ) for polystyrene tracer particles dispersed in hydrogel in three different regions (i: central, ii: left , iii: bottom). In all cases, all MSDs exhibited almost no time dependence with slope close to zero and an average MSD (red curve) value approximately $2 \cdot 10^{-4}$ μm^2. This result indicates that particles are highly constrained by the surrounding fluid, which is consistent with elastic trapping of particles in a gel-like network. Additionally, statistical analyses of the MSD distribution clearly reveals a homogeneous structure on the micrometer length scale with a small value of the non-Gaussian parameter α = 0.55, 0.56 and 0.41 determined at $\tau = 0.1$ s for central, left and bottom region of the hydrogel micropad respectively.[137] These results are also reflected in the variation of elastic and viscous moduli, G´ and G´´, respectively, calculated from the average MSD. As shown in **Figure 43 B**, independent of the region, a significant degree of elasticity was observed with $G'(\omega) > G''(\omega)$ and constant elastic modulus $G' = 14 \pm 4$ Pa in a broad frequency range. From this value, the mesh size ξ of the network was determined according to the classical theory of rubber elasticity with $G' = \frac{k_B T}{\xi^3}$. The mesh size was found to be 67 ±6 nm.

Overall, fluorescence, Raman and MPT microrheological analyses confirmed even distribution of printed solutions in nanoliter-sized droplets analogous to the synthesis on a macroscale.

4.2.5 Combinatorial screening of hydrogels

To confirm the applicability of the DMA platform for synthesis and assessment of the properties of responsive hydrogels, a proof-of-concept library with one photodegradable (methacrylate-based) and one non-degradable (acrylate-based) hydrogel was synthesized. Both hydrogels were printed on the DMA in a checkerboard pattern, which could not be recognized before irradiation; all hydrogels had identical appearance (**Figure 44i**). Given an inherent photodegradability of polymethacrylates and the UV-transparency of water, the remarkable minute-scale degradability of polymethacrylate-based hydrogels originates from the high swellability of the hydrogel network. Therefore, during UV irradiation, macroradicals are separated in space, and re-crosslinking is suppressed. In the case of polyPEG-acrylates, re-crosslinking reactions occur much faster than that of polyPEG-methacrylates, rendering acrylate-based hydrogels non-degradable under UV light, and allowing visualization of the hidden checkerboard pattern under UV irradiation (**Figure 44ii**):

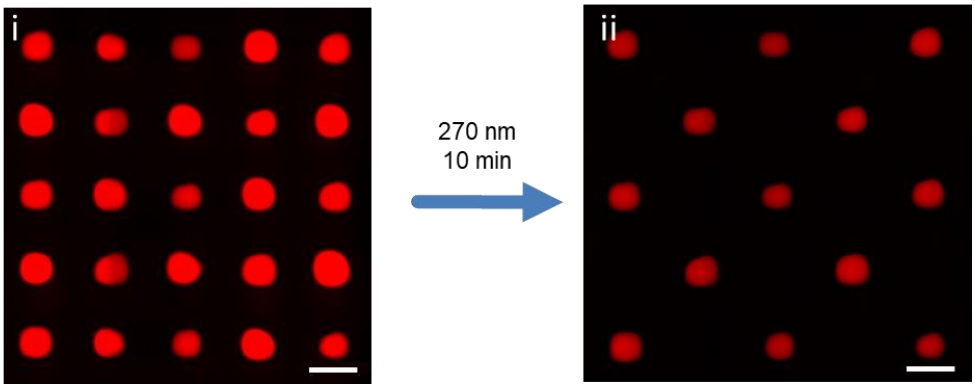

Figure 44. The fluorescent images of hydrogel array before and after UV irradiation. (i) Exemplary library of polyPEG acrylate and polyPEG methacrylate hydrogels arranged in a checkerboard-pattern on a microarray, colored with Rhodamine 6G; (ii) after illumination with UV light (270 nm, 22 mW/cm^2, 10 min) only non-degradable polyacrylates are left. Scale bars are 1 mm.

This proof-of-concept library, comprising one degradable and one non-degradable material, arranged in a preprogrammed pattern, represents a special case of temporal and spatial control over the degradation. Furthermore, high-throughput combinatorial synthesis can be used to rapidly customize the hydrogel degradation properties for each specific application.

Since the proof-of-concept library showed the possibility to distinguish between degradable and non-degradable hydrogels (yes/no), next hydrogels with different degradation times (therefore different degradability) on the DMA slide were assessed. As already mentioned, the swellability of the hydrogel network is the prerequisite for hydrogel photodegradation. Swellability correlates negatively with the amount of crosslinker, rendering hydrogels with higher crosslinker content (with respect to the monomer) less swellable, and therefore less degradable, compared to a hydrogel with a lower crosslinker content. To determine whether this behavior could be reproduced on the DMA, a library of three PEGMA-based hydrogels with different crosslinker concentrations (2.5, 5.0 and 10.0 mol% w.r.t. PEGMA) was synthesized. To verify the reproducibility of the degradation, each composition was synthesized in 16 replicates, resulting in 48 nanoliter-sized hydrogels that required only 6 µL of solution in total. After the synthesis, the hydrogel microarray was immersed in rhodamine 6G solution to color the hydrogels and was subsequently subjected to UV irradiation (270 nm, 1–3 min). The course of the degradation (i.e. the presence or disappearance of hydrogel micropads) was followed either by eye (pink rhodamine) or under a microscope in the fluorescent channel. If detection was made via fluorescence, hydrogel circles were detected automatically using specialized software. As expected and shown in **Figure 45**, hydrogels with 2.5 mol% crosslinker were completely degraded within 2 minutes of UV irradiation, whereas doubling the crosslinker content slowed degradation of the hydrogels to 4 minutes. Hydrogels with the highest crosslinker content did not degrade even after 10 minutes UV irradiation. It is

noteworthy that all 16 replicates of one composition degraded simultaneously, emphasizing the reproducibility of the synthesis.

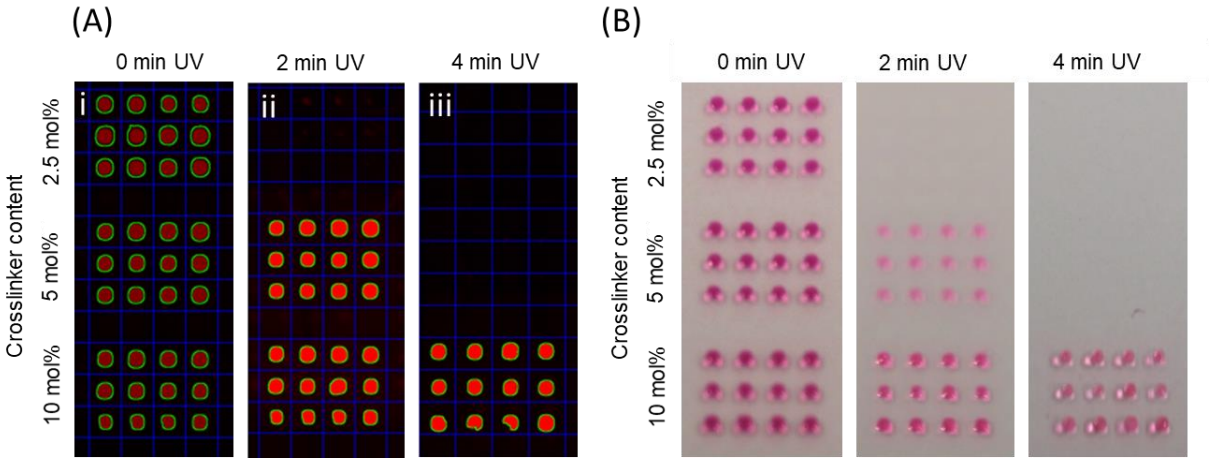

Figure 45. Different degradation ability of PEGMA-based hydrogels with varying amount of crosslinker. Degradation (270 nm, 22 mW/cm^2) can be followed (A) by software or (B) by eye.

Finally, the effect of supplementation of the prepolymerization mixtures from the previous library with different amounts of zwitterionic (2-(*N*-3-sulfopropyl-*N*,*N*-dimethyl ammonium)ethyl methacrylate (SAMA) on degradation of the resulting hydrogels was examined (**Figure 46**):

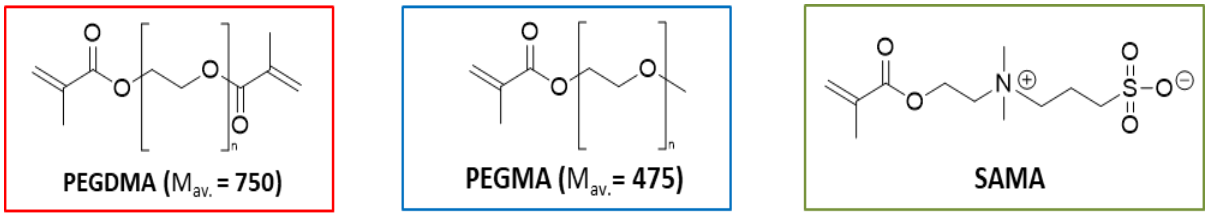

Figure 46. Components of a two-dimensional combinatorial library: PEGMA and SAMA as monomers as well as PEGDMA as a crosslinker.

To do so, the volume ratios of equimolar monomer solutions PEGMA:SAMA were varied from 6:1 to 1:6 with crosslinker concentrations 2.5, 5.0 and 10.0 mol% w.r.t. the combined amount of monomers, maintaining a constant ratio Σn(monomers)/n(crosslinker) for all compositions. Therefore, the combinatorial library was extended to another dimension, yielding 17 unique combinations with a total of 16 replicates each, resulting in 272 nanoliter-sized hydrogels that required only 34 µL of solution in total. SAMA is a charged monomer that is known to increase the swelling ratio of hydrogels; therefore, the ability of increased SAMA:PEGMA ratios to increase the rapidity of hydrogel degradation on the DMA was investigated.[129] Two trends were observed following exposure of the DMA slide with SAMA library to UV light. Generally, as was already shown, the rate of hydrogel degradation correlates negatively with the degree of crosslinking. Additionally, clear trends were observed within the group of hydrogels with the

same crosslinker content. As expected, progressively substituting PEGMA with SAMA rendered the hydrogels more degradable (**Figure 47**).

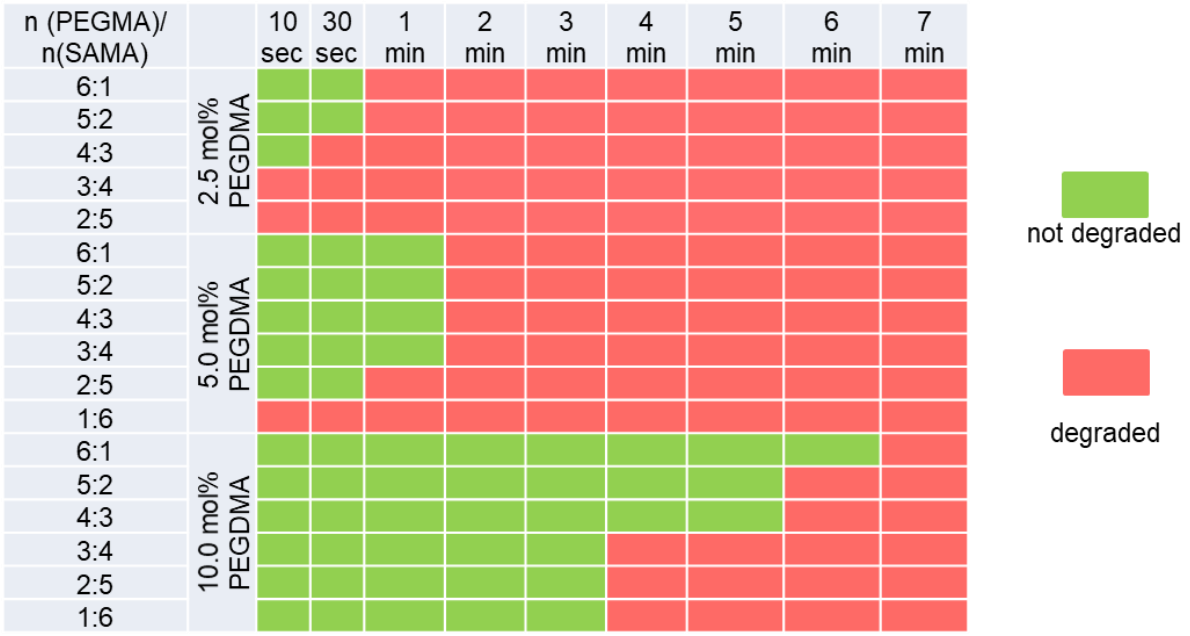

Figure 47. Photodegradation screening results of a two-dimensional combinatorial library, constructed by varying the amount of crosslinker PEGDMA and PEGMA/SAMA molar ratio. The degradation ability is inversly proportional to the amount of PEGDMA and PEGMA.

Four compositions (PEGMA:SAMA = 6:1 and 4:3 with crosslinker concentrations 2.5 and 10.0 mol% each) were upscaled from 130 nL to 180 µL to verify the reproducibility of the synthesis. It is noteworthy that the synthesis of four hydrogel compositions in triplicate at a submilliliter scale required 2.16 mL prepolymerization solutions, which is sufficient to synthesize more than 17,000 hydrogels on a DMA. After illumination of upscaled hydrogels with UV for 1.5 minutes, the mass loss was measured. For 2.5 mol% crosslinker, the rate of (PEGMA:SAMA 6:1)-hydrogel degradation was slower than that of the (PEGMA:SAMA 4:3)-hydrogel (58% vs. 88%). Both upscaled hydrogels with 10.0 mol% crosslinker showed almost no degradation after 1.5 min UV (1% vs. 6% for 6:1 and 4:3 PEGMA:SAMA proportions, respectively). This also reflects the hydrogel behavior on the DMA, with hydrogels with 10.0 mol% crosslinker still visible after 1.5 min UV exposure. Therefore, high SAMA content and low crosslinker content were shown to correlate with high degradability on both the micro- and nanoscales.

5 Designing inherently degradable gelatin methacrylate-based hydrogels[4]

5.1 Introduction

Responsiveness is a ubiquitous property of biological systems and a primary characteristic of living matter. To mimic living systems more effectively, extensive research has been devoted to hydrogels that resemble biological systems based on their responsive properties. Hydrogel design has sought to make hydrogels accessible for a variety of stimuli capable of either synthesizing[138-139] the hydrogel or inducing changes (e.g., degradation,[129] drug release,[140] and sol-gel transition[141]) in hydrogels. Certain stimuli, including enzymes,[58] pH,[142] and small molecules such as glucose,[143] induce responses via direct molecular contact with a hydrogel or its precursors. Other stimuli, such as temperature[142] and light[41], enable synthesis and manipulation of soft matter in a non-contact spatiotemporal manner, which is why stimuli have become increasingly important in biological settings. Photopolymerization and photodegradation are especially noteworthy given their high tunability of wavelength and intensity; the use of photomasks also enables sharp control of spatial resolution.

Usually, hydrogels can be made photodegradable through additional functionalization with photoresponsive groups that must be incorporated into the hydrogel network and act as fracture points for light. Various photolabile groups can be introduced into hydrogels; the most common one is the *o*-nitrobenzylester group[144-146], although other groups[147] such as coumarin,[148] disulfides,[149] and ruthenium (II) polypyridyl complexes[150] are also used. Sophisticated *o*-nitrobenzyl derivatives of gelatin can be used to support cell adhesion to yield matrices for 3D cell cultures.[151-152] Despite many accomplishments in this field, the limited number of photolabile moieties and associated synthetic challenges greatly constrain the monomers that can be used in synthesis. Flexibility and heterogeneity are needed to more accurately mimic complex biological systems. Also, highly simplified synthetic procedures are essential for the rapid development of nature-like hydrogels. Thus, cell-compatible innately photodegradable hydrogels without photoresponsive groups are urgently needed.

Recently, in our group the inherent photodegradability of poly(ethyleneglycol) methacrylate (PEGMA)-based hydrogels was demonstrated.[129] The remarkable minute-scale photodegradability of PEGMA hydrogels is attributable to the combination of inherent photodegradability of polymethacrylates, UV transparency of water and strong swelling of the

[4] This chapter is adapted from the following publication: **Alisa Rosenfeld**; Tobias Göckler; Markus Reischl; Ute Schepers; Pavel A. Levkin. Designing inherently photodegradable gelatin methacrylate-based hydrogels, submitted. Tobias Göckler performed precursor synthesis and analysis as well as cell viability tests upon encapsulation, degradation and medium exchange, and cell photorelease experiments. Dr. Ing. Markus Reischl (IAI, KIT) performed mathematical approximation calculations.

hydrogel network. High volumes of water restrict macroradical mobility and keep polymer chains separated in space during UV irradiation; therefore, chain scission and degradation reactions dominate over the re-crosslinking reaction. UV degradability is thus associated with hydrogel swellability, which can be influenced by e.g. introducing charged monomers.[153] These photopolymerizable, inherently photodegradable PEGMA-based hydrogels are biologically inert and nontoxic, similar to other PEG-based hydrogels, but lack cell adhesion and enzymatic degradation sites. By contrast, methacrylated gelatin (GelMA) displays excellent biocompatibility and biodegradability and can be conveniently photopolymerized.[108-109, 154-155] However, three factors influence the non-degradability of polymerized GelMA under 270 nm UV light on a reasonable timescale:1) reduced swellability of polymerized GelMA; 2) amide-bound methacrylates less prone to photomediated scission; and 3) the presence of aromatic UV-absorbing amino acids. Therefore, gelatin-based polymethacrylates do not demonstrate photodegradable behavior compared to PEG-based methacrylate hydrogels.

In this chapter, a biocompatible, easily accessible, photopolymerizable, and photodegradable material for 3D cell culture microstructuring has been demonstrated. The hypothesis that supplementing PEGMA hydrogels with GelMA can enhance the hydrogels´ cell encapsulation ability while retaining photodegradation properties was proved. The abovementioned synthetic challenge was addressed by constructing a combinatorial library of PEGMA/PEGDMA/GelMA hydrogels and investigating how the addition of GelMA influenced the photodegradation properties of PEG-based hydrogels (i.e., the structure-function relationship). The formulation with the fastest degradability was tested on two cell types and demonstrated good cell viability. The kinetics of photodegradation were evaluated, and customizable 3D cell cultures (e.g., hydrogel micropad arrays) were generated as examples.

5.2 Results and discussion

5.2.1 Synthesis of a combinatorial library

Despite being an attractive material for 3D cell culture,[108-109, 154-155] polymerized gelatin methacrylate is not degradable under 270 nm UV light for three reasons. GelMA substantially reduces the swellability of PEGDMA hydrogels because of its interaction with PEG.[156] One of the photodegradation mechanisms via formation of formyl radicals is less accessible for amides due to partial double bond character of the carbon-nitrogen bond in amides. Therefore, since methacrylate groups are tethered to gelatin's backbone via amide bonds, their photomediated scission is less favorable than ester-bound methacrylate groups in PEGMA. Furthermore, the aromatic amino acids of gelatin absorb UV light at 280 nm, thereby reducing its effective intensity. It was found that a 1% (w/v) GelMA solution exhibits an absorbance of

1.45 at 270 nm. Therefore, in order to identify a gelatin-containing PEG-composite hydrogel that, while still being cell-friendly, could be degraded in under 10 min, a combinatorial library comprising PEGMA, PEGDMA and GelMA (**Figure 48**) was constructed. The 10 min time frame was used as a benchmark for convenient handling. Also, sodium phenyl(2,4,6-trimethylbenzoyl)phosphinate (SAP) was synthesized and used as photoinitiator in cell-free experiments due to its enhanced solubility in water.

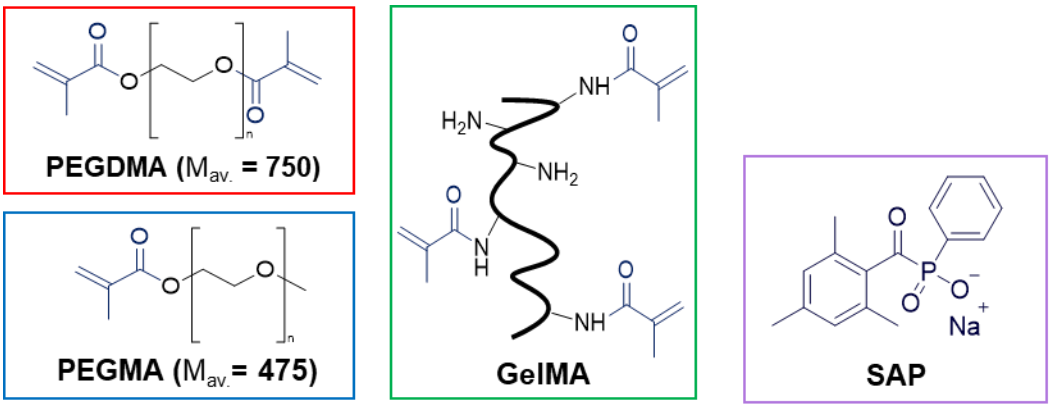

Figure 48. Chemical structure of monomers, crosslinker and photoinitiator used in the construction of a combinatorial library.

Through combinatorial synthesis, the dependance of several factors (i.e., amount of crosslinker, amount of monomers, and degree of monomer methacrylation) on photodegradability were systematically examined.

To map the structure-function relationship of each hydrogel composition and its degradability, the degree of GelMA methacrylation (20-35%, 50-60%, and 80-90% methacrylation, respectively defined as GelMA-low, medium, and high), its concentration in the prepolymerization mixture, and the concentration of PEGMA and PEGDMA were varied, resulting in 32 unique combinations (**Table 1**):

Number	MA	DMA	GelMA40	GelMA60	GelMA90	Degradability
1	7,77	0,52	0,032	0	0	91
2	7,77	0,52	0	0,048	0	81
3	7,77	0,52	0	0	0,072	71
4	5,18	0,52	0,064	0	0	54
5	5,18	0,52	0	0,096	0	57
6	5,18	0,52	0	0	0,144	43
7	2,59	0,52	0,096	0	0	30
8	2,59	0,52	0	0,144	0	35
9	2,59	0,52	0	0	0,216	33
10	7,77	0,312	0,032	0	0	100
11	7,77	0,312	0	0,048	0	100
12	7,77	0,312	0	0	0,072	83
13	5,18	0,312	0,064	0	0	64
14	5,18	0,312	0	0,096	0	66
15	5,18	0,312	0	0	0,144	67
16	2,59	0,312	0,096	0	0	34
17	2,59	0,312	0	0	0,216	25
18	3,45	0	0,10666667	0	0	33
19	3,45	0	0	0,16	0	37
20	3,45	0	0	0	0,24	27
21	5,18	0,156	0,064	0	0	31
22	5,18	0,156	0	0,096	0	27
23	7,77	0,156	0,064	0	0	23
23	7,77	0,156	0	0,096	0	24
25	3,89	0,104	0	0,128	0	28
26	6,48	0,37266667	0	0,072	0	54
27	5,00	0,52	0	0,072	0	67
28	3,97	0,52	0	0,072	0	83
29	3,97	0,52	0,096	0	0	45
30	5,18	0,52	0,048	0	0	70
31	5,18	0,52	0,072	0	0	40
32	4,7	0,52	0,06	0	0	70

Table 1. Combinatorial screening of 32 hydrogel prepolymerization mixtures with regard to their photodegradability after hydrogel formation. Entries in µmol per 240 µL prepolymerization mixture.

Crosslinking reactions and hydrogel formation were achieved via photopolymerization in a silicone mold (14 x 5 x 3 mm) at 360 nm at a lower intensity (6 mW/cm^2) for 2 min, benefiting from the non-contact, on-demand nature of photopolymerization and its biocompatibility. These characteristics will be important in subjecting the hit-composition to cell viability experiments.

After photopolymerization in a silicone mold, hydrogel pads were allowed to swell in deionized water for 24 h; pad dimensions were altered due to swelling (**Figure 49**). GelMA is known to reduce the swelling rate, hence why the swelling factor differed for each composition.

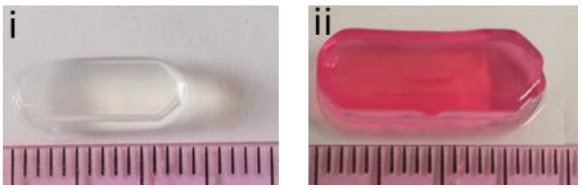

Figure 49. Photographs of an exemplary hydrogel (i) before swelling and (ii) after swelling in DMEM with scale.

Next, hydrogel pads were subjected to UV light (270 nm, 10 min, 22 mW/cm^2). Each hydrogel mass was measured before degradation and after removing liquid degradation products. The degradation ability was determined as follows:

$$degradation\ ability = \frac{m(before\ degradation) - m(after\ degradation)}{m(before\ degradation)}$$

The degradation ability ranged from completely degradable within 10 min (100% degradability) to only partially degradable (25%). Upon comparing gel compositions 1-3 with compositions 10-12, the proportion of bifunctional crosslinker PEGDMA declined 1.64-fold, leading to increased degradability for all GelMA functionalization degrees due to greater swellability. The degradability of GelMA-low- and -medium-containing gels thus shifted from 91% resp. 81% to complete degradability (100%). The correlations were identified for lower PEGMA concentrations with respect to water: a 1.64-fold reduction in crosslinker concentration led to an increase in degradability from 51% on average (gels 4–6) to 66% on average (gels 13–15). However, further dividing the crosslinker concentration by two resulted in reduced degradation, halving the degradation ability from 65% on average (gels 13 and 14) to 29% on average (gels 21 and 22) under the same PEGMA concentration.

The more GelMA was added, the worse the degradation behavior (**Table 1**, entries 4, 30 and 31). When using the same amounts of PEGMA and PEGDMA, 70% degradation was achieved with 1.88% GelMA-low with respect to water (gel 30). Adding 1.3x more GelMA-low reduced

the degradation to 54% (gel 4), and adding 1.5x GelMA-low slashed the degradation rate nearly twofold to 40% (gel 31).

Mathematic approximation was applied to map structure-function relationships. Absolute molar amounts of methacrylate moieties in PEGMA, PEGDMA, and in GelMA with different functionalization grades were used as input (x_1 to x_5, corresponding to PEGMA, PEGDMA, GelMA-low, GelMA-medium, and GelMA-high, respectively). The degradation ability was assessed as described earlier, expressed as a percentage and taken as an output variable. A multivariant square model without bilinear terms according to

$$y_{approx}=\mathbf{a}^T\mathbf{x}$$

with

$$\mathbf{a}^T=(a_1, \ldots, a_{11})$$

$$\mathbf{x}^T=(1, x_1, x_2, x_3, x_4, x_5, x_1^2, x_2^2, x_3^2, x_4^2, x_5^2)$$

was adapted for mathematical approximation, in which the ordinary least squares method was used. Over all 29 combinations, a mean error of degradation ability $\Sigma_{(i)}|y_i - y_{approx,i}|$ resulted in 6.6%, rendering the model reliable. This approximation resulted in the following quadratic equation for degradability (%), where n denotes the absolute amount of methacrylated moieties:

$$\text{Degradability} = 115.82 + 35.26\text{A} + 194.35\text{B} - 4763.23\text{C} - 3308.41\text{D} - 2252.01\text{E} - 3.48\text{A}^2 - 259.21\text{B}^2 + 29725.71\text{C}^2 + 14385.01\text{D}^2 + 6447.94\text{E}^2$$

A = n(PEGMA), B = n(PEGDMA), C = n(GelMA-low), D = n(GelMA-medium), and E = n(GelMA-high); substance amounts in µmol per 240 µL of prepolymerization mixture.

This equation confirms that adding any kind of GelMA to the prepolymerization mixture compromises degradation behavior, if applied to the following concentrations: C < 0.15, D < 0.23, and E < 0.35 (all tested compositions fell within these ranges).
The model also reveals the clear effect of the degree of GelMA functionalization on degradability. Specifically, GelMA-high influenced degradation most negatively, followed by GelMA-medium and GelMA-low. This finding aligns with GelMA-high exhibiting the worst swelling behavior, followed by GelMA-medium and GelMA-low.[157]

GelPEG-10 (15 wt% PEGMA with respect to water, 6.7 mol% PEGDMA with respect to PEGMA, 1.25 wt% GelMA-20 with respect to water) showed one of the highest degrees of degradability (i.e., completely degradable after 10 min UV irradiation) given more than twofold swelling after 24 h (from 5 × 13 × 4 mm to 7 × 18 × 5 mm). Therefore, this hydrogel composition was subjected to further biological experiments.

5.2.2 Cell experiments with a hit composition

A pure PEG-based polymethacrylate hydrogel exposes no bioactive sites and is therefore unsuitable for cell encapsulation. Supplementation with gelatin, offering Arg-Gly-Asp (RGD) sequences and matrix metalloproteinase (MMP) cleavage sites, promotes cell adherence and spreading within the hydrogel network. Conversely, combinatorial screening revealed the negative impact of GelMA on photodegradability, allowing the GelMA concentration to be as low as 1.25 wt% with respect to water in order to render the hydrogel completely photodegradable within 10 min. Supplementing PEGMA-gel with only 1.25 wt% GelMA-low was tested in regards of suitability of this hydrogel for cell encapsulation. The biocompatibility and cell viability of NHDF were tested for GelPEG-10 and for the analogous GelMA-free hydrogel, which served as a control. Whereas cells encapsulated in GelMA-free hydrogels showed low viability as expected, the composite GelPEG-10 hydrogel displayed advanced biocompatibility for at least 14 days upon photopolymerization (**Figure 50 A**) along with cell spreading (**Figure 50 B**).

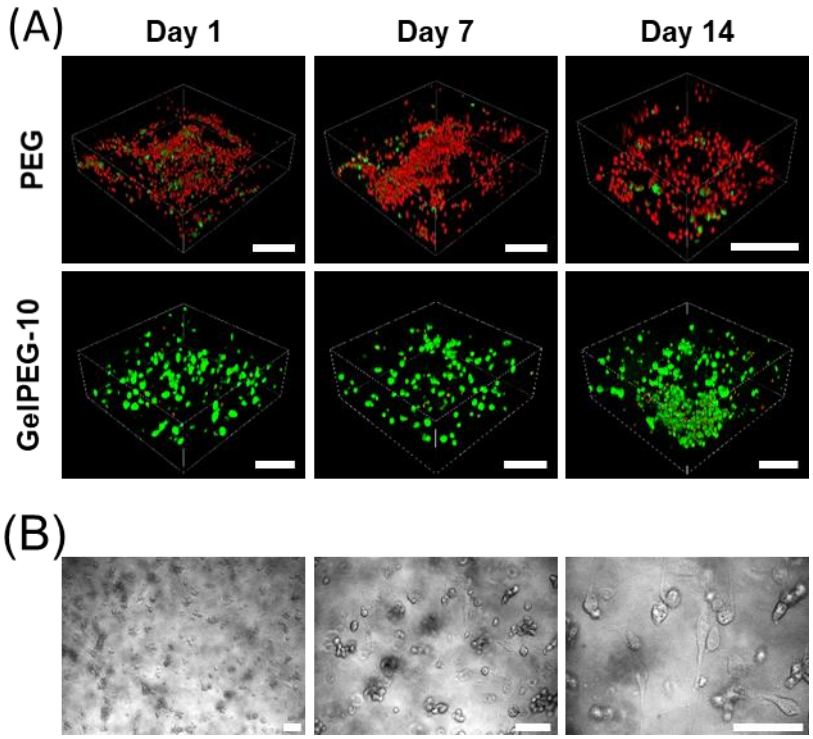

Figure 50. Cell encapsulation screenings of a "hit" hydrogel. (A) Live/dead staining of NHDF with calcein-AM (green, live cells) and PI (red, dead cells) embedded in PEG and GelPEG-10 hydrogels on day 1, 7, and 14 post-encapsulation, followed by imaging with confocal microscopy (Leica TCS SPE, scale bar: 200 µm). (B) Spreading of NHDF encapsulated in GelPEG-10 hydrogels on day 1 post-encapsulation (scale bar: 100 µm).

Altogether, the combinatorial screening resulted in a hydrogel composition that balances two counteracting forces and combines the advantageous properties of both: the strong encapsulation properties of GelMA and favorable UV degradability of PEGMA.

5.2.3 Optimization of a photodegradation procedure

Since the chosen cell medium (DMEM) contains UV-absorbing components (e.g., fetal calf serum [FCS] and phenol red [PR]), which could reduce the effective UV intensity required for complete hydrogel degradation, their influence on the degradation behavior of GelPEG-10 was assessed. In this experiment, GelPEG-10 was swollen in five liquids: 1) phosphate saline buffer (PBS); 2) PR- and FCS-free DMEM; 3) PR-containing and FCS-free DMEM; 4) FCS-containing and PR-free DMEM; and 5) FCS- and PR-containing DMEM **(Figure 51**).

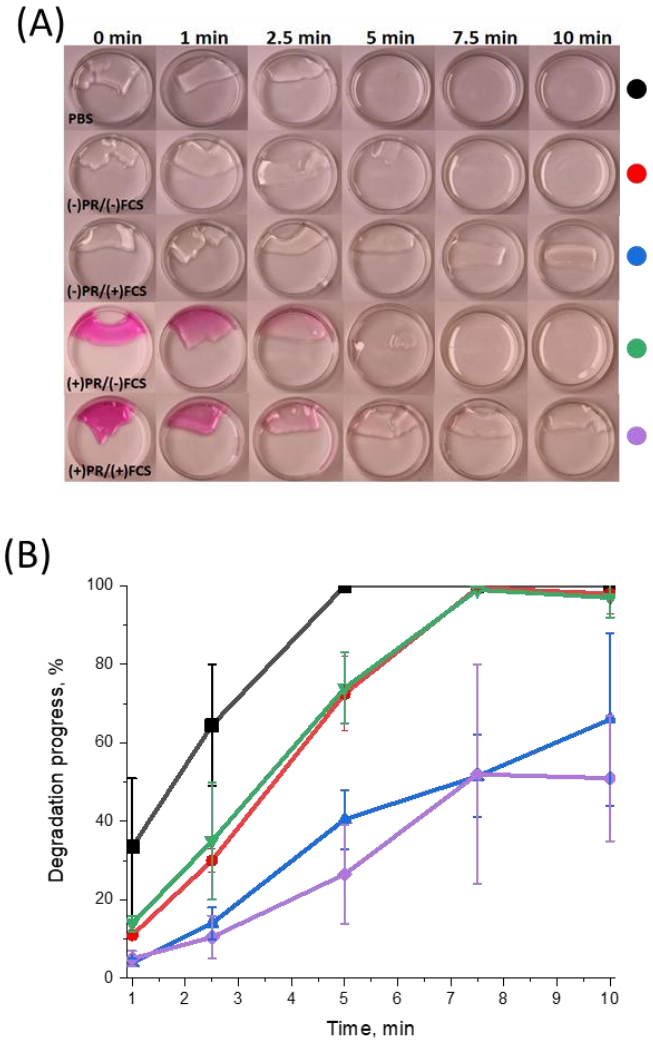

Figure 51. (A) Photograph depicting degradation behavior at different time points of GelPEG-10 swollen in PBS and in different PR-/FCS-containing/-lacking media. PR bleaching occurred within UV irradiation period, indicated by color shift from violet to colorless. (B) Quantification of gel degradation of GelPEG-10 swollen in PBS (black) and in different PR-/FCS-containing/-lacking DMEM (-PR, -FCS: red; -PR, +FCS: blue; +PR,-FCS: green; +PR, +FCS: lilac).

The GelPEG-10 swollen in PBS was completely degraded after 5 min irradiation. Although the presence of PR slowed complete degradation slightly, full degradation was reached after 10 min, similar to GelPEG-10 swollen in PBS. PR bleaching was observed prior to gel degradation. The degradation of GelPEG-10 swollen in FCS-free DMEM based on reduced gel thickness with increasing UV illumination time was also investigated; the fastest degradation occurred within the first 2 min (0.5 mm/min gel erosion; **Figure 52**):

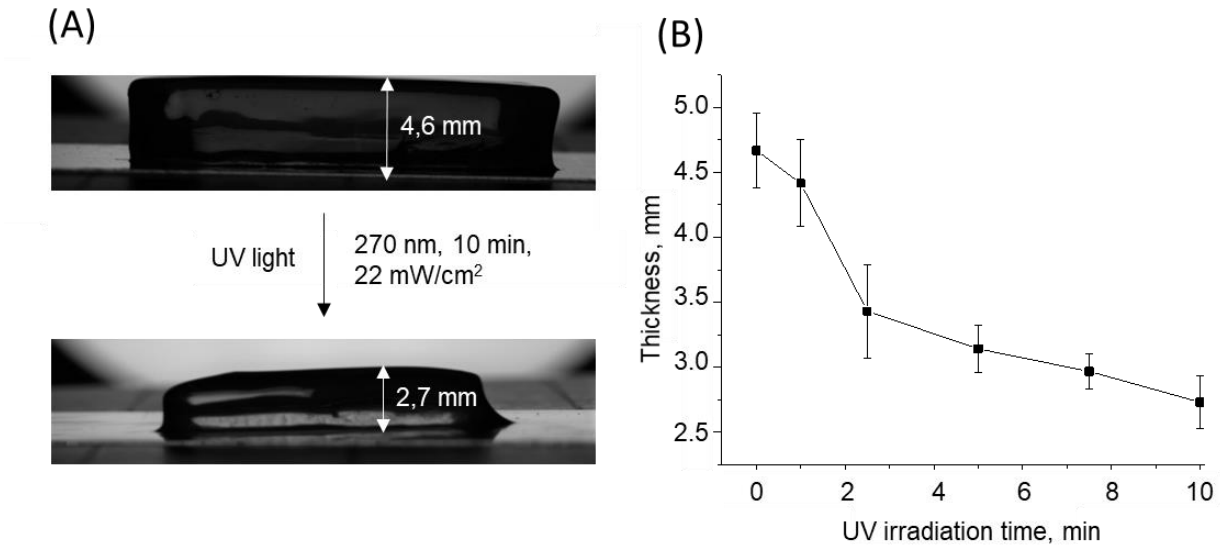

Figure 52. (A) Photograph depicting degradation behavior of GelPEG-10 swollen in FCS-free DMEM after 10 min UV irradiation. (B) Quantification of gel degradation of GelPEG-10 swollen in FCS-free DMEM, indicating dependence of gel thickness on irradiation time. Error bars are based on standard deviation of 3 repetitions in two independent experiments.

As anticipated, FCS containing a mixture of proteins and as the major component of DMEM (10%) significantly reduced the degradation ability of GelPEG-10 from 100% to about 60% after 10 min of UV exposure, with slightly worse degradation when combined with PR (**Figure 51**). Therefore, FCS must be eliminated prior to degradation to maintain a reasonable degradation time. Accordingly, cell viability upon FCS removal was examined. Three strategies were evaluated: 1) Incubation overnight in FCS-free medium; 2) Incubation overnight in FCS-containing medium and exchange against PBS to get rid of FCS; 3) Incubation overnight in FCS-containing medium and exchange against FCS-free medium to get rid of FCS. After cell-laden gels were incubated overnight and, if applicable, after FCS exchange, the gels were irradiated through the photomask with 270 nm UV light for 10 minutes. The viability was assessed after every step (before and after FCS exchange serving as a control); for irradiated gels the gel part covered with photomask was evaluated (**Figure 53**):

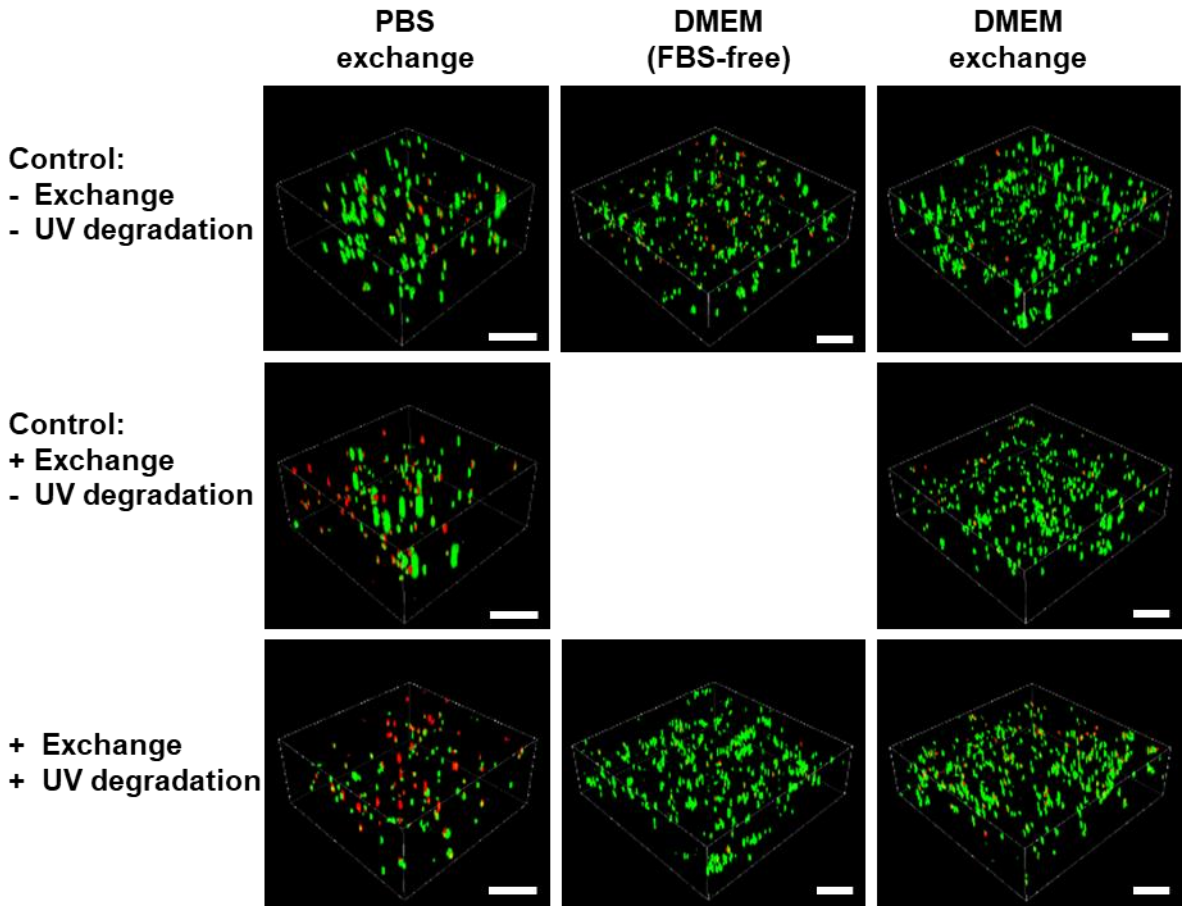

Figure 53. Live/dead staining of HeLa cells with calcein-AM (green, live cells) and PI (red, dead cells) embedded in GelPEG-10 hydrogels on day 3 post-encapsulation (on day 1 post-photodegradation respectively), followed by imaging via confocal microscopy (Leica TCS SPE; scale bar: 200 µm). FCS in cell media was removed using different approaches prior to photodegradation.

After gel incubation in FCS-containing DMEM, DMEM was exchanged against PBS for 3 h, which resulted in reduced cell viability because cells were not supplied with any nutrients during this period. DMEM exchange against FCS-free DMEM manifested as high cell viability despite the absence of growth factors for 4 h. Incubating cell-laden gels overnight in FCS-free DMEM yielded similar viability despite the absence of growth factors for 1 day. For further experiments, DMEM exchange against FCS-free DMEM was used.

5.2.4 Production of a free-standing hydrogel array

The hydrogel composition found in the combinatorial screening was used to produce an array of free-standing cell-containing hydrogel micropads, allowing for convenient on-demand production of arrayed matrices for 3D cell cultures (**Figure 54)**:

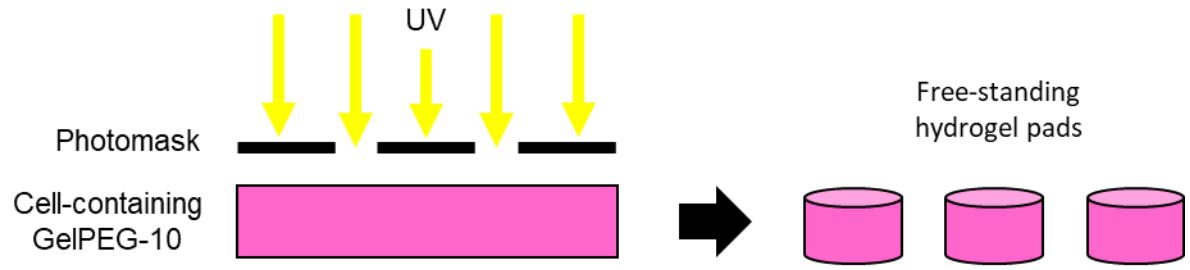

Figure 54. Schematic representation of on-demand hydrogel micropad array production.

First, a GelPEG-10 cell-containing hydrogel layer was produced and allowed to swell. After UV irradiation of the hydrogel layer through a photomask, array of free-standing hydrogel pads was obtained (**Figure 55**):

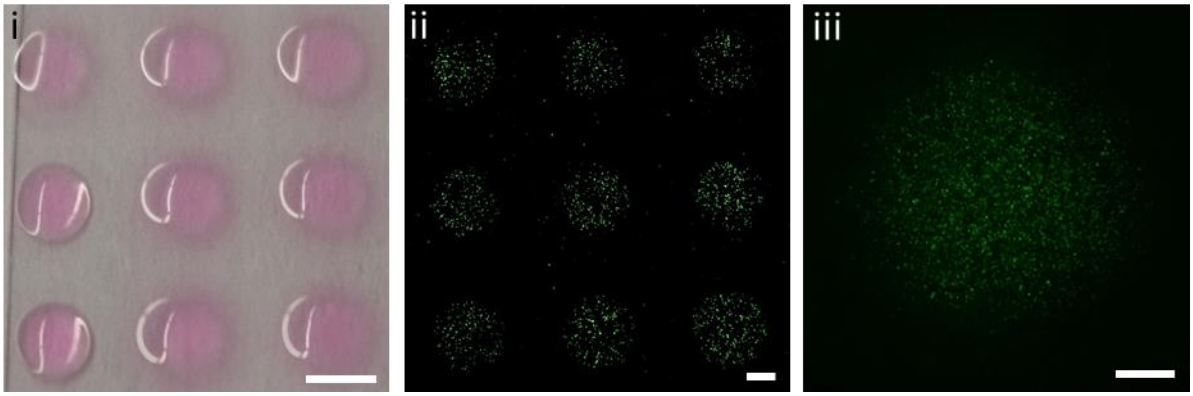

Figure 55. Free-standing hydrogel pads of various sizes incorporating HeLa-GFP cells, prepared by photodegradation of GelPEG-10 through a photomask of corresponding spot size (scale bar: 1 mm): (i) and (ii) 0.5-mm-thick hydrogel, 1.5 min UV; (iii) 4.5-mm-thick hydrogel, 10 min UV.

Two different photomasks (1 mm and 3 mm round spots) were used, highlighting the flexibility in the production of the hydrogel array. The black areas of the photomask prevented photodegradation of gel in the selected, customizable areas and enabled spatial control over degradation. The cells, which were not exposed to UV light due to coverage by chrome parts of the photomask, were not affected by UV light and exhibited high viability. Depending on the gel thickness, different illumination times were need to degrade the gel completely, whereas degradation time correlated with previously determined degradation curves (**Figure 52**).

5.2.5 Cell photoreleasing experiments

Light is a convenient non-contact and noncontaminant stimulus, which is readily used in biological settings, therefore, the possibility of photoreleasing cells from the hydrogels was assessed. Photorelease of cells benefits from high spatiotemporal and quantitative control by controlling the exposure time, place, and intensity. Importantly, to photorelease the cell from the gel, no prior installing of photoresponsive groups was needed, since the gel found via

combinatorial screening was inherently photodegradable by nature. The HeLa cell-containing GelPEG-10 gel was polymerized, incubated overnight, and the medium was exchange against FCS-free medium as described before. Afterwards, the gel was illuminated for 10 min with 270 nm UV light. HeLa cells released from 4.5-mm-thick GelPEG-10 gels after 10 min irradiation were transferred to an ibidi µ-slide and incubated overnight; live-dead staining indicated that 68% of cells were viable (**Figure 53):**

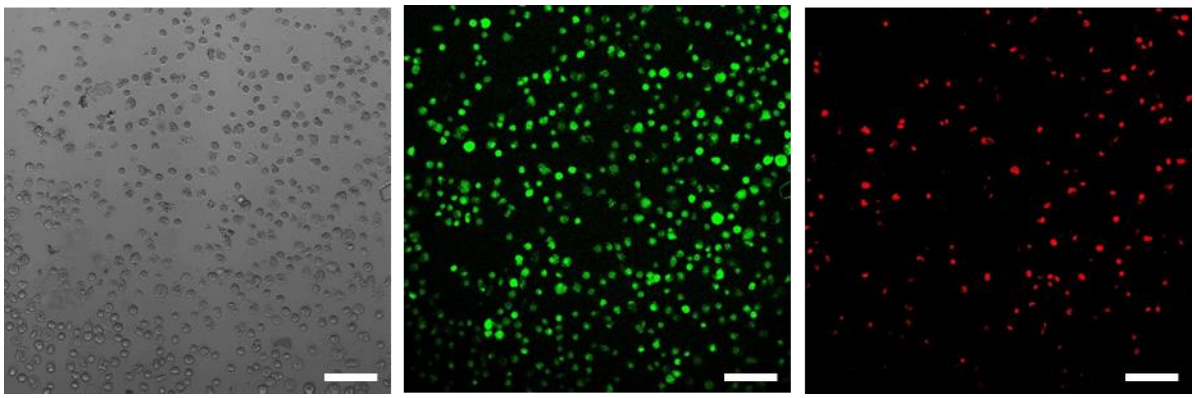

Figure 53. Live/dead staining of released HeLa cells from photodegraded GelPEG-10 hydrogel (scale bar: 100 µm): (i) brightfield; (ii) calcein-AM (green, live cells); (iii) PI (red, dead cells)

Even though the cells were exposed to short-wavelength UV light, their viability was comparatively high. Cells not exposed to UV light (i.e., due to a photomask) survived the process without damage (>90 % viability).

6 Conclusions and outlook

In this PhD work, Droplet Microarray was exploited for miniaturized high-throughput combinatorial synthesis of small molecules and smart materials, combining the synthesis with biological screening on the same chip and showing the potential to be used as a platform in the early stages of drug and material development. For both small molecule and smart material synthesis, the results indicated significant increase of the throughput and decrease of material consumption due to miniaturization. Furthermore, a novel cell-friendly inherently photodegradable hydrogel material was developed using the droplet microarray platform and combinatorial synthesis.

In Chapter 3, a potential of DMA as a miniaturized platform combining the possibility to perform combinatorial solid-phase synthesis with high-throughput cell screenings was demonstrated. The platform comprised a standard glass slide coated with nanoporous poly(2-hydroxyethyl methacrylate-*co*-ethylene dimethacrylate) layer, which was patterned with hydrophilic spots separated from each other by superhydrophobic liquid-impermeable barriers. The porous polymer inside the hydrophilic spots was functionalized with a nitrobenzene-based photolabile linker, which was used as a support to conduct solid-phase synthesis of an exemplary peptide library. The procedure of linker attachment was followed via XPS, ToF-SIMS and ATR-IR, and was optimized to reach the even loading. It was shown that reagent solutions (i.e. linker solution) wet the hydrophilic spot on surface as well in the bulk of the polymer, superhydrophobic borders preventing the liquid from spreading into the neighboring spots. Therefore, compartmentalization as a crucial prerequisite for contamination-free miniaturized combinatorial synthesis was confirmed. Upon irradiation with UV-light, products of the solid-phase synthesis could be released from the porous polymer and delivered into the separate droplets. It was shown that the amount of released compounds could be controlled by altering the irradiation time. Arrayed format enabled the combinatorial approach without the need for decoding. Thus, the light-induced release of the products allowed me to control the release spatially, temporally and quantitatively. In order to demonstrate the versatility and usability of the platform, high cell viability of HEK293 cells on the linker-modified surface, as well as upon UV exposure (360 nm, 6mW/cm^2, up to 15 min) was demonstrated.

To ensure convenient manual handling, round spots 2.83 mm in diameter were used for the optimization of linker loading and construction of combinatorial library. Being patterned with 2.83 mm round spot pattern, a standard microscopic glass slide in the size of 75 x 26 mm can accommodate 80 different reactions (less reactions if replicates are used). Smaller spots can be produced by utilizing corresponding photomask in the slide production process and can accommodate smaller volumes of liquid. For example, hydrophilic squares of 333x333 µm accommodate ca. 4 nL, and one patterned slide can be potentially used for running 6048

different reactions, increasing the throughput more than 75-fold. While conducting chemical synthesis on arrays with smaller features drastically increases the throughput and reduces material consumption, it inherently makes automated liquid handling robotics necessary. On this scale, precise handling and dispensing of low volumes in lower nanoliter range, evaporation of liquids, and reaction monitoring as well as analysis of the reaction yield and product purity are the challenges to address. These aspects of the chemBIOS pipeline, as well as expanding the reaction toolbox, are currently being under investigation. Thereby, the ability not only to synthesize libraries of compounds but also release them into individual cell microreservoirs with spatio-temporal control, possesses the potential for further advancement of miniaturized and high-throughput cell-based assays.

Similar to drug development, the traditional pipeline of hydrogel development includes individual one-by-one synthesis and characterization of hydrogels. This approach is associated with the disadvantages of low-throughput and high cost. As an alternative approach to classical one-by-one synthesis, high-throughput development of hydrogels is still tremendously under-represented in the field of responsive (especially photoresponsive) material development, despite the urgent requirement for such techniques. Furthermore, most high-throughput experimental set-ups lack confinement of every single polymer, rendering development of smart materials for cell encapsulation or materials for drug encapsulation impossible. In Chapter 4, DMA was used to develop methods of high-throughput combinatorial synthesis of responsive hydrogels. In DMA, hydrophilic regions separated by superhydrophobic liquid-impermeable barriers allowed deposition of various precursor solutions onto the hydrophilic spots without cross-contamination. The confinement of these solutions provided by the hydrophilic/superhydrophobic pattern allowed encapsulation of cells within the hydrogel, and enabled variation in hydrogel height and width. Proper mixing of chemicals within the nanoliter-sized droplets was proved by fluorescence measurements, Raman mapping and multiple particle tracking experiments. DMA was implemented for the synthesis of inherently photodegradable polymethacrylate-based hydrogels, constructing 53 unique hydrogels, to demonstrate the versatility and utility of the platform. The polymerization procedure was optimized concerning oxygen scavenging on 33 out of 36 unique prepolymerization mixtures, comprising variable proportion of monomers PEGMA and DMAEMA, as well as variable content of crosslinker PEGDMA. All starting material combinations were printed in quadruplicates, yielding 128 distinct hydrogel micropads pro experiment. Photodegradation studies were performed on 20 hydrogel compositions constructed of PEGMA, SAMA and PEGDMA, which vary in concentration of monomers and crosslinker. To ensure high reproducibility of the screening, 16 replicates of each composition were screened, amounting to 320 distinct hydrogel micropads. Arrayed format enabled the combinatorial approach without the need for decoding. The screening revealed strong positive correlation of the

photodegradation ability with crosslinker content, covering the range of degradability from non-degradable to rapidly degradable materials. (2-(*N*-3-sulfopropyl-*N*,*N*-dimethyl ammonium)ethyl methacrylate (SAMA) content revealed a smaller impact on the degradability, rendering high-SAMA-content hydrogels more photodegradable. In total, the number of replicates amounted to approximately 450 hydrogel micropads, which required less than 60 µL of precursor solutions, highlighting the highly miniaturized nature of developed pipeline. High-throughput synthesis and screening gave quick insights into the structure/function relationships, enabling a customized variation of degradation kinetics by the choice of particular hydrogel precursors. Importantly, the temporal and spatial control over the degradation allowed facile one-step on-demand formation of arbitrary hydrogel patterns by UV-irradiation, as shown exemplarily by construction of a checkerboard pattern.

Since the number of printable additives is immense, one can cover a large combinatorial space through high-throughput screening over a multitude of hydrogel pre-polymerization mixtures (including for example peptides that promote cell adhesion, fibronectin, laminin, hyaluronic acid, dextran, chitosan to identify biomaterials). By its compartmentalized features, DMA offers the possibility to study cell encapsulation parameters; therefore, the proposed workflow represents an imaginably promising approach to facilitate fine-tuning of the biochemical and/or biophysical properties of hydrogels and identification of optimal candidates for a certain application such as recapitulation of the complexity of extracellular matrix to optimize materials for cell encapsulation. Deliberate employment of high-throughput methodologies has a great potential to develop materials that tangentially attain the complexity of natural dynamic systems. Given the complex interplay of multiple stimuli in vivo, methods for the in vivo testing of such combinatorial libraries of responsive materials should also be further explored.[158]

Considering that proposed hydrogel synthesis takes place in confined microenvironment, elaborated workflow can be particularly useful in developing hydrogels for drug-delivery applications. Variety of stimuli can be exploited to trigger drug release into the confined microcompartments. Thereupon, released drugs can be subjected to further analytical methods to e.g. determine the kinetics of release. Compartmentalization prevents cross-contamination between the spots, which is inevitable on state-of-the-art nonpatterned surfaces. Materials for drug release are often not designed rationally, so combinatorial high-throughput screening over random libraries might play an ever-bigger role in their development. Confined spaces themselves could be potentially used as a trigger, i.e. in development of injectable hydrogels that react differently to different pore size. Finally, high-throughput combinatorial synthesis of responsive hydrogels can be of importance to develop materials with complex stimulus/response patterns **(Figure 54).** The following patterns are conceivable: A) external stimulus is used to first synthesize the material and then trigger the

response (e.g. photo-polymerizable and photo-degradable hydrogels);[130] B) one stimulus triggers several responses (simplifying the application of the material); C) multiple responses are orthogonal (independent from each other) and can occur simultaneously or delayed from each other in time (the time and chronological order of responses can be fine-tuned); D) multiple responses are coupled (upon trigger, a material responds in a certain manner, which causes other responses via the domino principle); E) multiple stimuli trigger one response (allows more flexibility in application); F) chronologically first stimulus can switch on/off or fine-tune the response upon second stimulus (as e.g. presence of ions, redox factors and light can trigger next response, e.g. thermoresponsiveness).[159]

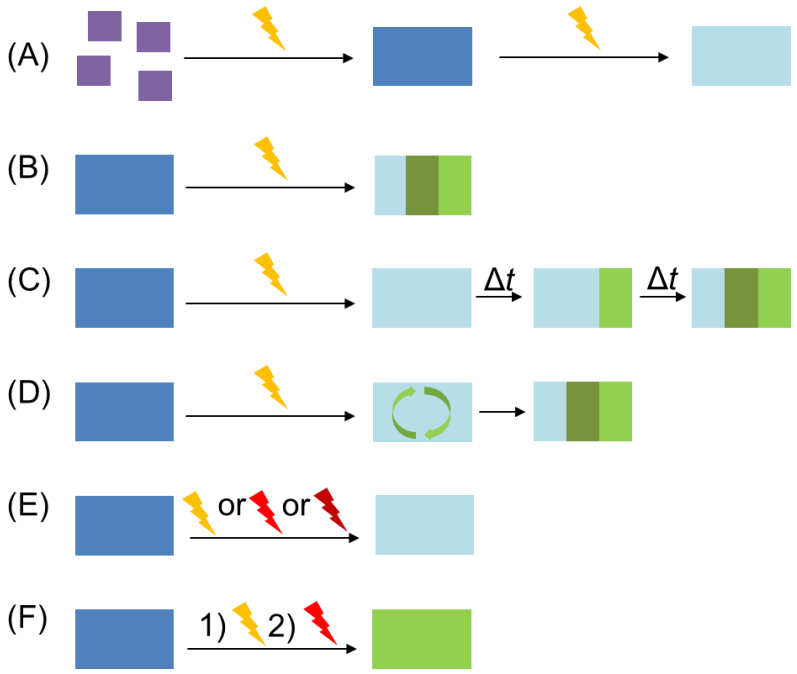

Figure 54. Combinatorial high-throughput methods can accelerate the search for materials with complex stimuli-responsive patterns. Examples of possible patterns are described. Alisa Rosenfeld; Pavel A. Levkin. High-Throughput Combinatorial Synthesis of Stimuli-Responsive Materials. Advanced Biosystems, 2019, 1800293, Copyright Wiley-VCH GmbH. Reproduced with permission.

As already mentioned, light-based microfabrication techniques constitute an indispensable approach to fabricate tissue assemblies, benefiting from non-contact spatially and temporarily controlled manipulation of soft matter. Light-triggered degradation of soft materials, such as hydrogels, is also important in tissue engineering, bioprinting, and related fields. The photoresponsiveness of hydrogels is generally not intrinsic and requires complex synthetic procedures wherein photoresponsive groups are incorporated into the hydrogel. As an exception, poly(PEG)-methacrylate-based hydrogels are intrinsically photodegradable by 270 nm UV light.[129] However, due to non-adhesiveness of PEG chains for cells, cells cannot be encapsulated within poly(PEG)-methacrylate hydrogels. In contrary, gelatin methacrylate is a well-suited substrate for 3D cell culture. Yet, preliminary experiments have shown the non-degradability of gelatin polymethacrylate under 270 nm UV light. In chapter 5, a novel

biocompatible and inherently photodegradable poly(ethyleneglycol) methacrylate (PEGMA)-based gelatin methacrylate (GelMA)-containing hydrogel was presented, which balances the cell adhesiveness of gelatin and proneness to photodegradability of PEG-polymethacrylate. This hydrogel was found as a result of combinatorial synthesis of 32 hydrogels and can be used as a 3D matrix for culturing cells for at least 14 days. The hydrogel degradation procedure was optimized in regards to swelling liquid. It was demonstrated that developed cell-containing gels could be conveniently and quickly degraded via UV irradiation for 10 min to produce free-standing cell-laden hydrogel particles without damaging the cells. These structures can be flexibly produced on demand. In particular, polymerization, swelling and subsequent photodegradation using a photomask has several advantages over using a photomask already at the stage of photopolymerization. First, photodegradation being separated in time from the polymerization offers flexibility in experimental design (e.g., first a hydrogel layer, then an array of hydrogel micropads), whereas using the photomask already during the photopolymerization determines the geometrical form of the hydrogel from the very beginning. In addition, if the hydrogels are allowed to swell after polymerization, the photodegradation leads to stable high-resolved features. This avoids the swelling-induced distortion of the features in hydrogels produced by photopolymerization using a photomask. Furthermore, the synthetic character of methacrylates enables finetuning of hydrogel properties, thus encouraging the use of miniaturized combinatorial screening of hydrogels to ensure rapid adjustment for specific applications. The described approach could be useful in applications of photoresponsive and biocompatible materials (e.g., as sacrificial layers to mirror vascular systems), micrometer-scale cell-laden hydrogel particles for modular biofabrication, and responsive bimodal hydrogel systems.

7 References

1. https://www.fda.gov/Drugs/DevelopmentApprovalProcess/DrugInnovation/ucm534863.htm (accessed 19.01.18).

2. Eder, J.; Sedrani, R.; Wiesmann, C., The discovery of first-in-class drugs: origins and evolution. *Nature Reviews Drug Discovery* **2014,** *13* (8), 577-587.

3. Chong, C. R.; Sullivan Jr, D. J., New uses for old drugs. *Nature* **2007,** *448*, 645.

4. DiMasi, J. A.; Grabowski, H. G.; Hansen, R. W., Innovation in the pharmaceutical industry: New estimates of R&D costs. *Journal of Health Economics* **2016,** *47*, 20-33.

5. Hong, J. A.; Neel, D. V.; Wassaf, D.; Caballero, F.; Koehler, A. N., Recent discoveries and applications involving small-molecule microarrays. *Current opinion in chemical biology* **2014,** *18*, 21-28.

6. http://zinc.docking.org/browse/subsets/ http://zinc.docking.org/browse/subsets/ (accessed 09.01.2018).

7. Smith, A., Screening for drug discovery: The leading question. *Nature* **2002,** *418*, 453.

8. Fernandes, T. G.; Diogo, M. M.; Clark, D. S.; Dordick, J. S.; Cabral, J. M. S., High-throughput cellular microarray platforms: applications in drug discovery, toxicology and stem cell research. *Trends in biotechnology* **2009,** *27* (6), 342-349.

9. Trevino, V.; Falciani, F.; Barrera-Saldaña, H. A., DNA microarrays: a powerful genomic tool for biomedical and clinical research. *Molecular Medicine* **2007,** *13* (9-10), 527-541.

10. Wang, L.; Li, P. C. H., Microfluidic DNA microarray analysis: A review. *Analytica Chimica Acta* **2011,** *687* (1), 12-27.

11. Heller, M. J., DNA Microarray Technology: Devices, Systems, and Applications. *Annual Review of Biomedical Engineering* **2002,** *4* (1), 129-153.

12. Falsey, J. R.; Renil, M.; Park, S.; Li, S.; Lam, K. S., Peptide and Small Molecule Microarray for High Throughput Cell Adhesion and Functional Assays. *Bioconjugate Chemistry* **2001,** *12* (3), 346-353.

13. Frank, R., Spot-synthesis: an easy technique for the positionally addressable, parallel chemical synthesis on a membrane support. *Tetrahedron* **1992,** *48* (42), 9217-9232.

14. MacBeath, G.; Schreiber, S. L., Printing Proteins as Microarrays for High-Throughput Function Determination. *Science* **2000,** *289* (5485), 1760-1763.

15. MacBeath, G.; Koehler, A. N.; Schreiber, S. L., Printing Small Molecules as Microarrays and Detecting Protein−Ligand Interactions en Masse. *Journal of the American Chemical Society* **1999,** *121* (34), 7967-7968.

16. Blackwell, H. E., Hitting the SPOT: small-molecule macroarrays advance combinatorial synthesis. *Current Opinion in Chemical Biology* **2006,** *10* (3), 203-212.

17. Manimala, J. C.; Roach, T. A.; Li, Z.; Gildersleeve, J. C., High-Throughput Carbohydrate Microarray Analysis of 24 Lectins. *Angewandte Chemie International Edition* **2006,** *45* (22), 3607-3610.

18. Ban, L.; Mrksich, M., On-Chip Synthesis and Label-Free Assays of Oligosaccharide Arrays. *Angewandte Chemie International Edition* **2008,** *47* (18), 3396-3399.

19. Anderson, D. G.; Levenberg, S.; Langer, R., Nanoliter-scale synthesis of arrayed biomaterials and application to human embryonic stem cells. *Nature Biotechnology* **2004,** *22*, 863.

20. Maskos, U.; Southern, E. M., Oligonucleotide hybridizations on glass supports: a novel linker for oligonucleotide synthesis and hybridization properties of oligonucleotides synthesised in situ. *Nucleic acids research* **1992,** *20* (7), 1679-1684.

21. Trevino, V.; Falciani, F.; Barrera-Saldaña, H. A., DNA microarrays: a powerful genomic tool for biomedical and clinical research. *Mol Med* **2007,** *13* (9-10), 527-541.

22. Fodor, S.; Read, J.; Pirrung, M.; Stryer, L.; Lu, A.; Solas, D., Light-directed, spatially addressable parallel chemical synthesis. *Science* **1991,** *251* (4995), 767-773.

23. Beyer, M.; Nesterov, A.; Block, I.; König, K.; Felgenhauer, T.; Fernandez, S.; Leibe, K.; Torralba, G.; Hausmann, M.; Trunk, U.; Lindenstruth, V.; Bischoff, F. R.; Stadler, V.; Breitling, F., Combinatorial Synthesis of Peptide Arrays onto a Microchip. *Science* **2007,** *318* (5858), 1888-1888.

24. Atwater, J.; Mattes, D. S.; Streit, B.; von Bojničić-Kninski, C.; Loeffler, F. F.; Breitling, F.; Fuchs, H.; Hirtz, M., Combinatorial Synthesis of Macromolecular Arrays by Microchannel Cantilever Spotting (μCS). *Advanced Materials* **2018,** *30* (31), 1801632.

25. Manimala, J. C.; Roach, T. A.; Li, Z.; Gildersleeve, J. C., High-Throughput Carbohydrate Microarray Analysis of 24 Lectins. *Angewandte Chemie* **2006,** *118* (22), 3689-3692.

26. Ban, L.; Mrksich, M., On-chip synthesis and label-free assays of oligosaccharide arrays. *Angew Chem Int Ed Engl* **2008,** *47* (18), 3396-3399.

27. Goldflam, M.; Ullman, C. G., Recent Advances Toward the Discovery of Drug-Like Peptides De novo. *Frontiers in chemistry* **2015,** *3*, 69-69.

28. Carbonell, C.; Stylianou, K. C.; Hernando, J.; Evangelio, E.; Barnett, S. A.; Nettikadan, S.; Imaz, I.; Maspoch, D., Femtolitre chemistry assisted by microfluidic pen lithography. *Nature Communications* **2013,** *4* (1), 2173.

29. Yang, J.; Rose, F. R. A. J.; Gadegaard, N.; Alexander, M. R., A High-Throughput Assay of Cell-Surface Interactions using Topographical and Chemical Gradients. *Advanced Materials* **2009,** *21* (3), 300-304.

30. Ankam, S.; Teo, B. K. K.; Kukumberg, M.; Yim, E. K. F., High throughput screening to investigate the interaction of stem cells with their extracellular microenvironment. *Organogenesis* **2013,** *9* (3), 128-142.

31. Flaim, C. J.; Chien, S.; Bhatia, S. N., An extracellular matrix microarray for probing cellular differentiation. *Nature Methods* **2005,** *2*, 119.

32. Hilpert, K.; Elliott, M.; Jenssen, H.; Kindrachuk, J.; Fjell, C. D.; Körner, J.; Winkler, D. F. H.; Weaver, L. L.; Henklein, P.; Ulrich, A. S.; Chiang, S. H. Y.; Farmer, S. W.; Pante, N.; Volkmer, R.; Hancock, R. E. W., Screening and Characterization of Surface-Tethered Cationic Peptides for Antimicrobial Activity. *Chemistry & Biology* **2009,** *16* (1), 58-69.

33. Reineke, U.; Sabat, R.; Misselwitz, R.; Welfle, H.; Volk, H.-D.; Schneider-Mergener, J., A synthetic mimic of a discontinuous binding site on interleukin-10. *Nature Biotechnology* **1999,** *17*, 271.

34. Wenschuh, H.; Volkmer-Engert, R.; Schmidt, M.; Schulz, M.; Schneider-Mergener, J.; Reineke, U., Coherent membrane supports for parallel microsynthesis and screening of bioactive peptides. *Peptide Science* **2000,** *55* (3), 188-206.

35. Kleiner, R. E.; Dumelin, C. E.; Liu, D. R., Small-Molecule Discovery from DNA-Encoded Chemical Libraries(). *Chemical Society reviews* **2011,** *40* (12), 5707-5717.

36. Duncombe, T. A.; Tentori, A. M.; Herr, A. E., Microfluidics: reframing biological enquiry. *Nature Reviews Molecular Cell Biology* **2015,** *16*, 554.

37. Klouda, L., Thermoresponsive hydrogels in biomedical applications: A seven-year update. *European Journal of Pharmaceutics and Biopharmaceutics* **2015,** *97*, 338-349.

38. Kim, Y.-J.; Matsunaga, Y. T., Thermo-responsive polymers and their application as smart biomaterials. *Journal of Materials Chemistry B* **2017,** *5* (23), 4307-4321.

39. Bertrand, O.; Gohy, J.-F., Photo-responsive polymers: synthesis and applications. *Polymer Chemistry* **2017,** *8* (1), 52-73.

40. Manouras, T.; Vamvakaki, M., Field responsive materials: photo-, electro-, magnetic- and ultrasound-sensitive polymers. *Polymer Chemistry* **2017,** *8* (1), 74-96.

41. Li, L.; Scheiger, J. M.; Levkin, P. A., Design and Applications of Photoresponsive Hydrogels. *Advanced Materials* **2019,** *31* (26), 1807333.

42. Wiggins, K. M.; Brantley, J. N.; Bielawski, C. W., Methods for activating and characterizing mechanically responsive polymers. *Chemical Society Reviews* **2013,** *42* (17), 7130-7147.

43. Kocak, G.; Tuncer, C.; Butun, V., pH-Responsive polymers. *Polymer Chemistry* **2017,** *8* (1), 144-176.

44. Dai, S.; Ravi, P.; Tam, K., *pH-Responsive polymers: Synthesis, properties and applications*. 2008; Vol. 4, p 435-449.

45. Nucara, L.; Piazza, V.; Greco, F.; Robbiano, V.; Cappello, V.; Gemmi, M.; Cacialli, F.; Mattoli, V., Ionic Strength Responsive Sulfonated Polystyrene Opals. *ACS Applied Materials & Interfaces* **2017,** *9* (5), 4818-4827.

46. Wen, H.; Chen, S.; Ge, Z.; Zhuo, H.; Ling, J.; Liu, Q., Development of humidity-responsive self-healing zwitterionic polyurethanes for renewable shape memory applications. *RSC Advances* **2017,** *7* (50), 31525-31534.

47. Yang, T.; Ji, R.; Deng, X.-X.; Du, F.-S.; Li, Z.-C., Glucose-responsive hydrogels based on dynamic covalent chemistry and inclusion complexation. *Soft Matter* **2014,** *10* (15), 2671-2678.

48. Dong, Y.; Wang, W.; Veiseh, O.; Appel, E. A.; Xue, K.; Webber, M. J.; Tang, B. C.; Yang, X.-W.; Weir, G. C.; Langer, R.; Anderson, D. G., Injectable and Glucose-Responsive Hydrogels Based on Boronic Acid–Glucose Complexation. *Langmuir* **2016,** *32* (34), 8743-8747.

49. Liu, H.; Lin, S.; Feng, Y.; Theato, P., CO2-Responsive polymer materials. *Polymer Chemistry* **2017,** *8* (1), 12-23.

50. Darabi, A.; Jessop, P. G.; Cunningham, M. F., CO2-responsive polymeric materials: synthesis, self-assembly, and functional applications. *Chemical Society Reviews* **2016,** *45* (15), 4391-4436.

51. Huo, M.; Yuan, J.; Tao, L.; Wei, Y., Redox-responsive polymers for drug delivery: from molecular design to applications. *Polymer Chemistry* **2014,** *5* (5), 1519-1528.

52. Zhang, X.; Han, L.; Liu, M.; Wang, K.; Tao, L.; Wan, Q.; Wei, Y., Recent progress and advances in redox-responsive polymers as controlled delivery nanoplatforms. *Materials Chemistry Frontiers* **2017,** *1* (5), 807-822.

53. Zelzer, M.; Ulijn, R. V., 6 - Enzyme-responsive polymers: properties, synthesis and applications. In *Smart Polymers and their Applications*, Aguilar, M. R.; San Román, J., Eds. Woodhead Publishing: 2014; pp 166-203.

54. Xu, F.-J.; Kang, E.-T.; Neoh, K.-G., pH- and temperature-responsive hydrogels from crosslinked triblock copolymers prepared via consecutive atom transfer radical polymerizations. *Biomaterials* **2006,** *27* (14), 2787-2797.

55. Jochum, F. D.; Theato, P., Temperature- and light-responsive smart polymer materials. *Chemical Society Reviews* **2013,** *42* (17), 7468-7483.

56. Zhuang, J.; Gordon, M. R.; Ventura, J.; Li, L.; Thayumanavan, S., Multi-stimuli responsive macromolecules and their assemblies. *Chemical Society Reviews* **2013,** *42* (17), 7421-7435.

57. Cremaldi, J. C.; Bhushan, B., Bioinspired self-healing materials: lessons from nature. *Beilstein J Nanotechnol* **2018,** *9*, 907-935.

58. Ulijn, R. V., Enzyme-responsive materials: a new class of smart biomaterials. *Journal of Materials Chemistry* **2006,** *16* (23), 2217-2225.

59. Yoshida, R., Self-Oscillating Gels Driven by the Belousov–Zhabotinsky Reaction as Novel Smart Materials. *Advanced Materials* **2010,** *22* (31), 3463-3483.

60. Yoshida, R.; Ueki, T., Evolution of self-oscillating polymer gels as autonomous polymer systems. *Npg Asia Materials* **2014,** *6*, e107.

61. Rosso, F.; Marino, G.; Giordano, A.; Barbarisi, M.; Parmeggiani, D.; Barbarisi, A., Smart materials as scaffolds for tissue engineering. *Journal of Cellular Physiology* **2005,** *203* (3), 465-470.

62. Hawkes, E. W.; Cutkosky, M. R., Design of Materials and Mechanisms for Responsive Robots. *Annual Review of Control, Robotics, and Autonomous Systems* **2018,** *1* (1), 359-384.

63. Tzou, H. S.; Lee, H. J.; Arnold, S. M., Smart Materials, Precision Sensors/Actuators, Smart Structures, and Structronic Systems. *Mechanics of Advanced Materials and Structures* **2004,** *11* (4-5), 367-393.

64. da Silva, R. M. P.; Mano, J. F.; Reis, R. L., Smart thermoresponsive coatings and surfaces for tissue engineering: switching cell-material boundaries. *Trends in Biotechnology* **2007,** *25* (12), 577-583.

65. Zhang, R.; Liberski, A.; Sanchez-Martin, R.; Bradley, M., Microarrays of over 2000 hydrogels – Identification of substrates for cellular trapping and thermally triggered release. *Biomaterials* **2009,** *30* (31), 6193-6201.

66. Zhang, R.; Mjoseng, H. K.; Hoeve, M. A.; Bauer, N. G.; Pells, S.; Besseling, R.; Velugotla, S.; Tourniaire, G.; Kishen, R. E. B.; Tsenkina, Y.; Armit, C.; Duffy, C. R. E.; Helfen, M.; Edenhofer, F.; de Sousa, P. A.; Bradley, M., A thermoresponsive and chemically defined hydrogel for long-term culture of human embryonic stem cells. *Nature communications* **2013,** *4*, 1335-1335.

67. Hook, A. L.; Scurr, D. J.; Anderson, D. G.; Langer, R.; Williams, P.; Davies, M.; Alexander, M., High throughput discovery of thermo-responsive materials using water contact angle measurements and time-of-flight secondary ion mass spectrometry. *Surface and Interface Analysis* **2013,** *45* (1), 181-184.

68. Hook, A. L.; Chang, C.-Y.; Scurr, D. J.; Langer, R.; Anderson, D. G.; Williams, P.; Davies, M. C.; Alexander, M. R., Thermally switchable polymers achieve controlled Escherichia coli detachment. *Advanced healthcare materials* **2014,** *3* (7), 1020-1025.

69. Wang, G.; Duan, Z.; Sheng, Y.; Neumann, K.; Deng, L.; Li, J.; Bradley, M.; Zhang, R., Tuning the emission properties of a fluorescent polymer using a polymer microarray approach - identification of an optothermo responsive polymer. *Chemical Communications* **2016,** *52* (69), 10521-10524.

70. Becer, C. R.; Hahn, S.; Fijten, M. W. M.; Thijs, H. M. L.; Hoogenboom, R.; Schubert, U. S., Libraries of methacrylic acid and oligo(ethylene glycol) methacrylate copolymers with LCST behavior. *Journal of Polymer Science Part A: Polymer Chemistry* **2008,** *46* (21), 7138-7147.

71. Hook, A. L.; Yang, J.; Chen, X.; Roberts, C. J.; Mei, Y.; Anderson, D. G.; Langer, R.; Alexander, M. R.; Davies, M. C., Polymers with hydro-responsive topography identified using high throughput AFM of an acrylate microarray. *Soft Matter* **2011,** *7* (16), 7194-7197.

72. Lynn, D. M.; Anderson, D. G.; Putnam, D.; Langer, R., Accelerated Discovery of Synthetic Transfection Vectors: Parallel Synthesis and Screening of a Degradable Polymer Library. *Journal of the American Chemical Society* **2001,** *123* (33), 8155-8156.

73. Anderson, D. G.; Lynn, D. M.; Langer, R., Semi-Automated Synthesis and Screening of a Large Library of Degradable Cationic Polymers for Gene Delivery. *Angewandte Chemie International Edition* **2003,** *42* (27), 3153-3158.

74. Khan, F.; Valere, S.; Fuhrmann, S.; Arrighi, V.; Bradley, M., Synthesis and cellular compatibility of multi-block biodegradable poly(?-caprolactone)-based polyurethanes. *Journal of Materials Chemistry B* **2013,** *1* (20), 2590-2600.

75. Drury, J. L.; Mooney, D. J., Hydrogels for tissue engineering: scaffold design variables and applications. *Biomaterials* **2003,** *24* (24), 4337-4351.

76. Anderson, D. G.; Tweedie, C. A.; Hossain, N.; Navarro, S. M.; Brey, D. M.; Van Vliet, K. J.; Langer, R.; Burdick, J. A., A Combinatorial Library of Photocrosslinkable and Degradable Materials. *Advanced Materials* **2006,** *18* (19), 2614-2618.

77. Brey, D. M.; Chung, C.; Hankenson, K. D.; Garino, J. P.; Burdick, J. A., Identification of Osteoconductive and Biodegradable Polymers from a Combinatorial Polymer Library. *Journal of Biomedical Materials Research. Part a* **2010,** *93* (2), 807-816.

78. Luef, K. P.; Petit, C.; Ottersböck, B.; Oreski, G.; Ehrenfeld, F.; Grassl, B.; Reynaud, S.; Wiesbrock, F., UV-mediated thiol-ene click reactions for the synthesis of drug-loadable and degradable gels based on copoly(2-oxazoline)s. *European Polymer Journal* **2017,** *88*, 701-712.

79. Deng, X.; Zheng, N.; Song, Z.; Yin, L.; Cheng, J., Trigger-responsive, fast-degradable poly(β-amino ester)s for enhanced DNA unpackaging and reduced toxicity. *Biomaterials* **2014,** *35* (18), 5006-5015.

80. Nehls, E. M.; Rosales, A. M.; Anseth, K. S., Enhanced user-control of small molecule drug release from a poly(ethylene glycol) hydrogel via azobenzene/cyclodextrin complex tethers. *Journal of Materials Chemistry B* **2016,** *4* (6), 1035-1039.

81. Qiu, M.; Wang, D.; Liang, W.; Liu, L.; Zhang, Y.; Chen, X.; Sang, D. K.; Xing, C.; Li, Z.; Dong, B.; Xing, F.; Fan, D.; Bao, S.; Zhang, H.; Cao, Y., Novel concept of the smart NIR-light-controlled drug release of black phosphorus nanostructure for cancer therapy. *Proceedings of the National Academy of Sciences of the United States of America* **2018,** *115* (3), 501-506.

82. Lee, T. T.; García, J. R.; Paez, J. I.; Singh, A.; Phelps, E. A.; Weis, S.; Shafiq, Z.; Shekaran, A.; Del Campo, A.; García, A. J., Light-triggered in vivo activation of adhesive peptides regulates cell adhesion, inflammation and vascularization of biomaterials. *Nature materials* **2015,** *14* (3), 352-360.

83. Hahn, M. S.; Miller, J. S.; West, J. L., Three-Dimensional Biochemical and Biomechanical Patterning of Hydrogels for Guiding Cell Behavior. *Advanced Materials* **2006,** *18* (20), 2679-2684.

84. DeForest, C. A.; Polizzotti, B. D.; Anseth, K. S., Sequential click reactions for synthesizing and patterning three-dimensional cell microenvironments. *Nature materials* **2009,** *8* (8), 659-664.

85. Griffin, D. R.; Kasko, A. M., Photodegradable macromers and hydrogels for live cell encapsulation and release. *Journal of the American Chemical Society* **2012,** *134* (31), 13103-13107.

86. Bai, T.; Sinclair, A.; Sun, F.; Jain, P.; Hung, H.-C.; Zhang, P.; Ella-Menye, J.-R.; Liu, W.; Jiang, S., Harnessing isomerization-mediated manipulation of nonspecific cell/matrix interactions to reversibly trigger and suspend stem cell differentiation. *Chemical Science* **2016,** *7* (1), 333-338.

87. Lee, I. N.; Dobre, O.; Richards, D.; Ballestrem, C.; Curran, J. M.; Hunt, J. A.; Richardson, S. M.; Swift, J.; Wong, L. S., Photoresponsive Hydrogels with Photoswitchable Mechanical Properties Allow Time-Resolved Analysis of Cellular Responses to Matrix Stiffening. *ACS applied materials & interfaces* **2018,** *10* (9), 7765-7776.

88. Stowers, R. S.; Allen, S. C.; Suggs, L. J., Dynamic phototuning of 3D hydrogel stiffness. *Proceedings of the National Academy of Sciences of the United States of America* **2015,** *112* (7), 1953-1958.

89. Liu, D.; Bastiaansen, C. W. M.; den Toonder, J. M. J.; Broer, D. J., (Photo-)Thermally Induced Formation of Dynamic Surface Topographies in Polymer Hydrogel Networks. *Langmuir* **2013,** *29* (18), 5622-5629.

90. Wang, N.; Li, Y.; Zhang, Y.; Liao, Y.; Liu, W., High-Strength Photoresponsive Hydrogels Enable Surface-Mediated Gene Delivery and Light-Induced Reversible Cell Adhesion/Detachment. *Langmuir* **2014,** *30* (39), 11823-11832.

91. Ueda, E.; Feng, W.; Levkin, P. A., Superhydrophilic–Superhydrophobic Patterned Surfaces as High-Density Cell Microarrays: Optimization of Reverse Transfection. *Advanced Healthcare Materials* **2016,** *5* (20), 2646-2654.

92. Popova, A. A.; Demir, K.; Hartanto, T. G.; Schmitt, E.; Levkin, P. A., Droplet-microarray on superhydrophobic-superhydrophilic patterns for high-throughput live cell screenings. *RSC Advances* **2016,** *6* (44), 38263-38276.

93. Ueda, E.; Geyer, F. L.; Nedashkivska, V.; Levkin, P. A., DropletMicroarray: facile formation of arrays of microdroplets and hydrogel micropads for cell screening applications. *Lab on a Chip* **2012,** *12* (24), 5218-5224.

94. Jogia, G. E.; Tronser, T.; Popova, A. A.; Levkin, P. A., Droplet Microarray Based on Superhydrophobic-Superhydrophilic Patterns for Single Cell Analysis. *Microarrays* **2016,** *5* (4), 28.

95. Popova, A. A.; Depew, C.; Permana, K. M.; Trubitsyn, A.; Peravali, R.; Ordiano, J. Á. G.; Reischl, M.; Levkin, P. A., Evaluation of the Droplet-Microarray Platform for High-Throughput Screening of Suspension Cells. *SLAS TECHNOLOGY: Translating Life Sciences Innovation* **2017,** *22* (2), 163-175.

96. Popova, A. A.; Tronser, T.; Demir, K.; Haitz, P.; Kuodyte, K.; Starkuviene, V.; Wajda, P.; Levkin, P. A., Facile One Step Formation and Screening of Tumor Spheroids Using Droplet-Microarray Platform. *Small* **2019,** *15* (25), 1901299.

97. Lei, W.; Bruchmann, J.; Rüping, J. L.; Levkin, P. A.; Schwartz, T., Biofilm Bridges Forming Structural Networks on Patterned Lubricant-Infused Surfaces. *Advanced Science* **2019,** *6* (13), 1900519.

98. Popova, A. A.; Marcato, D.; Peravali, R.; Wehl, I.; Schepers, U.; Levkin, P. A., Fish-Microarray: A Miniaturized Platform for Single-Embryo High-Throughput Screenings. *Advanced Functional Materials* **2018,** *28* (3), 1703486.

99. Tronser, T.; Popova, A. A.; Levkin, P. A., Miniaturized platform for high-throughput screening of stem cells. *Current Opinion in Biotechnology* **2017,** *46*, 141-149.

100. Tronser, T.; Popova, A. A.; Jaggy, M.; Bastmeyer, M.; Levkin, P. A., Droplet Microarray Based on Patterned Superhydrophobic Surfaces Prevents Stem Cell Differentiation and Enables High-Throughput Stem Cell Screening. *Advanced Healthcare Materials* **2017,** *6* (23), 1700622.

101. Tronser, T.; Demir, K.; Reischl, M.; Bastmeyer, M.; Levkin, P. A., Droplet microarray: miniaturized platform for rapid formation and high-throughput screening of embryoid bodies. *Lab on a Chip* **2018,** *18* (15), 2257-2269.

102. Popova, A. A.; Schillo, S. M.; Demir, K.; Ueda, E.; Nesterov-Mueller, A.; Levkin, P. A., Droplet-Array (DA) Sandwich Chip: A Versatile Platform for High-Throughput Cell Screening Based on Superhydrophobic–Superhydrophilic Micropatterning. *Advanced Materials* **2015,** *27* (35), 5217-5222.

103. Brehm, M.; Heissler, S.; Afonin, S.; Levkin, P. A., Nanomolar Synthesis in Droplet Microarrays with UV-Triggered On-Chip Cell Screening. *Small* **2020,** *n/a* (n/a), 1905971.

104. Benz, M.; Molla, M. R.; Böser, A.; Rosenfeld, A.; Levkin, P. A., Marrying chemistry with biology by combining on-chip solution-based combinatorial synthesis and cellular screening. *Nature Communications* **2019,** *10* (1), 2879.

105. Rosenfeld, A.; Levkin, P. A., High-Throughput Combinatorial Synthesis of Stimuli-Responsive Materials. *Advanced Biosystems* **2019,** *3* (3), 1800293.

106. Neto, A. I.; Demir, K.; Popova, A. A.; Oliveira, M. B.; Mano, J. F.; Levkin, P. A., Fabrication of Hydrogel Particles of Defined Shapes Using Superhydrophobic-Hydrophilic Micropatterns. *Advanced Materials* **2016,** *28* (35), 7613-7619.

107. Scofield, J. H., Hartree-Slater subshell photoionization cross-sections at 1254 and 1487 eV. *Journal of Electron Spectroscopy and Related Phenomena* **1976,** *8* (2), 129-137.

108. Yue, K.; Trujillo-de Santiago, G.; Alvarez, M. M.; Tamayol, A.; Annabi, N.; Khademhosseini, A., Synthesis, properties, and biomedical applications of gelatin methacryloyl (GelMA) hydrogels. *Biomaterials* **2015,** *73*, 254-271.

109. Van Den Bulcke, A. I.; Bogdanov, B.; De Rooze, N.; Schacht, E. H.; Cornelissen, M.; Berghmans, H., Structural and Rheological Properties of Methacrylamide Modified Gelatin Hydrogels. *Biomacromolecules* **2000,** *1* (1), 31-38.

110. Holmes, C. P., Model Studies for New o-Nitrobenzyl Photolabile Linkers: Substituent Effects on the Rates of Photochemical Cleavage. *The Journal of Organic Chemistry* **1997,** *62* (8), 2370-2380.

111. Klán, P.; Šolomek, T.; Bochet, C. G.; Blanc, A.; Givens, R.; Rubina, M.; Popik, V.; Kostikov, A.; Wirz, J., Photoremovable Protecting Groups in Chemistry and Biology: Reaction Mechanisms and Efficacy. *Chemical Reviews* **2013,** *113* (1), 119-191.

112. Usui, K.; Kikuchi, T.; Tomizaki, K.-y.; Kakiyama, T.; Mihara, H., A novel array format for monitoring cellular uptake using a photo-cleavable linker for peptide release. *Chemical Communications* **2013,** *49* (57), 6394-6396.

113. Kakiyama, T.; Usui, K.; Tomizaki, K.-y.; Mie, M.; Kobatake, E.; Mihara, H., A peptide release system using a photo-cleavable linker in a cell array format for cell-toxicity analysis. *Polym J* **2013,** *45* (5), 535-539.

114. Sarin, V. K.; Kent, S. B. H.; Tam, J. P.; Merrifield, R. B., Quantitative monitoring of solid-phase peptide synthesis by the ninhydrin reaction. *Analytical Biochemistry* **1981,** *117* (1), 147-157.

115. Ast, T.; Heine, N.; Germeroth, L.; Schneider-Mergener, J.; Wenschuh, H., Efficient assembly of peptomers on continuous surfaces. *Tetrahedron Letters* **1999,** *40* (23), 4317-4318.

116. Groups Containing N□O Bonds, or Si, P, S, or Halogen Atoms. In *Course Notes on the Interpretation of Infrared and Raman Spectra*, pp 217-246.

117. Allazetta, S.; Negro, A.; Lutolf, M. P., Microfluidic Programming of Compositional Hydrogel Landscapes. *Macromolecular Rapid Communications* **2017,** *38* (15), 1700255.

118. Tourniaire, G.; Collins, J.; Campbell, S.; Mizomoto, H.; Ogawa, S.; Thaburet, J.-F.; Bradley, M., Polymer microarrays for cellular adhesion. *Chemical Communications* **2006,** (20), 2118-2120.

119. Khan, F.; Smith, J. O.; Kanczler, J. M.; Tare, R. S.; Oreffo, R. O. C.; Bradley, M., Discovery and Evaluation of a Functional Ternary Polymer Blend for Bone Repair: Translation from a Microarray to a Clinical Model. *Advanced Functional Materials* **2013,** *23* (22), 2850-2862.

120. Santoro, R.; Venkateswaran, S.; Amadeo, F.; Zhang, R.; Brioschi, M.; Callanan, A.; Agrifoglio, M.; Banfi, C.; Bradley, M.; Pesce, M., Acrylate-based materials for heart valve scaffold engineering. *Biomaterials Science* **2018,** *6* (1), 154-167.

121. Wu, M.; Bridle, H.; Bradley, M., Targeting Cryptosporidium parvum capture. *Water Research* **2012,** *46* (6), 1715-1722.

122. Venkateswaran, S.; Wu, M.; Gwynne, P. J.; Hardman, A.; Lilienkampf, A.; Pernagallo, S.; Blakely, G.; Swann, D. G.; Gallagher, M. P.; Bradley, M., Bacteria repelling poly(methylmethacrylate-co-dimethylacrylamide) coatings for biomedical devices. *Journal of Materials Chemistry B* **2014,** *2* (39), 6723-6729.

123. Patel, A. K.; Tibbitt, M. W.; Celiz, A. D.; Davies, M. C.; Langer, R.; Denning, C.; Alexander, M. R.; Anderson, D. G., High throughput screening for discovery of materials that control stem cell fate. *Current Opinion in Solid State and Materials Science* **2016,** *20* (4), 202-211.

124. Hansen, A.; Mjoseng, H. K.; Zhang, R.; Kalloudis, M.; Koutsos, V.; de Sousa, P. A.; Bradley, M., High-Density Polymer Microarrays: Identifying Synthetic Polymers that Control Human Embryonic Stem Cell Growth. *Advanced Healthcare Materials* **2014,** *3* (6), 848-853.

125. Yang, F.; Mei, Y.; Langer, R.; Anderson, D. G., High Throughput Optimization of Stem Cell Microenvironments. *Combinatorial chemistry & high throughput screening* **2009,** *12* (6), 554-561.

126. Jia, J.; Coyle, R. C.; Richards, D. J.; Berry, C. L.; Barrs, R. W.; Biggs, J.; James Chou, C.; Trusk, T. C.; Mei, Y., Development of peptide-functionalized synthetic hydrogel microarrays for stem cell and tissue engineering applications. *Acta Biomaterialia* **2016,** *45*, 110-120.

127. Le, N. N. T.; Zorn, S.; Schmitt, S. K.; Gopalan, P.; Murphy, W. L., Hydrogel arrays formed via differential wettability patterning enable combinatorial screening of stem cell behavior. *Acta Biomaterialia* **2016,** *34*, 93-103.

128. Schober, L.; Büttner, E.; Laske, C.; Traube, A.; Brode, T.; Traube, A. F.; Bauernhansl, T., Cell Dispensing in Low-Volume Range with the Immediate Drop-on-Demand Technology (I-DOT). *Journal of Laboratory Automation* **2015,** *20* (2), 154-163.

129. Li, L.; Scheiger, J. M.; Tronser, T.; Long, C.; Demir, K.; Wilson, C. L.; Kuzina, M. A.; Levkin, P. A., Inherent Photodegradability of Polymethacrylate Hydrogels: Straightforward Access to Biocompatible Soft Microstructures. *Advanced Functional Materials* **2019,** *29* (33), 1902906.

130. Scheiger, J. M.; Levkin, P. A., Hydrogels with Preprogrammable Lifetime via UV-Induced Polymerization and Degradation. *Advanced Functional Materials n/a* (n/a), 1909800.

131. Chen, M.; Zhong, M.; Johnson, J. A., Light-Controlled Radical Polymerization: Mechanisms, Methods, and Applications. *Chemical Reviews* **2016,** *116* (17), 10167-10211.

132. Chapman, R.; Gormley, A. J.; Stenzel, M. H.; Stevens, M. M., Combinatorial Low-Volume Synthesis of Well-Defined Polymers by Enzyme Degassing. *Angewandte Chemie International Edition* **2016,** *55* (14), 4500-4503.

133. Chapman, R.; Gormley, A. J.; Herpoldt, K.-L.; Stevens, M. M., Highly Controlled Open Vessel RAFT Polymerizations by Enzyme Degassing. *Macromolecules* **2014,** *47* (24), 8541-8547.

134. Oytun, F.; Kahveci, M. U.; Yagci, Y., Sugar overcomes oxygen inhibition in photoinitiated free radical polymerization. *Journal of Polymer Science Part A: Polymer Chemistry* **2013,** *51* (8), 1685-1689.

135. Gormley, A. J.; Chapman, R.; Stevens, M. M., Polymerization Amplified Detection for Nanoparticle-Based Biosensing. *Nano Letters* **2014,** *14* (11), 6368-6373.

136. Kröber, P.; Delaney, J. T.; Perelaer, J.; Schubert, U. S., Reactive inkjet printing of polyurethanes. *Journal of Materials Chemistry* **2009,** *19* (29), 5234-5238.

137. Weeks, E. R.; Crocker, J. C.; Levitt, A. C.; Schofield, A.; Weitz, D. A., Three-Dimensional Direct Imaging of Structural Relaxation Near the Colloidal Glass Transition. *Science* **2000,** *287* (5453), 627.

138. Johnson, L. M.; Fairbanks, B. D.; Anseth, K. S.; Bowman, C. N., Enzyme-Mediated Redox Initiation for Hydrogel Generation and Cellular Encapsulation. *Biomacromolecules* **2009,** *10* (11), 3114-3121.

139. Nguyen, K. T.; West, J. L., Photopolymerizable hydrogels for tissue engineering applications. *Biomaterials* **2002,** *23* (22), 4307-4314.

140. Gupta, P.; Vermani, K.; Garg, S., Hydrogels: from controlled release to pH-responsive drug delivery. *Drug Discovery Today* **2002,** *7* (10), 569-579.

141. Matsumoto, S.; Yamaguchi, S.; Ueno, S.; Komatsu, H.; Ikeda, M.; Ishizuka, K.; Iko, Y.; Tabata, K. V.; Aoki, H.; Ito, S.; Noji, H.; Hamachi, I., Photo Gel–Sol/Sol–Gel Transition and Its Patterning of a Supramolecular Hydrogel as Stimuli-Responsive Biomaterials. *Chemistry – A European Journal* **2008,** *14* (13), 3977-3986.

142. Schmaljohann, D., Thermo- and pH-responsive polymers in drug delivery. *Advanced Drug Delivery Reviews* **2006,** *58* (15), 1655-1670.

143. Wu, Q.; Wang, L.; Yu, H.; Wang, J.; Chen, Z., Organization of Glucose-Responsive Systems and Their Properties. *Chemical Reviews* **2011,** *111* (12), 7855-7875.

144. Kloxin, A. M.; Kasko, A. M.; Salinas, C. N.; Anseth, K. S., Photodegradable Hydrogels for Dynamic Tuning of Physical and Chemical Properties. *Science* **2009,** *324* (5923), 59-63.

145. Siltanen, C.; Shin, D.-S.; Sutcliffe, J.; Revzin, A., Micropatterned Photodegradable Hydrogels for the Sorting of Microbeads and Cells. *Angewandte Chemie International Edition* **2013,** *52* (35), 9224-9228.

146. Rosales, A. M.; Vega, S. L.; DelRio, F. W.; Burdick, J. A.; Anseth, K. S., Hydrogels with Reversible Mechanics to Probe Dynamic Cell Microenvironments. *Angewandte Chemie International Edition* **2017,** *56* (40), 12132-12136.

147. Tomatsu, I.; Peng, K.; Kros, A., Photoresponsive hydrogels for biomedical applications. *Advanced Drug Delivery Reviews* **2011,** *63* (14), 1257-1266.

148. Azagarsamy, M. A.; McKinnon, D. D.; Alge, D. L.; Anseth, K. S., Coumarin-Based Photodegradable Hydrogel: Design, Synthesis, Gelation, and Degradation Kinetics. *ACS Macro Letters* **2014,** *3* (6), 515-519.

149. Fairbanks, B. D.; Singh, S. P.; Bowman, C. N.; Anseth, K. S., Photodegradable, Photoadaptable Hydrogels via Radical-Mediated Disulfide Fragmentation Reaction. *Macromolecules* **2011,** *44* (8), 2444-2450.

150. Rapp, T. L.; Highley, C. B.; Manor, B. C.; Burdick, J. A.; Dmochowski, I. J., Ruthenium-Crosslinked Hydrogels with Rapid, Visible-Light Degradation. *Chemistry – A European Journal* **2018,** *24* (10), 2328-2333.

151. Truong, V. X.; Tsang, K. M.; Simon, G. P.; Boyd, R. L.; Evans, R. A.; Thissen, H.; Forsythe, J. S., Photodegradable Gelatin-Based Hydrogels Prepared by Bioorthogonal Click Chemistry for Cell Encapsulation and Release. *Biomacromolecules* **2015,** *16* (7), 2246-2253.

152. Yanagawa, F.; Sugiura, S.; Takagi, T.; Sumaru, K.; Camci-Unal, G.; Patel, A.; Khademhosseini, A.; Kanamori, T., Activated-Ester-Type Photocleavable Crosslinker for Preparation of Photodegradable Hydrogels Using a Two-Component Mixing Reaction. *Advanced Healthcare Materials* **2015,** *4* (2), 246-254.

153. Mann, B. A.; Kremer, K.; Holm, C., The Swelling Behavior of Charged Hydrogels. *Macromolecular Symposia* **2006,** *237* (1), 90-107.

154. Benton, J. A.; DeForest, C. A.; Vivekanandan, V.; Anseth, K. S., Photocrosslinking of gelatin macromers to synthesize porous hydrogels that promote valvular interstitial cell function. *Tissue Eng Part A* **2009,** *15* (11), 3221-3230.

155. Nichol, J. W.; Koshy, S. T.; Bae, H.; Hwang, C. M.; Yamanlar, S.; Khademhosseini, A., Cell-laden microengineered gelatin methacrylate hydrogels. *Biomaterials* **2010,** *31* (21), 5536-5544.

156. Hutson, C. B.; Nichol, J. W.; Aubin, H.; Bae, H.; Yamanlar, S.; Al-Haque, S.; Koshy, S. T.; Khademhosseini, A., Synthesis and characterization of tunable poly(ethylene glycol): gelatin methacrylate composite hydrogels. *Tissue Eng Part A* **2011,** *17* (13-14), 1713-1723.

157. Yoon, H.; Shin, S.; Cha, J.; Lee, S.-H.; Kim, J.-H.; Do, J. T.; Song, H.; Bae, H., Cold Water Fish Gelatin Methacryloyl Hydrogel for Tissue Engineering Application. *PLOS ONE* **2016,** *11*, e0163902.

158. Oliveira, M. B.; Ribeiro, M. P.; Miguel, S. P.; Neto, A. I.; Coutinho, P.; Correia, I. J.; Mano, J. F., In vivo high-content evaluation of three-dimensional scaffolds biocompatibility. *Tissue engineering. Part C, Methods* **2014,** *20* (11), 851-864.

159. Niskanen, J.; Tenhu, H., How to manipulate the upper critical solution temperature (UCST)? *Polymer Chemistry* **2017,** *8* (1), 220-232.

8 Acknowledgements

Firstly, I would like to thank my supervisor, PRIV.-DOZ. DR. PAVEL LEVKIN, for giving me the chance to work on this exciting topic, for his supportive guidance through my PhD-journey, for his fair and respectful treatment of even craziest ideas, as well as for keeping me on track to reach the deadlines.

I would like to thank the members of the Thesis Advisory Committee, PROF. DR. VERONIQUE ORIAN-ROUSSEAU (IBCS-FMS, KIT) and PROF. DR. STEFAN BRÄSE (IBCS-FMS, KIT), for committed scientific assistance and giving me the full-fledged vision of the impact of my work. I would also like to thank PROF. DR. UTE SCHEPERS for agreeing to act as a second examiner for my thesis.

Further, I would like to express my gratitude to the collaborators, especially STEFAN HEISSLER, DR. ALEXANDER WELLE, VANESSA TROUILLET, DR. RICHARD THELEN, DR.-ING. MARKUS REISCHL and DR. CLAUDE OELSCHLAEGER for their help with Raman spectrometry (IFG, KIT), Time-of-Flight Secondary Ion Mass Spectrometry (IFG, KIT), X-ray photoelectron spectroscopy (IAM, KIT), white light scattering spectroscopy (IMT, KIT), mathematical approximation calculations (IAI, KIT) and multiple particle tracking experiments (AME, KIT). I am especially grateful to TOBIAS GÖCKLER (IFG, KIT), for his substantial contribution to one of my main projects and multiple careful proofreading of the manuscript, but primarily for his exceptionally friendly nature and sanguine views towards the future.

I would like to acknowledge my former and current colleagues, who made these three years unforgettable, for a pleasant working atmosphere and great time outside the working hours, especially DR. ANNA POPOVA, MAXIMILIAN BENZ, YANXI LIU, JOHANNES SCHEIGER, DR. SHRADDHA CHAKRABORTY and DR. FARID BEHBOODI SADABAD. ANNA, thank you for being my secret role model throughout the years. MAX, you could always find the right words to go through all the up´s and down´s. YANXI, thank you for always being there for me. JOHANNES, thanks for supporting me scientifically and cheering me up on Mondays. SCHRADDHA, without your calm and optimistic perspective my PhD-days would be much darker. FARID, thanks for all the support and guidance in writing the papers and the thesis.

Finally yet importantly, I want to thank my friends for staying my friends down the years, especially JULIA and ANNA. I also thank my best friend DARIA for giving me the necessary tailwind. My deepest gratitude goes to my family, for their deliberate support of all my initiatives since I was a child. Thanks for noticing me pipetting soap water from one shampoo bottle into

another at the age of three and buying me the Young Chemist Kit some years later. Thanks for deliberately distracting me from my research and pushing me to go and grasp some fresh air. Ultimately, I would like to thank my dearest fiancée, soulmate and partner in crime EUGEN, who, despite his own extremely time-consuming and mentally exhausting job, surrounded me with love and support I could never have dreamt of.